Multiscale models of atmospheric mercury: bromine chemistry, air-sea exchange, and global transport

A dissertation presented

by

Christopher D. Holmes

to

The Department of Earth and Planetary Sciences

in partial fulfillment of the requirements
for the degree of
Doctor of Philosophy
in the subject of
Earth and Planetary Sciences

Harvard University
Cambridge, Massachusetts

April, 2010

Dissertation Advisor

Professor Daniel J. Jacob

Author

Christopher D. Holmes

Multiscale models of atmospheric mercury: bromine chemistry, air-sea exchange, and global transport

Abstract

This dissertation uses multiple modeling approaches to identify the key reactions and processes controlling atmospheric mercury globally, with particular emphasis on the upper troposphere and marine boundary layer. We first calculate the global mean atmospheric lifetime of elemental mercury (Hg^0) against oxidation by atomic bromine (Br) in the troposphere by combining kinetic data for the Hg-Br system with modeled global concentrations of tropospheric Br. We obtain a lifetime of 0.5–1.7 years based on the range of kinetic data, implying that oxidation of Hg^0 by Br is a major, and possibly dominant, global sink for Hg^0.

Halogens in marine air are proposed to be major oxidants of Hg^0. We construct a box model of the marine boundary layer (MBL) to interpret observations of reactive gaseous mercury (RGM) in terms of its sources and sinks. The morning RGM rise and midday maximum are consistent with oxidation of Hg^0 by Br atoms, requiring $<$2 ppt BrO in most conditions. Oxidation of Hg^0 by Br accounts for 35-60% of the RGM source in our model MBL, with most of the remainder contributed by oxidation of Hg^0 by ozone (5–20%) and

entrainment of RGM-rich air from the free troposphere (25–40%). Oxidation of Hg^0 by Cl is minor (3–7%), and oxidation by OH cannot reproduce the observed RGM diurnal cycle, suggesting that it is unimportant.

Finally, we compare a global atmospheric model for mercury (GEOS-Chem) in which atomic bromine is the sole oxidant of $Hg^0$with an alternative model in which OH and ozone are oxidants. Our model also includes updated emissions (8600 Mg a^{-1}), improved scavenging by ice and snow, a new parameterization of Hg^{II} uptake and deposition through sea-salt aerosol, and a coupled snowpack emission model. Bromine concentrations here derive from atmospheric models constrained by source gas distributions and match satellite BrO columns. We find that the observed spatial distribution and seasonal cycle of total gaseous mercury (TGM) are equally consistent with either the bromine-only mechanism or the OH and O_3 mechanism, while mercury oxidation in summer subsidence events over Antarctica is more consistent with the bromine mechanism. Wet deposition measurements over the US are also consistent with the bromine mechanism, but require some additional bromine in the free troposphere, perhaps from sea-salt. Aircraft observations in Arctic spring find complete Hg^0 oxidation in the lower stratosphere that the model cannot reproduce, except possibly with oxidation by chlorine species in the winter vortex. Atmospheric reduction, which has no known mechanism, is not required to reproduce any major features of mercury observations.

Contents

List of Figures

List of Tables

Citations to Previously Published Work

Chapters 2 and 3 have appeared previously in the following papers:

Holmes, C.D., D.J. Jacob, R.P. Mason, D.A. Jaffe (2009) Sources and deposition of reactive gaseous mercury in the marine atmosphere, *Atmospheric Environment* **43**, 2278–2285, doi: 10.1016/j.atmosenv.2009.01.051.

Holmes, C.D., D.J. Jacob, and X. Yang (2006) Global lifetime of elemental mercury against oxidation by atomic bromine in the free troposphere, *Geophysical Research Letters* **33**, L20808, doi:10.1029/2006GL027176.

Acknowledgments

I am deeply grateful to many people for their invaluable contributions to this work.

Daniel Jacob has been a great advisor and mentor during my PhD study, introducing me to atmospheric chemistry and offering field research opportunities that have been the highlight of my studies. His insights have pushed me in new and exciting directions. And his exhortations to focus on big issues have sharpened my scientific vision.

Daniel and Jennifer Logan have assembled a wonderful group of scientists and accomplished individuals in the Atmospheric Chemistry Modeling Group. These graduate students, postdocs and scientists have provided helpful ideas, lighthearted breaks, and many friendships. Thanks especially to Elsie Sunderland, Bob Yantosca, Philippe LeSager and the members of Team Hg: Bess, Noelle, Anne, Nicole and Helen.

My officemates—Lin Zhang, Monika Kopacz and Eric Leibensperger, in particular—have shaped my thoughts on science, life, and the world.

The Earth and Planetary Science department staff have guided me over bureaucratic hurdles and provided a continuous supply of cookies, coffee, pizza and encouragement.

My parents, Tom and Grace, sister Laura, and Alla provided concern, advice, support and love.

to the memory of my grandmothers

Catherine Denton (1912-2004) and Bertha Holmes (1911-2007)

"From these dark sayings of this mystical Author, we may gather these things...

That it is of a strange and wonderful nature not easily by labour found out: which made Helmont confess that he had spent thirty years sub ferula Mercurii, and that it had not its compeer in Nature."

—John Webster, METALLOGRAPHIA (1671)

Chapter 1

Overview

1.1 Mercury in society and the environment

For millennia people have sought mercury for its useful, aesthetic and supposed magical properties. Romans mined it in Spain for metallurgy. Chinese emperors drank it to achieve immortality. Cultures around the world have used it in traditional medicine, art, and cosmetics. And alchemists believed that the right proportions of mercury and other elements might transmute common metals into great wealth. With the rise of industrial chemistry in the 18th century and later, mercury became even more central to modern life. As a catalyst for organic synthesis, chloralkali manufacture, and a common electrical component, mercury became essential to producing paper, textiles, medicines, plastics, lighting and countless everyday consumer products.

The bright reputation of mercury grew darker in the 20th century. Although some mercury compounds were known as poisons for centuries, the metallic liquid form used in many of the industrial processes was generally thought to be safe—mid-century science

kits for children contained open vials of quicksilver. This benign view changed as epidemiologists traced the cause of birth deformities, neurological disease and death that afflicted Minimata, Japan throughout the 1950s. The source was eventually traced to mercury-laden effluent from industrial acetate production, which drained into the bay where residents harvested fish and shellfish bearing toxic levels of methyl-mercury (McAlpine and Araki, 1958). Since the chemical plant used the supposedly non-toxic elemental mercury, the tragic lesson was that natural environments—now thought to be anaerobic bacteria in water and sediments—could convert inorganic mercury to organic species that biomagnify to toxic doses within food webs.

Severe industrial poisonings recurred in the following decades, from fishing in the wastewater downstream of a chloralkali producer in Ontario, Canada in the 1960s and from consuming grain treated with an organic mercury fungicide in southern Iraq in 1971–3. Similar outbreaks might have occurred near Syracuse, New York where a chloralkali manufacturer released over 50 tons of mercury into Onondaga Lake, but environmental agencies banned all fishing in the lake as a protective measure (Effler, 1987).

A new pattern of mercury exposure emerged in the 1970s; high mercury concentrations were found fish and water from northern Scandinavia and remote lakes in North America without wastewater contamination. Rainwater measurements then found that atmospheric transport and deposition was the mercury source, meaning that mercury is more mobile and widespread than other metal pollutants (Bjorklund et al., 1984; Evans, 1986). Simultaneous work in the Arctic established that mercury reaches the most remote ecosystems through

the air. And reconstructions of past mercury deposition from ice cores and animal tissues show that humans are mainly responsible for present-day mercury deposition, enhancing deposition 3–5 fold over the preindustrial past (Schuster et al., 2002; Dietz et al., 2009). Today, atmospheric emission and transport are the first steps to exposure for most Americans (Figure 1.1), who consume mercury mainly from marine fish like tuna and swordfish (Sunderland, 2007). Although rarely acute, present-day exposures reduce IQ, delay childhood development, and may increase cardiovascular disease (Mergler et al., 2007).

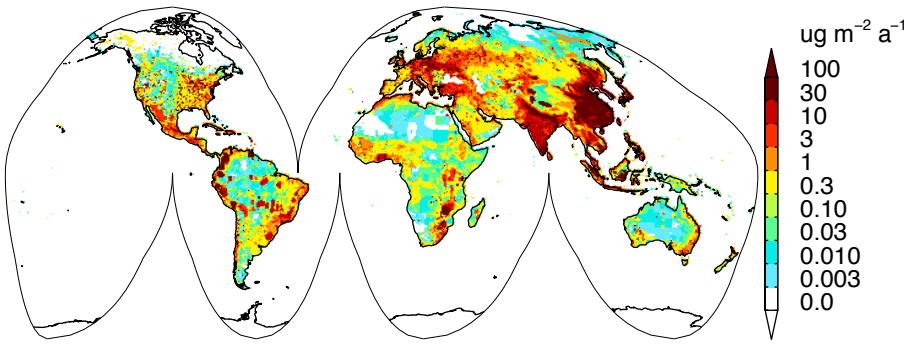

Figure 1.1: Global anthropogenic mercury emissions in 2005 from United Nations Environment Program.

As governments enact regulations and agreements to limit mercury emissions and reduce exposure, they rely heavily on atmospheric mercury models. These are used to attribute mercury deposition to emission regions and processes, and to predict the impact of policy actions—all of which require accurate process representation in the models.

This dissertation arises from the desire to understand and model the pathways of environmental mercury dispersion and from simple curiosity about a global elemental cycle with air, water and living parts. My focus here is the atmospheric portion of the mercury cy-

cle, with special emphasis on the chemical and physical processes that control its lifetime, distribution and deposition fate.

1.2 Atmospheric mercury: the redox problem

The atmosphere contains mercury in elemental (Hg^0) and divalent (Hg^{II}) forms, with field measurements generally finding about 95% as Hg^0. Hg^0 has low solubility in water, which imparts an atmospheric lifetime (0.5-2 years) long enough to enable global transport. Hg^{II} species likely consist of salts and oxides, all of which are highly soluble in water (Henry's Law coefficient $> 10^6$ M atm^{-1}) and therefore have a lifetime against deposition of days in the lower troposphere. The Hg^{II} gases can also condense onto atmospheric aerosols, which are similarly short-lived.

Mercury emissions are mainly Hg^0, including nearly all emissions from natural processes and around 60% of anthropogenic emissions—only high-temperature combustion releases Hg^{II}—while Hg^{II} dominates wet deposition. Therefore net oxidation is required to close the atmospheric mercury budget and redox chemistry will control the distribution and fate of mercury emissions.

When I began this research in 2004 it was commonly accepted that gas-phase OH and O_3 were the globally dominant oxidants of Hg^0, and that fast photoreduction of Hg^{II}—likely by aqueous HO_2—led to active redox cycling. This was supported by laboratory studies finding fast kinetics for these reactions (Hall, 1995; Pehkonen and Lin, 1998; Sommar et al., 2001; Pal and Ariya, 2004a,b), and by the relatively well-known distribution of

these trace gas reactants. Models including these oxidants and fast aqueous reduction simulated major features of mercury observations, providing further support for the consensus (Shia et al., 1999; Bergan and Rodhe, 2001; Bullock and Brehme, 2002; Selin et al., 2007).

Cracks in this basic picture of atmospheric mercury oxidation arose in 2003-2005. Shepler and Peterson (2003) recalculated the binding energy of HgO with improved *ab initio* methods and found that gas-phase $Hg + O_3 \rightarrow HgO + O_2$ is endothermic and that gaseous HgO is very weakly bound. Shortly thereafter Goodsite et al. (2004) calculated that the intermediate product, HgOH, formed from $Hg + OH$ is extremely unstable at atmospheric temperatures and should decompose to reactants rather than react further to stable Hg^{II}. In light of these studies Calvert and Lindberg (2005) reviewed the laboratory studies of these reactions and concluded that the experimental methods did not quantify important secondary chemistry and interfering heterogeneous reaction pathways. Therefore, they argued, the reported rate coefficients were too high and do not apply to the atmosphere. Furthermore, Gårdfeldt and Jonsson (2003) reexamined the Hg^{II} reduction pathways and concluded that single-electron reduction, whether by HO_2 or other species, could not occur in oxygenated water, and other known reductants are much slower (Ariya et al., 2008). Thus the mercury research field was thrown into fundamental uncertainty about the dominant atmospheric redox reactions

1.3 Research questions and methods

This work aims to better quantify the fluxes of atmospheric mercury, their distribution and role in the global biogeochemical cycle of mercury. The following questions are central to this work.

- What are the dominant redox reactions affecting atmospheric mercury?
- What implications do alternative oxidants and kinetic rate coefficients have for the mercury cycle?
- What are the major chemical and physical processes controlling mercury exchange with the ocean?

I address these questions with atmospheric models ranging in complexity from a box model to a 3-D global atmospheric chemical transport model with coupled surface soil, ocean and snow sub-models. The simplified models provide insights into key processes whose consequences are evaluated in the global model. Given the conflicting claims about reaction kinetics and processes, these models are useful platforms to test the consistency of alternative chemical mechanisms with atmospheric observations. Observations used for comparison here include surface monitoring sites, ship cruises and recently available aircraft data from the NASA INTEX-B and ARCTAS field experiments.

1.4 Dissertation outline and major results

Chapter 2 provides a first estimate of the impact of bromine on mercury oxidation throughout the troposphere. I calculate the local and global lifetimes of Hg^0 within a 2-D zonally-

symmetric atmosphere containing bromine concentrations derived from a process-based model. The range of kinetic data imply a global Hg^0 lifetime of 0.5–1.7 years due to bromine, which matches the lifetime inferred from observations and establishes bromine as a globally important oxidant of Hg^0.

In Chapter 3, I interpret observed diurnal cycles of reactive gaseous mercury (RGM)—the gaseous part of Hg^{II}–in the marine boundary layer (MBL) with a box model of chemistry and air-sea exchange. Earlier field and modeling studies proposed that halogens are important oxidants in the mid-latitude MBL (Hedgecock and Pirrone, 2004; Laurier and Mason, 2007; Selin et al., 2007), and I test this against all available RGM data from the Pacific and Atlantic oceans (Jaffe et al., 2005; Laurier et al., 2003; Laurier and Mason, 2007). I find that Hg^0 oxidation by bromine fits observations better than oxidation by OH and O_3. I also provide a new method to calculate Hg^{II} uptake into sea-salt aerosols based on observed wind speeds and relative humidities and find that this is the dominant pathway for Hg^{II} deposition to the ocean.

Chapter 4 integrates the key processes identified in the earlier chapters into the GEOS-Chem global atmospheric chemistry and transport model. In particular, I implement mercury-bromine chemistry, provide an efficient parameterization of Hg^{II} uptake into sea-salt aerosols, and develop a snowpack model for mercury emissions in polar regions. The model includes two alternative Hg^0 oxidation mechanisms—Br only vs. OH and O_3—both of which are compared with against the distribution and seasonal cycle of Hg^0, wet deposition, and vertical profiles from aircraft. In nearly all cases, Hg^0 oxidation by Br fits observations as

well or better than oxidation by OH and O_3, and this implies greater mercury deposition at higher latitudes than expected from previous models. Fast atmospheric reduction, which has no established mechanism, is not required in the bromine mechanism when the kinetic coefficients are adjusted within their uncertainties. Arctic Hg^0 observations are most consistent with 40% surface retention of mercury deposited to snow, representing a significant input to ecosystems. Inconsistencies between model and observations in the upper troposphere and lower stratosphere suggest additional chemistry, perhaps involving reactive chlorine. Finally, I identify observations in the tropics and southern hemisphere that could best clarify our understanding of atmospheric mercury cycling.

Bibliography

Ariya, P., Peterson, K., Snider, G., and Amyot, M. (2008). Mercury chemical transformation in the gas, aqueous and heterogeneous phases: state-of-the-art science and uncertainties. In *Mercury Fate and Transport in the Global Atmosphere*. United Nations Environment Programme.

Bergan, T. and Rodhe, H. (2001). Oxidation of elemental mercury in the atmosphere; constraints imposed by global scale modelling. *J Atmos Chem*, 40(2):191–212.

Bjorklund, I., Borg, H., and Johansson, K. (1984). Mercury in Swedish lakes - its regional distribution and causes. *Ambio*, 13(2):118–121.

Bullock, O. and Brehme, K. (2002). Atmospheric mercury simulation using the cmaq model: formulation description and analysis of wet deposition results. *Atmos Environ*, 36(13):2135–2146.

Calvert, J. and Lindberg, S. (2005). Mechanisms of mercury removal by O-3 and OH in the atmosphere. *Atmos Environ*, 39(18):3355–3367.

Dietz, R., Outridge, P. M., and Hobson, K. A. (2009). Anthropogenic contributions to mercury levels in present-day arctic animals-a review. *Sci Total Environ*, 407(24):6120–6131.

Effler, S. (1987). The impact of a chloralkali plant on onondaga lake and adjoining systems. *Water Air Soil Poll*, 33(1-2):85–115.

Evans, R. (1986). Sources of mercury contamination in the sediments of small headwater lakes in south-central ontario, canada. *Arch Environ Con Tox*, 15(5):505–512.

Gårdfeldt, K. and Jonsson, M. (2003). Is bimolecular reduction of Hg(II) complexes possible in aqueous systems of environmental importance. *J Phys Chem A*, 107(22):4478–4482.

Goodsite, M., Plane, J., and Skov, H. (2004). A theoretical study of the oxidation of Hg-0 to HgBr2 in the troposphere. *Environ Sci Technol*, 38(6):1772–1776.

Hall, B. (1995). The gas phase oxidation of elemental mercury by ozone. *Water, Air, and Soil Pollution*, 80:301–315.

Hedgecock, I. and Pirrone, N. (2004). Chasing quicksilver: Modeling the atmospheric lifetime of Hg-(g)(0) in the marine boundary layer at various latitudes. *Environ Sci Technol*, 38(1):69–76.

Jaffe, D., Prestbo, E., Swartzendruber, P., Weiss-Penzias, P., Kato, S., Takami, A., Hatakeyama, S., and Kajii, Y. (2005). Export of atmospheric mercury from Asia. *Atmos Environ*, 39(17):3029–3038.

Laurier, F. and Mason, R. (2007). Mercury concentration and speciation in the coastal and open ocean boundary layer. *J Geophys Res*, 112(D6):D06302.

Laurier, F., Mason, R., Whalin, L., and Kato, S. (2003). Reactive gaseous mercury formation in the North Pacific Ocean's marine boundary layer: A potential role of halogen chemistry. *J Geophys Res*, 108(D17):4529.

McAlpine, D. and Araki, S. (1958). Minamata disease - an unusual neurological disorder caused by contaminated fish. *Lancet*, 2:629–631.

Mergler, D., Anderson, H., Chan, L., Mahaffey, K., Murray, M., Sakamoto, M., and Stern, A. (2007). Methylmercury exposure and health effects in humans: A worldwide concern. *Ambio*, 36(1):3–11.

Pal, B. and Ariya, P. A. (2004a). Gas-phase HO·-initiated reactions of elemental mercury: Kinetics, product studies, and atmospheric implications. *Environ Sci Technol*, 38(21):5555–5566.

Pal, B. and Ariya, P. A. (2004b). Studies of ozone initiated reactions of gaseous mercury: kinetics, product studies, and atmospheric implications. *Phys Chem Chem Phys*, 6(3):572–579.

Pehkonen, S. and Lin, C. (1998). Aqueous photochemistry of mercury with organic acids. *Journal of the Air & Waste Management Association*, 48(2):144–150.

Schuster, P., Krabbenhoft, D., Naftz, D., Cecil, L., Olson, M., Dewild, J., Susong, D., Green, J., and Abbott, M. (2002). Atmospheric mercury deposition during the last 270 years: A glacial ice core record of natural and anthropogenic sources. *Environ Sci Technol*, 36:2303–2310.

Selin, N. E., Jacob, D. J., Park, R. J., Yantosca, R. M., Strode, S., Jaeglé, L., and Jaffe, D. (2007). Chemical cycling and deposition of atmospheric mercury: Global constraints from observations. *J Geophys Res*, 112(D2):1–14.

Shepler, B. and Peterson, K. (2003). Mercury monoxide: A systematic investigation of its ground electronic state. *J Phys Chem A*, 107(11):1783–1787.

Shia, R., Seigneur, C., Pai, P., Ko, M., and Sze, N. (1999). Global simulation of atmospheric mercury concentrations and deposition fluxes. *J Geophys Res*, 104(D19):23747–23760.

Sommar, J., Gardfeldt, K., Stromberg, D., and Feng, X. (2001). A kinetic study of the gas-phase reaction between the hydroxyl radical and atomic mercury. *Atmos Environ*, 35(17):3049–3054.

Sunderland, E. M. (2007). Mercury exposure from domestic and imported estuarine and marine fish in the us seafood market. *Environmental Health Perspectives*, 115(2):235–242.

Chapter 2

Global lifetime of elemental mercury against oxidation by atomic bromine in the free troposphere

Abstract

We calculate the global mean atmospheric lifetime of elemental mercury (Hg^0) against oxidation by atomic bromine (Br) in the troposphere by combining recent kinetic data for the Hg-Br system with modeled global concentrations of tropospheric Br. We obtain a lifetime of 0.5-1.7 years based on the range of kinetic data, implying that oxidation of Hg^0 by Br is a major, and possibly dominant, global sink for Hg^0. Most of the oxidation takes place in the middle and upper troposphere, where Br concentrations are high and where cold temperatures suppress thermal decomposition of the HgBr intermediate. This oxidation mechanism is consistent with mercury observations, including in particular high gaseous Hg^{II} concentrations in Antarctic summer. Better free-tropospheric measurements of bromine radicals and further kinetic study of the Hg-Br system are essential to more accurately assess the global importance of Br as an oxidant of atmospheric Hg^0.

Mercury is present in the atmosphere principally in its elemental form, Hg^0, which can be transported globally, as indicated by the uniformity of its atmospheric concentration. Hg^0 is eventually oxidized to divalent Hg^{II}, which may be reduced back to Hg^0 but also partitions into atmospheric water and reacts with surfaces, leading to mercury deposition and accumulation in ecosystems. Some deposited mercury is subsequently reduced and re-emitted as Hg^0. Unlike other heavy metals, mercury transits among surface reservoirs primarily through atmospheric fluxes (Mason and Sheu, 2002). Therefore, understanding the atmospheric redox chemistry of mercury is critical to determining source-receptor relationships of this toxic element.

Current models assume that gaseous hydroxyl radicals (OH) and gaseous ozone (O_3) are the main global oxidants of Hg^0 (e.g. Bergan and Rodhe, 2001). Laboratory kinetic studies imply that the global mean lifetime of Hg^0 is 120-210 days against oxidation by OH (Sommar et al., 2001; Pal and Ariya, 2004a) and 60-1500 days against oxidation by O_3 (Hall, 1995; Pal and Ariya, 2004b). However, in light of the expected rapid thermal dissociation of HgOH (Goodsite et al., 2004), Calvert and Lindberg (2005) concluded that oxidation of Hg^0 by OH is much slower than reported by the above studies and is insignificant under atmospheric conditions. Atmospheric observations constrain the residence time of total atmospheric mercury (Hg^0 + Hg^{II}) to 0.5-2 years (Schroeder and Munthe, 1998), which places an upper limit on the lifetime of Hg^0 against oxidation (depending on competition between reduction and deposition of Hg^{II}). Ozone alone cannot be the main oxidant of Hg^0 because it explains neither the observed seasonal variation of Hg^0 and dissolved

Hg^{II} in rainwater (Bergan and Rodhe, 2001; Selin et al., 2007), nor the observed diurnal cycle of gaseous Hg^{II} (Laurier et al., 2003; Hedgecock et al., 2005). These observations imply that oxidation of Hg^0 must be photochemically mediated.

Goodsite et al. (2004) developed a homogeneous mechanism for Hg-Br chemistry in the troposphere based on theoretical kinetic calculations, and showed that gas-phase oxidation of Hg^0 by Br atoms could explain mercury depletion events (MDEs) in the Arctic springtime boundary layer. They suggested that this mechanism would be important more generally in the marine boundary layer and on the global scale. Lin et al. (2006) suggested that Hg-Br chemistry is also significant in the upper troposphere. We present here a quantitative analysis of the global lifetime of Hg^0 against oxidation by tropospheric Br by combining the mechanism of Goodsite et al. (2004) with Br concentrations from a global 3-D simulation of tropospheric bromine chemistry (Yang et al., 2005) as well as updated kinetic data. We find that oxidation by Br in the middle and upper troposphere could be an important sink for Hg^0, and that the mechanism yields an atmospheric lifetime of Hg^0 consistent with observational constraints.

Recent observations indicate that the free troposphere contains significant BrO. Satellite instruments (GOME and SCIAMACHY) observe BrO columns with $1-4\times10^{13}$ molecules cm^{-2} in excess of the known stratospheric abundance (Salawitch et al., 2005; Sinnhuber et al., 2005). This corresponds to $0.5-2$ pptv BrO distributed throughout the tropospheric column. Balloon measurements in the northern mid-latitudes and tropics give independent evidence for $0.5-2$ pptv BrO in the troposphere (Fitzenberger et al., 2000; Pundt et al.,

2002; Van Roozendael et al., 2002). Tropospheric sources include activation from sea salt; oxidation and photolysis of bromocarbons; transport from the stratosphere; and recycling from reservoir species (Br_2, HOBr, $BrNO_2$, $BrONO_2$, HBr) by homogeneous and heterogeneous processes (von Glasow et al., 2002; Platt and Honninger, 2003; Yang et al., 2005; Salawitch, 2006).

Some ground-based observations have found lower abundances of tropospheric BrO. Schofield et al. (2004) found an upper limit of 1.2×10^{13} molecules cm^{-2} in the tropospheric column over Lauder, New Zealand. The maximum tropospheric column observed by Leser et al. (2003) during an Atlantic cruise was 0.6×10^{13} molecules BrO cm^{-2}. However, neither method was sensitive to BrO near the tropopause and therefore both could be reconciled with satellite observations if much of the satellites' nominally tropospheric BrO column were concentrated in the upper troposphere or lowermost stratosphere (Salawitch et al., 2005).

Raofie and Ariya (2004) reported a gas-phase reaction of BrO with Hg^0, but could not exclude the possibility of heterogeneous mechanisms in their experimental system. Homogeneous oxidation of Hg^0 by BrO is endothermic and has a large energy barrier, making its atmospheric relevance unlikely (Balabanov and Peterson, 2003; Tossell, 2003). However, oxidation by Br atoms is fast (Calvert and Lindberg, 2004; Goodsite et al., 2004). Rapid chemical cycling between BrO and Br through BrO photolysis, self-reaction, and reaction with NO, balanced by Br oxidation by O_3, maintains Br:BrO molar ratios of $0.01 - 2$ in the daytime troposphere (Platt and Janssen, 1995; Yang et al., 2005).

We estimate here the global impact of atomic bromine on atmospheric oxidation of mercury through the two-step recombination reactions (R1) + (R3), in competition with thermal dissociation (R2), following Goodsite et al. (2004):

$$\mathrm{Hg} + \mathrm{Br} \xrightarrow{\mathrm{M}} \mathrm{HgBr} \tag{R1}$$

$$\mathrm{HgBr} \xrightarrow{\mathrm{M}} \mathrm{Hg} + \mathrm{Br} \tag{R2}$$

$$\mathrm{HgBr} + \mathrm{X} \xrightarrow{\mathrm{M}} \mathrm{HgBrX} \qquad (\mathrm{X} = \mathrm{Br}, \mathrm{OH}) \tag{R3}$$

Other species (e.g. X = I, O_2) may also contribute to reaction (R3) (Goodsite et al., 2004), but their effect is probably minor and we disregard them. The local lifetime of Hg^0 against oxidation to chemically stable Hg^{II} by (R1) – (R3) is

$$\tau_{\mathrm{local}} = \frac{k_2 + k_{3,\mathrm{Br}}[\mathrm{Br}] + k_{3,\mathrm{OH}}[\mathrm{OH}]}{k_1[\mathrm{Br}]\left(k_{3,\mathrm{Br}}[\mathrm{Br}] + k_{3,\mathrm{OH}}[\mathrm{OH}]\right)}. \tag{2.1}$$

Table 2.1 compiles literature values of k_1, k_2, and k_3. Reaction (R2) makes τ_{local} extremely sensitive to temperature, as k_2 doubles with every increase of 6 K (at 273 K) (Goodsite et al., 2004). There is limited information about the temperature (T) and pressure (p) dependences of k_1 and k_3. Donohoue et al. (2006) found that reaction (R1) is in the low pressure regime for $p \leq 1$ atm. Balabanov et al. (2005) reported high and low pressure limits for $k_{3,\mathrm{Br}}$, while Goodsite et al. (2004) found that the reaction is in the high pressure regime at 1 atm.

We calculate the global mean tropospheric lifetime of Hg^0 against conversion to Hg^{II}

Table 2.1: Rate coefficients for oxidation of Hg^0 by Br under atmospheric conditions

Rate coefficient[a]		Conditions	Reference[b]
k_1	3.2×10^{-12}	1 atm, 298 K	(1)
	$1.0 \times 10^{-12} \exp(209/T)$	1 atm[c]	(2)
	$1.1 \times 10^{-12} (T/298)^{-2.37}$	1 atm[c]	(3)
	$3.0 - 9.7 \times 10^{-13}$	1 atm, 298 K[d]	(4)
	$1.5 \times 10^{-32} (T/298)^{-1.86}$ [M]		(5)
k_2	$1.2 \times 10^{10} \exp(-8357/T)$	1 atm	(3)
$k_{3,\mathrm{Br}}$	$2.5 \times 10^{-10} (T/298)^{-0.57}$	1 atm, high p limit	(3)
	3.0×10^{-11}	2 body, 298 K[e]	(5)
	3.0×10^{-11}	high p limit, 298 K	(5)
$k_{3,\mathrm{OH}}$	$2.5 \times 10^{-10} (T/298)^{-0.57}$	1 atm, high p limit [f]	(3)
k_4	3.9×10^{-11}	298 K	(5)

[a] Rate coefficients are in units of cm^3 $molecule^{-1}$ s^{-1}, except for k_2 (s^{-1}). T is temperature in K. [M] is the number density of air.
[b] (1) Ariya et al. (2002); (2) Khalizov et al. (2003); (3) Goodsite et al. (2004); (4) Donohoue et al. (2006); (5) Balabanov et al. (2005)
[c] We assume in our calculations that k_1 is in the low-pressure regime at 1 atm, following Donohoue et al. (2006), and thus scale k_1 with [M].
[d] Unpublished data from Spicer et al. [2002] cited by Donohoue et al. (2006).
[e] Rate coefficient in the absence of a third body, i.e., with stabilization of the activated complex solely by internal energy dissipation.
[f] Inferred by analogy with $k_{3,\mathrm{Br}}$.

by (R1) – (R3) by integrating the loss over the troposphere using global distributions of Br, OH, and temperature, and assuming a uniform tropospheric Hg^0 mixing ratio. For the Br concentration, we use monthly and zonally averaged values for four months (January, April, July, and October) from the global chemical transport model (CTM) of tropospheric bromine described by Yang et al. (2005) (Figure 2.1). This model includes budgets of the dominant bromocarbons and an empirical parameterization of halogen release from sea salt aerosols based on wind speed and observed bromide depletion. It simulates daytime tropospheric BrO columns ($0.2 - 1.6 \times 10^{13}$ molecules cm^{-2}) that are at the low end of the range of satellite observations; thus, the model provides a conservative, process-based estimate of bromine abundance. We use monthly mean temperatures from the NASA Goddard Earth

Observing System (GEOS-4) assimilated meteorology for 1999. Monthly mean OH distributions are from a detailed simulation of tropospheric chemistry (Park et al., 2004). OH and Br are present only during daylight, so we distribute the average monthly concentrations over the daytime hours.

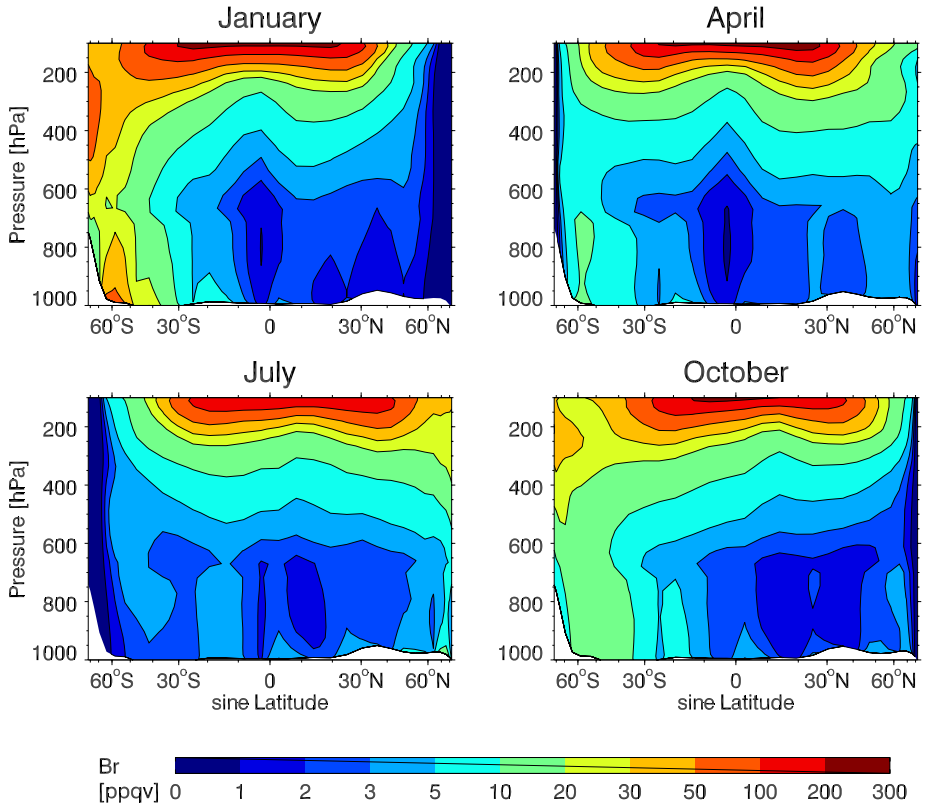

Figure 2.1: Monthly and zonally averaged atomic Br mixing ratios [ppqv] from the Yang et al. (2005) chemical transport model (CTM), which includes inorganic bromine released from sea salt and by photolysis and oxidation of bromocarbons. 1 ppqv = 10^{-15} mol mol^{-1}.

Partitioning among inorganic bromine species explains much of the variability of atomic Br in Figure 2.1 (Yang et al., 2005). Br constitutes 10% of inorganic bromine near the tropical tropopause, where HBr and $BrONO_2$ photolyze rapidly, but less than 1% near the surface. Seasonal changes in BrO photolysis increase atomic Br concentrations in the sum-

mer hemisphere. Atomic Br is generally more abundant in the southern hemisphere than in the north because high wind speeds over the southern ocean drive large emissions from sea salt aerosols.

Figure 2.2 shows the lifetime of Hg^0 against conversion to Hg^{II} by (R1) – (R3), computed from Equation 2.1 for the months of January, April, July, and October. For this base case estimate we use the most recent kinetic data with T and p dependences—k_1 from Donohoue et al. (2006); $k_{3,Br}$ and $k_{3,OH}$ from Goodsite et al. (2004); and k_2 calculated to maintain the k_1:k_2 balance (Goodsite et al., 2004).

From Figure 2.2 we see that the lifetime of Hg^0 is less than 300 days in all seasons near the tropical tropopause due to high Br concentrations and low temperatures (suppressing (R2)). This is consistent with recent aircraft observations of high concentrations of aerosol-bound mercury (presumably Hg^{II}) associated with bromine and iodine near the tropopause (Murphy et al., 2006). Assuming a uniform mixing ratio of Hg^0 up to the tropopause (taken as 150 hPa in the tropics and 300 hPa elsewhere), we find that 47% of Hg^0 tropospheric oxidation occurs in the upper troposphere (above 500 hPa), 32% in the middle troposphere ($800 - 500$ hPa), and 21% in the lower troposphere. The lifetime we calculate for the northern mid-latitude boundary layer (< 500 days) is much longer than a previous lower bound of 160 days for the marine boundary layer in that region (Goodsite et al., 2004) mainly because our zonal-mean lifetime accounts for the lower Br abundances over land. The seasonal cycle in Figure 2.2 shows that despite the opposing influence of temperature, the increased concentrations of Br and OH in summer shorten τ_{local} relative to winter, in

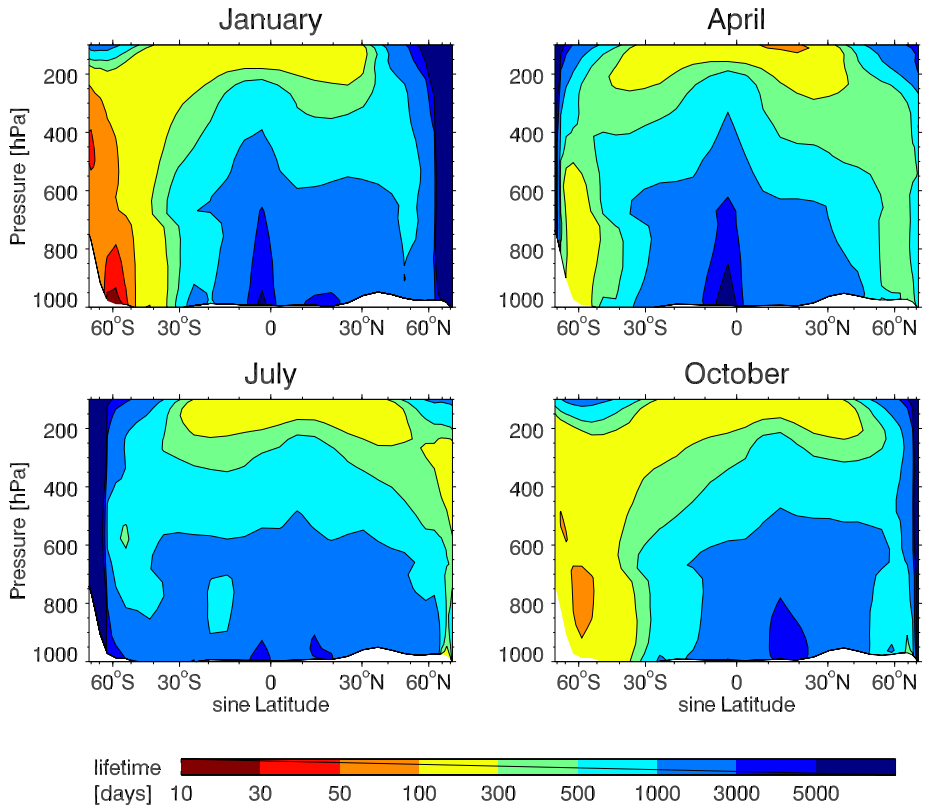

Figure 2.2: Lifetime [days] of atmospheric Hg^0 against oxidation to Hg^{II} by two-step recombination with Br atoms and OH (reactions (R1) – (R1) forming $HgBr_2$ or HgBrOH), using base case rate coefficients from Donohoue et al. (2006) and Goodsite et al. (2004) with the bromine distribution shown in Figure 2.1. The corresponding global-mean tropospheric lifetime of Hg^0 is 510 days, assuming a uniform Hg^0 mixing ratio. The text describes results with other rate coefficients from Table 2.1, all of which yield qualitatively similar distributions of Hg^0 lifetime.

agreement with the observed seasonal cycle of Hg^0 (e.g. Ebinghaus et al., 2002; Selin et al., 2007).

Mass-weighted integration of the Hg^0 loss rates ($1/\tau_{local}$) from Figure 2.2 yields a global mean tropospheric Hg^0 lifetime, τ_{global}, of 510 days against conversion to Hg^{II} by (R1) – (R3). This is similar to current estimates of the lifetime of Hg^0 against oxidation by ozone (e.g. Selin et al., 2007) and could account for a large part of the Hg^0 loss within the 0.5-2 yr observational constraint on the atmospheric lifetime of total mercury. We find that 85% of

the Hg^{II} formed is HgBrOH. This assumes, following Goodsite et al. (2004), that the value of $k_{3,OH}$ is the same as that of $k_{3,Br}$ which they explicitly calculated. If reaction (R3) with OH were insignificant (i.e. $k_{3,OH} = 0$) then the global Hg^0 lifetime would be 50% greater, with the largest changes in the lower troposphere.

Our calculations predict rapid summertime oxidation of Hg^0 ($\tau_{local} = 10 - 100$ days) at all altitudes in Antarctic summer. Sprovieri et al. (2002) and Temme et al. (2003) have observed high concentrations of gaseous Hg^{II} on the Antarctic coast during November through January; these differ from springtime mercury depletion events in that they observe positive correlations between gaseous Hg^{II} and ozone. As OH, O_3 and other known oxidants of Hg^0 could not explain the observed Hg^{II} concentrations, Sprovieri et al. (2002) hypothesized a role for bromine radicals or photochemical oxidants generated immediately above the snowpack. Brooks et al. (2006) also observed high gaseous Hg^{II} at the South Pole under unstable atmospheric conditions, which they attributed to halogen reactions in the upper troposphere. Our work shows that subsiding air from any part of the troposphere could bring to the surface gaseous Hg^{II} formed by reactions with Br, together with elevated ozone.

Thus far our base case calculations have used one combination of rate coefficients (k_1 from Donohoue et al. (2006); $k_{3,Br}$, $k_{3,OH}$, and k_1:k_2 from Goodsite et al. (2004)). Other theoretical (Khalizov et al., 2003; Goodsite et al., 2004) and experimental (Ariya et al., 2002) estimates of k_1 are faster (see Table 2.1), although Donohoue et al. (2006) argue that these values are less accurate. The fastest k_1 value with reported temperature dependence

(Khalizov et al., 2003) implies τ_{global} = 160 days, after recalculating k_2 to keep the k_1:k_2 balance (Goodsite et al., 2004).

The calculated value of τ_{global} also depends on competition between reactions (R2) and (R3). Balabanov et al. (2005) studied reaction (R3) as well as several additional reactions that could occur in the Hg-Br system. Their high-pressure limit for $k_{3,Br}$ is half that of Goodsite et al. (2004). They also found that abstraction of Br from HgBr by reaction (R4) decreases the rate of Hg^{II} formation.

$$HgBr + Br \longrightarrow Hg + Br_2 \qquad \text{(R4)}$$

Calculating the global lifetime of Hg^0 against reactions (R1) – (R4) with the high pressure k_3 and k_4 values from Balabanov et al. (2005), and other rates the same as our base case, yields τ_{global} = 630 days. Additional oxidants for HgBr in reaction (R3) suggested by Balabanov et al. (2005), such as BrO and Br_2, would decrease τ_{global}.

The amount and distribution of tropospheric Br is a large uncertainty in our lifetime estimates. Our calculations show that in order to have a globally significant impact on Hg^0, atomic Br must be present in the middle and upper troposphere, where cold temperatures suppress the thermal dissociation of HgBr. While global models predict peak Br concentrations in this region from bromocarbon sources (von Glasow et al., 2004; Yang et al., 2005), observational evidence is indirect and does not clearly resolve the upper troposphere and lowermost stratosphere (Salawitch et al., 2005). Even in the lowermost stratosphere, atomic Br could significantly shorten the lifetime of Hg^0 through relatively rapid air exchange with

the troposphere.

In conclusion, oxidation by atomic bromine could result in an atmospheric lifetime of Hg^0 against conversion to Hg^{II} of 1.4–1.7 years, and possibly as short as 0.5 years, with most reaction taking place in the free troposphere. This would be an important, and possibly dominant, global pathway for oxidation and deposition of atmospheric mercury. It could reconcile the atmospheric evidence that Hg^0 oxidation is photochemically mediated (Bergan and Rodhe, 2001; Selin et al., 2007) with the evidence against a major role for oxidation by OH (Calvert and Lindberg, 2005). The mechanism appears qualitatively consistent with mercury observations—the seasonal cycle of Hg^0; airborne particulate mercury measurements; and gaseous Hg^{II} in Antarctic summer—but global CTMs are necessary for more stringent quantitative tests. Improved atmospheric measurements of inorganic bromine and its radicals, particularly in the middle and upper troposphere, are needed. Uncertainties in the kinetic data, especially for reactions involving HgBr as a reactant, need to be resolved in order to more narrowly constrain the lifetime of Hg^0 and the Hg^{II} product distribution.

Bibliography

Ariya, P. A., Khalizov, A., and Gidas, A. (2002). Reactions of gaseous mercury with atomic and molecular halogens: Kinetics, product studies, and atmospheric implications. *J Phys Chem A*, 106(32):7310–7320.

Balabanov, N. and Peterson, K. (2003). Mercury and reactive halogens: The thermochemistry of Hg+Cl-2, Br-2, BrCl, ClO, and BrO. *J Phys Chem A*, 107(38):7465–7470.

Balabanov, N., Shepler, B., and Peterson, K. (2005). Accurate global potential en-

ergy surface and reaction dynamics for the ground state of HgBr2. *J Phys Chem A*, 109(39):8765–8773.

Bergan, T. and Rodhe, H. (2001). Oxidation of elemental mercury in the atmosphere; constraints imposed by global scale modelling. *J Atmos Chem*, 40(2):191–212.

Brooks, S., Saiz-Lopez, A., Skov, H., Lindberg, S., Plane, J., and Goodsite, M. (2006). The mass balance of mercury in the springtime Arctic environment. *Geophys Res Lett*, 33(13):L13812.

Calvert, J. and Lindberg, S. (2004). The potential influence of iodine-containing compounds on the chemistry of the troposphere in the polar spring. II. mercury depletion. *Atmos Environ*, 38(30):5105–5116.

Calvert, J. and Lindberg, S. (2005). Mechanisms of mercury removal by O-3 and OH in the atmosphere. *Atmos Environ*, 39(18):3355–3367.

Donohoue, D., Bauer, D., Cossairt, B., and Hynes, A. (2006). Temperature and pressure dependent rate coefficients for the reaction of Hg with Br and the reaction of Br with Br: A pulsed laser photolysis-pulsed laser induced fluorescence study. *J Phys Chem A*, 110(21):6623–6632.

Ebinghaus, R., Kock, H., Coggins, A., Spain, T., Jennings, S., and Temme, C. (2002). Long-term measurements of atmospheric mercury at Mace Head, Irish west coast, between 1995 and 2001. *Atmos Environ*, 36(34):5267–5276.

Fitzenberger, R., Bosch, H., Camy-Peyret, C., Chipperfield, M., Harder, H., Platt, U., Sinnhuber, B., Wagner, T., and Pfeilsticker, K. (2000). First profile measurements of tropospheric BrO. *Geophys Res Lett*, 27(18):2921–2924.

Goodsite, M., Plane, J., and Skov, H. (2004). A theoretical study of the oxidation of Hg-0 to HgBr2 in the troposphere. *Environ Sci Technol*, 38(6):1772–1776.

Hall, B. (1995). The gas phase oxidation of elemental mercury by ozone. *Water, Air, and Soil Pollution*, 80:301–315.

Hedgecock, I., Trunfio, G., Pirrone, N., and Sprovieri, F. (2005). Mercury chemistry in the MBL: Mediterranean case and sensitivity studies using the AMCOTS (Atmospheric Mercury Chemistry over the Sea) model. *Atmos Environ*, 39(38):7217–7230.

Khalizov, A., Viswanathan, B., Larregaray, P., and Ariya, P. (2003). A theoretical study on the reactions of Hg with halogens: Atmospheric implications. *J Phys Chem A*, 107(33):6360–6365.

Laurier, F., Mason, R., Whalin, L., and Kato, S. (2003). Reactive gaseous mercury formation in the North Pacific Ocean's marine boundary layer: A potential role of halogen chemistry. *J Geophys Res*, 108(D17):4529.

Leser, H., Honninger, G., and Platt, U. (2003). MAX-DOAS measurements of BrO and NO2 in the marine boundary layer. *Geophysical Research Letters*, 30(10):1537.

Lin, C., Pongprueksa, P., Lindberg, S., Pehkonen, S., Byun, D., and Jang, C. (2006). Scientific uncertainties in atmospheric mercury models I: Model science evaluation. *Atmos Environ*, 40(16):2911–2928.

Mason, R. and Sheu, G. (2002). Role of the ocean in the global mercury cycle. *Global Biogeochem. Cycles*, 16(4):1093.

Murphy, D., Hudson, P., Thomson, D., Sheridan, P., and Wilson, J. (2006). Observations of mercury-containing aerosols. *Environ Sci Technol*, 40(10):3163–3167.

Pal, B. and Ariya, P. A. (2004a). Gas-phase HO·-initiated reactions of elemental mercury: Kinetics, product studies, and atmospheric implications. *Environ Sci Technol*, 38(21):5555–5566.

Pal, B. and Ariya, P. A. (2004b). Studies of ozone initiated reactions of gaseous mercury: kinetics, product studies, and atmospheric implications. *Phys Chem Chem Phys*, 6(3):572–579.

Park, R., Jacob, D., Field, B., Yantosca, R., and Chin, M. (2004). Natural and transboundary pollution influences on sulfate-nitrate-ammonium aerosols in the United States: implications for policy. *J Geophys Res*, 109:D15204.

Platt, U. and Honninger, G. (2003). The role of halogen species in the troposphere. *Chemosphere*, 52(2):325–338.

Platt, U. and Janssen, C. (1995). Observation and role of the free radicals NO_3, ClO, BrO and IO in the troposphere. *Faraday Discussions*, 100:175–198.

Pundt, I., Pommereau, J., Chipperfield, M., Roozendael, M. V., and Goutail, F. (2002). Climatology of the stratospheric BrO vertical distribution by balloon-borne UV-visible spectrometry. *J Geophys Res*, 107(D24):4806.

Raofie, F. and Ariya, P. (2004). Product study of the gas-phase BrO-initiated oxidation of Hg-0: evidence for stable Hg1+ compounds. *Environ Sci Technol*, 38(16):4319–4326.

Salawitch, R. (2006). Atmospheric chemistry - biogenic bromine. *Nature*, 439(7074):275–277.

Salawitch, R., Weisenstein, D., Kovalenko, L., Sioris, C., Wennberg, P., Chance, K., Ko, M., and McLinden, C. (2005). Sensitivity of ozone to bromine in the lower stratosphere. *Geophysical Research Letters*, 32(5):L05811.

Schofield, R., Kreher, K., Connor, B., Johnston, P., Thomas, A., Shooter, D., Chipperfield, M., Rodgers, C., and Mount, G. (2004). Retrieved tropospheric and stratospheric BrO columns over Lauder, New Zealand. *J Geophys Res*, 109(D14):D14304.

Schroeder, W. and Munthe, J. (1998). Atmospheric mercury — an overview. *Atmos Environ*, 32(5):809–822.

Selin, N. E., Jacob, D. J., Park, R. J., Yantosca, R. M., Strode, S., Jaeglé, L., and Jaffe, D. (2007). Chemical cycling and deposition of atmospheric mercury: Global constraints from observations. *J Geophys Res*, 112(D2):1–14.

Sinnhuber, B., Rozanov, A., Sheode, N., Afe, O., Richter, A., Sinnhuber, M., Wittrock, F., Burrows, J., Stiller, G., von Clarmann, T., and Linden, A. (2005). Global observations of stratospheric bromine monoxide from SCIAMACHY. *Geophysical Research Letters*, 32(20):L20810.

Sommar, J., Gardfeldt, K., Stromberg, D., and Feng, X. (2001). A kinetic study of the gas-phase reaction between the hydroxyl radical and atomic mercury. *Atmos Environ*, 35(17):3049–3054.

Sprovieri, F., Pirrone, N., Hedgecock, I., Landis, M., and Stevens, R. (2002). Intensive atmospheric mercury measurements at Terra Nova Bay in Antarctica during November and December 2000. *J Geophys Res*, 107(D23):4722.

Temme, C., Einax, J., Ebinghaus, R., and Schroeder, W. (2003). Measurements of atmospheric mercury species at a coastal site in the Antarctic and over the South Atlantic Ocean during polar summer. *Environ Sci Technol*, 37(1):22–31.

Tossell, J. (2003). Calculation of the energetics for oxidation of gas-phase elemental Hg by Br and BrO. *J Phys Chem A*, 107(39):7804–7808.

Van Roozendael, M., Wagner, T., Richter, A., Pundt, I., Arlander, D., Burrows, J., Chipperfield, M., Fayt, C., Johnston, P., Lambert, J., Kreher, K., Pfeilsticker, K., Platt, U., Pommereau, J., Sinnhuber, B., Tornkvist, K., and Wittrock, F. (2002). Intercomparison of BrO measurements from ERS-2 GOME, ground-based and balloon platforms. *Advances in Space Research*, 29:1661–1666.

von Glasow, R., Sander, R., Bott, A., and Crutzen, P. (2002). Modeling halogen chemistry in the marine boundary layer - 1. cloud-free MBL. *J Geophys Res*, 107(D17):4341.

von Glasow, R., von Kuhlmann, R., Lawrence, M., Platt, U., and Crutzen, P. (2004). Impact of reactive bromine chemistry in the troposphere. *Atmos Chem Phys*, 4:2481–2497.

Yang, X., Cox, R., Warwick, N., Pyle, J., Carver, G., O'Connor, F., and Savage, N. (2005). Tropospheric bromine chemistry and its impacts on ozone: A model study. *J Geophys Res*, 110(D23):D23311.

Chapter 3

Sources and deposition of reactive gaseous mercury in the marine atmosphere

Abstract

Observations of reactive gaseous mercury (RGM) in marine air show a consistent diurnal cycle with minimum at night, rapid increase at sunrise, maximum at midday, and rapid decline in afternoon. We use a box model for the marine boundary layer (MBL) to interpret these observations in terms of RGM sources and sinks. The morning rise and midday maximum are consistent with oxidation of elemental mercury (Hg^0) by Br atoms, requiring < 2 ppt BrO in most conditions. Oxidation of Hg^0 by Br accounts for 35–60% of the RGM source in our model MBL, with most of the remainder contributed by oxidation of Hg^0 by ozone (5–20%) and entrainment of RGM-rich air from the free troposphere (25–40%). Oxidation of Hg^0 by Cl is minor (3–7%), and oxidation by OH cannot reproduce the observed RGM diurnal cycle, suggesting that it is unimportant. Fitting the RGM observations could be achieved in the model without oxidation of Hg^0 by ozone (leaving Br as the only significant oxidant) by increasing the entrainment flux from the free troposphere. The large relative diurnal amplitude of RGM concentrations implies rapid loss with a lifetime of only a few hours. We show that this can be quantitatively explained by rapid, mass-transfer-limited uptake of RGM into sea-salt aerosols as $HgCl_3^-$ and $HgCl_4^{2-}$. Our results suggest that 80–95% of Hg^{II} in the MBL should be present in sea-salt aerosol rather than gas-phase, and that deposition of sea-salt aerosols is the major pathway delivering Hg^{II} to the ocean.

3.1 Introduction

Atmospheric deposition is the principal source of mercury to the ocean (Lindberg et al., 2007). Human industry has increased this source by about a factor of three relative to natural conditions (Mason and Sheu, 2002), resulting in a corresponding increase in the surface ocean pool and raising concerns about mercury accumulation in marine biota (Mergler et al., 2007). Mercury is emitted to the atmosphere mainly as elemental mercury (Hg^0) and is oxidized within the atmosphere to Hg^{II}, which is highly water-soluble and the major depositing form (Lindberg et al., 2007). A critical step towards understanding the deposition of mercury to the ocean is quantifying the supply of Hg^{II} to the atmospheric marine boundary layer (MBL), which extends about 1 km above the ocean surface and is in turbulent contact with it. We apply here a box model for the MBL to analyze several recent data sets of reactive gaseous mercury (RGM, representing gaseous Hg^{II}) over the North Atlantic and Pacific Oceans (Laurier et al., 2003; Jaffe et al., 2005; Laurier and Mason, 2007), in order to better understand the Hg^{II} budget in the MBL and the implications for ocean uptake.

Mercury has an atmospheric lifetime of 0.5-1 years, enabling transport on a global scale (Lindberg et al., 2007). Oxidation of Hg^0 must be photochemical, as evidenced by the observed seasonal cycle of Hg^0 (Selin et al., 2007) and by the diurnal cycle of RGM (Laurier and Mason, 2007). But it is still unclear which oxidants dominate. Standard models assume gas-phase OH and ozone to be the main oxidants (Shia et al., 1999; Petersen et al., 2001; Cohen et al., 2004; Lin et al., 2006; Seigneur et al., 2006; Selin et al., 2007; Sillman et al., 2007). However, recent thermodynamic and kinetic analyses suggest that

these reactions are extremely slow in the atmosphere (Calvert and Lindberg, 2005; Hynes et al., 2008). Gas-phase oxidation by Br atoms is known to cause rapid loss of Hg^0 in the Arctic boundary layer in spring, an environment with particularly active bromine chemistry (Goodsite et al., 2004; Brooks et al., 2006; Tackett et al., 2007). Holmes et al. (2006) suggested that Br atoms in the free troposphere (above the boundary layer) could provide the main global sink of Hg^0.

Mercury-bromine chemistry could also be active within the MBL at low and middle latitudes. Mason and Sheu (2002) proposed that 40% of Hg^0 emitted from the ocean is oxidized within the MBL and deposited back; they implicated halogen oxidants but did not offer a specific mechanism. A direct test of Hg-halogen chemistry at a midlatitude coastal site by simultaneous BrO and RGM measurements was inconclusive due to the high BrO detection limit (2 pptv) (Keene et al., 2007; Laurier and Mason, 2007), but Br could still be important as a Hg^0 oxidant at lower BrO concentrations, as demonstrated below. Hedgecock et al. (2003; 2004; 2005; 2006) showed that a box model for the MBL with atomic Br released from sea-salt aerosols could reproduce the mean concentrations and diurnal amplitudes of RGM observed over the Mediterranean Sea. However, the Hg+Br reaction kinetics that they used (Ariya et al., 2002) seem too fast in light of recent data (Goodsite et al., 2004; Balabanov et al., 2005; Donohoue et al., 2006; Ariya et al., 2008). As a result, their model required a diurnal cycle in marine Hg^0 emission to balance oxidation and thus account for the observed lack of diurnal variation in atmospheric Hg^0 concentrations (Hedgecock and Pirrone, 2004). A diurnal cycle of Hg^0 emission is difficult to justify, even

with photoreduction of Hg^{II} in surface water, because the gaseous ventilation time of the marine photic zone is 1 month (Strode et al., 2007). We will show that these shortcomings can be corrected while preserving Hedgecocks central result that Br is a major Hg^0 oxidant in the MBL.

3.2 Observed RGM diurnal variability

We analyze reactive gaseous mercury (RGM) data from cruises in the remote Atlantic (Laurier and Mason, 2007) and Pacific Oceans (Laurier et al., 2003), and from coastal measurements in Okinawa, Japan (Jaffe et al., 2005). RGM is the measured gas-phase component of Hg^{II}, collected here using a KCl denuder (Landis et al., 2002). The Pacific data were collected between Osaka, Japan and Honolulu, Hawaii over 20 days during May – June 2002. We separated the midlatitude and subtropical data at 27 °N based on a sharp rise in water and air temperatures. The Atlantic data were collected in subtropical waters between Bermuda and Barbados over 11 days during August – September 2003. In both data sets the RGM concentrations are 2-h averages and the detection limit for individual measurements is 3 pg m^{-3}. We removed data contaminated by the ships exhaust, which occurred on only one day during the Pacific cruise. The ships also measured Hg^0, O_3, and CO concentrations in addition to standard oceanographic and meteorological variables. Laurier et al. (2003) and Laurier and Mason (2007) provide further details on the cruise tracks and sampling methods.

The Okinawa data span 40 days during March – May 2004. They were collected at the

northern tip of the island (26.8 °N, 128.2 °E, 60 m a.s.l.) with prevailing onshore flow. The site has minimal impact from anthropogenic sources on the island. Averaging times for the measurements were 5 minutes for Hg^0 and 3 hours for RGM and particulate mercury (radii $< 1.3\mu$m). The RGM detection limit for individual measurements is 1 pg m^{-3}. Hg^0 at Okinawa is strongly correlated with CO, indicating an East Asian industrial origin, but RGM is not (Jaffe et al., 2005; Strode et al., 2008). We discard 5 days of observations with the greatest pollution transport from continental Asia.

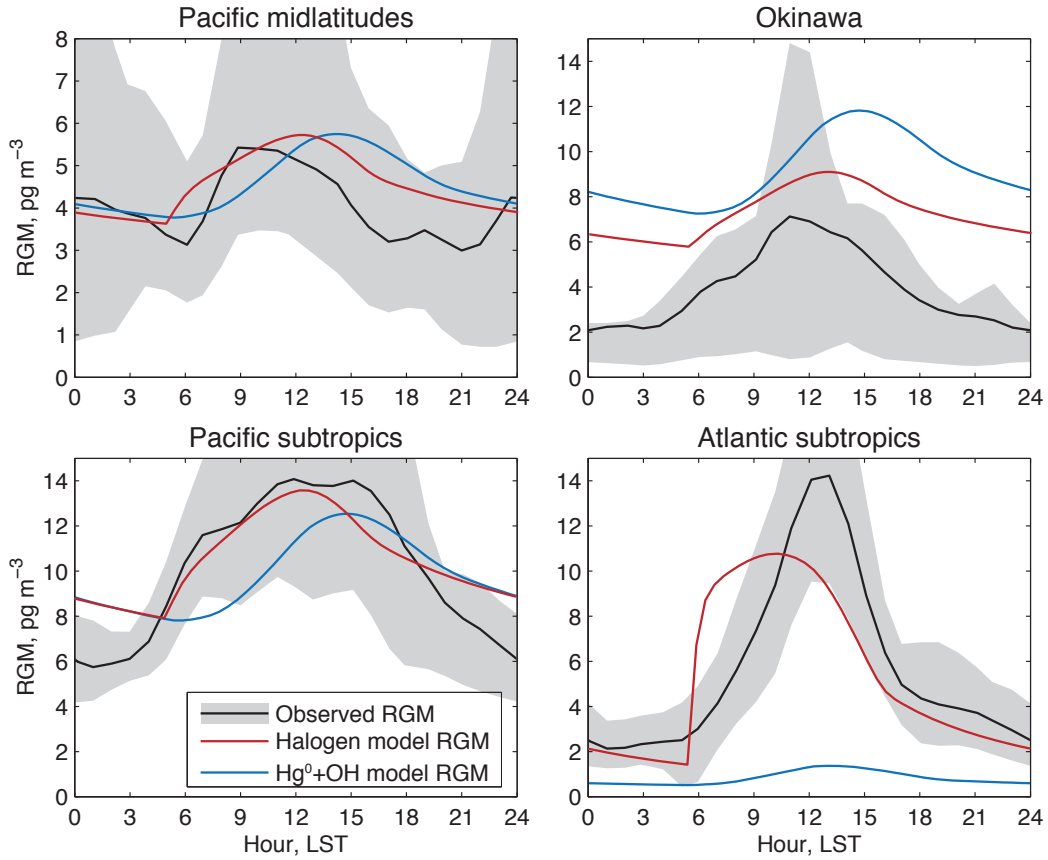

Figure 3.1: Mean diurnal cycles of reactive gaseous mercury (RGM) observed in the MBL (black line), with shaded areas showing the interquartile range of observations. The red line shows the steady state simulation of RGM in the base model with Hg^0 oxidation initiated by Br, Cl and O_3 as specified in Figure 3.3 and Table 3.1. The blue line shows RGM simulated with Hg^0 oxidation initiated by OH and O_3. Notice different scale in top left panel

The dominant feature of RGM temporal variability is its diurnal cycle, as shown in Figure 3.1. The diurnal cycle is statistically significant ($p \leq 0.05$ from Kruskal-Wallis test of constant mean) at Okinawa and in the subtropical Atlantic and Pacific data, but is much weaker and does not reach statistical significance in the midlatitude Pacific data ($p = 0.2$). RGM increases rapidly at sunrise, peaks at midday, declines through the afternoon, and falls near detection limit at night. Neither deposition nor boundary layer growth can drive this diurnal cycle, since the winds and MBL depth have little diurnal variability (Hignett, 1991). Rather, RGM production due to changing oxidant levels must be responsible. Although the amplitude of the RGM diurnal cycle varies between the data sets in Figure 3.1, the consistent shape and phase argues for a common driving mechanism.

The RGM increase at sunrise suggests a photochemical oxidant produced by photolysis of weakly-bound nighttime reservoirs. Br and Cl can exhibit this behavior (von Glasow et al., 2002). By contrast, OH in the MBL increases only slowly after sunrise and peaks at midday (Nowak et al., 2001). Selin et al. (2007) previously noted that Hg^0 oxidation by OH yields an afternoon peak of RGM delayed by several hours relative to the observations at Okinawa. In contrast to RGM, the Hg^0 concentrations in all data sets show no significant diurnal cycle, which places an upper bound on the Hg^0 oxidation rate. Given 10% measurement uncertainty for Hg^0 (Jaffe et al., 2005), daytime oxidation must be less than 3–5% d^{-1} or 4–8 pg m^{-3} h^{-1}.

The relative diurnal amplitude of RGM, expressed as the difference between maximum and minimum concentrations divided by the 24-hour mean, ranges from 1 to 3 depending

on the data set. Concentrations decrease by 40–70% over the 12-18 Local Solar Time (LST) period, implying a lifetime of a few hours at most. Nighttime RGM observations tend to decrease as wind speed increases (Figure 3.2), suggesting a fast deposition sink rather than chemical loss. Hedgecock and Pirrone (2001) and Selin et al. (2007) previously speculated that uptake by sea-salt aerosols might provide such a fast deposition sink, and we provide further mechanistic support for this hypothesis below.

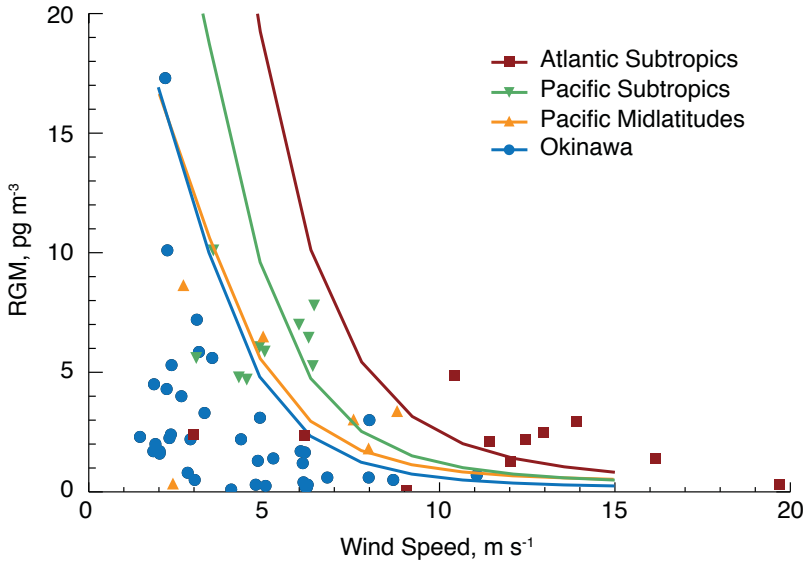

Figure 3.2: Nighttime RGM concentrations (0–5 LST) vs. wind speed. Symbols show observed means for individual days. Lines show the relationship predicted by the box model for each data set by varying wind speed while holding other parameters constant.

3.3 Model description

We interpret the observed diurnal cycles of RGM with a box model of the MBL applied to the different data sets of Figure 3.1. The model calculates the concentration of gaseous Hg^{II} (c, mol m^{-3}) based on chemical production and loss (P and L, mol m^{-3} s^{-1}), dry

deposition to the ocean surface (F_d, mol m^{-2} s^{-1}), entrainment at the top of the MBL (F_e, mol m^{-2} s^{-1}), and uptake by sea-salt aerosols (J, mol m^{-3} s^{-1}):

$$\frac{dc}{dt} = P - L + \frac{F_e - F_d}{Z} - J \tag{3.1}$$

where Z is the MBL depth. Downward fluxes are positive. For comparison with observations we assume that all gas-phase Hg^{II} species are measured as RGM.

Table 3.1 summarizes the model parameters, which are taken from measurements when available. Other parameters are typical MBL values, which suffice to compare proposed alternative Hg^{II} formation and loss pathways against RGM data. We choose the concentrations of Br and free-tropospheric RGM to best match the amplitude and mean of the RGM diurnal cycle in each data set, as described below, then evaluate these concentrations against the few available measurements.

Table 3.1: Marine boundary layer box model parameters

Parameter	Region			
	Okinawa	Pacific mid-latitudes	Pacific subtropics	Atlantic subtropics
Measured[a]				
$[Hg^0]$, ng m^{-3}	2.0	2.5	2.5	1.6
$[O_3]$, ppb	31	35	10	13
Temperature, K	294	283	298	301
10-m wind speed, m s^{-1}	4.4	5.9	5.1	11.2
Relative humidity, %	80	77	84	75
Derived[b]				
v_d, cm s^{-1}	0.38	0.56	0.46	1.4
$[Cl^-]$, M	4.5	5.1	3.8	5.4
H, M atm^{-1}	2.6×10^9	3.2×10^9	1.8×10^9	3.7×10^9
$L, m^3_{water}\ m^{-3}_{air}$	8.3×10^{-11}	1.6×10^{-10}	1.3×10^{-10}	5.3×10^{-10}
$F_V, m^3_{water}\ m^{-2}_{ocean}\ s^{-1}$	3.6×10^{-13}	1.1×10^{-12}	7.1×10^{-13}	8.8×10^{-12}
Hg^0 lifetime, d	120	140	90	10
RGM lifetime, h	8.1	3.8	6.7	0.7
Other[c]				
v_e, cm s^{-1}	0.5	0.5	0.5	0.5
Z, m	750	750	750	750
$[Br], cm^{-3}$	4.3×10^5	2.0×10^5	8.7×10^5	4.3×10^6
$[Cl], cm^{-3}$	1.5×10^4	1.5×10^4	1.5×10^4	1.5×10^4
$[OH], cm^{-3}$	1.1×10^6	6.3×10^5	1.2×10^6	1.1×10^6
c_{FT}, pg m^{-3}	10	20	20	20

[a] Means over the observation period

[b] We display H in conventional units here, so one should multiple this by 24 atm M^{-1} to obtain the dimensionless form used in Equation 3.9. F_V is the volumetric production flux of sea-salt aerosols from the ocean surface. Lifetimes are calculated with the 24-h mean fluxes in Figure 3.4. the RGM lifetime accounts for ventilation, while the Hg^0lifetime includes only chemical loss in the MBL. Other derived parameters are calculated from the measurements with the equations in Section 3.3.

[c] Other parameters are from literature and models as described in Section 3.3. [Br], [Cl], and [OH] are 24-h means which multiply the relative amplitudes in Figure 3.3.

Table 3.2 lists the kinetic data used to calculate P and L. Oxidation to Hg^{II} by halogen atoms and OH proceeds in two addition reactions, in competition with thermal dissociation of the intermediate HgX (X ≡ Br,Cl, OH). We neglect oxidation initiated by OH in our reference model due to the instability of HgOH under atmospheric conditions (Goodsite et al., 2004; Calvert and Lindberg, 2005; Hynes et al., 2008), but we include it in a sensitivity test.

The entrainment flux at the top of the boundary layer is the product of an assumed entrainment velocity v_e = 0.5 cm s^{-1} (Faloona et al., 2005) and the concentration difference between the MBL and the free troposphere (c_{FT}):

$$F_e = v_e \left(c_{FT} - c\right) \tag{3.2}$$

The dry deposition flux is calculated by applying a deposition velocity (v_d) to the RGM concentration:

$$F_d = v_d c. \tag{3.3}$$

Due to the high solubility of Hg^{II} species in water (Table 3.2), v_d is limited by aerodynamic resistance. For neutrally stable conditions typical of the marine atmosphere,

$$v_d(z) = \frac{k u_*}{\ln(z/z_0)} \tag{3.4}$$

where k = 0.4 is the von Kármán constant (Seinfeld and Pandis, 2006). Most aerodynamic resistance to deposition occurs in the lowest few meters, so we use a reference height z =

Table 3.2: Chemical reactions and equilibria in the MBL box model

Reaction or equilibrium[a]	Rate or equilibrium coefficient[b]	Reference[c]
$Hg^0 + O_3 \rightarrow HgO + O_2$[d]	3.0×10^{-20}	(1)
$Hg^0 + Br \xrightarrow{M} HgBr$	$1.1 \times 10^{-12}(T/298)^{-2.37}$	(2)
$HgBr \xrightarrow{M} Hg^0 + Br$	$1.2 \times 10^{10} \exp(-8357/T)$	(2)
$HgBr + Br \xrightarrow{M} HgBr_2$	$2.5 \times 10^{-10}(T/298)^{-0.57}$	(2)
$HgBr + OH \xrightarrow{M} HgBrOH$	$2.5 \times 10^{-10}(T/298)^{-0.57}$	(2)
$HgBr + Br \rightarrow Hg^0 + Br_2$	3.9×10^{-11}	(3)
$Hg^0 + Cl \xrightarrow{Y,M} HgClY$[e]	$2.2 \times 10^{-32} \exp(680(1/T - 1/298))[M]$	(4)
$HgCl_2 \leftrightarrow HgCl_{2(aq)}$[f]	1.4×10^6 M atm^{-1}	(5)
$HgCl_{2(aq)} + Cl^- \leftrightarrow HgCl^-_{3(aq)}$	6.7 M^{-1}	(6)
$HgCl^-_{3(aq)} + Cl^- \leftrightarrow HgCl^{2-}_{4(aq)}$	13 M^{-1}	(6)
$Hg^0 + OH \rightarrow Hg^{II}$	0	g

[a] Species are gas-phase except where (aq) indicates aqueous-phase.

[b] Rate coefficients are in units of cm^3 molecule^{-1} s^{-1} or s^{-1}. Equilibrium coefficients are in units of M atm^{-1} or M^{-1}, as indicated. T is temperature in K. [M] is the number density of air in molecules cm^{-3}.

[c] (1) Hall (1995); (2) Goodsite et al. (2004); (3) Balabanov et al. (2005); (4) Donohoue et al. (2005); (5) Lindqvist and Rodhe (1985); (6) Clever et al. (1985)

[d] The mechanism and products of this reaction are poorly understood, and the reaction might be insignificant under atmospheric conditions (Calvert and Lindberg, 2005; Hynes et al., 2008). In our standard simulation, we assume a gas-phase HgO product with the same solubility as $HgCl_2$. Suppression of this reaction in the model can be accommodated by increasing the entrainment flux from the free troposphere as discussed in Section 3.4.

[e] Assumed to be limited by the rate of HgCl formation, with Y representing a radical oxidant (Y ≡ Cl, Br, OH) that subsequently adds to HgCl to form stable Hg^{II}. The dissociation rate coefficient of HgCl, k_{-1}, can be estimated from $\Delta G = -RT \ln(k_1/k_{-1})$ where ΔG = -80.3 kJ mol^{-1} is the Gibbs free energy of HgCl (Linstrom and Mallard, 2005), R = 8.3 J K^{-1} mol^{-1} is the ideal gas constant and k_1 is the rate coefficient for $Hg^0 + Cl \xrightarrow{M} HgCl$ (from the table above). We find a dissociation rate $k_{-1} = 10^{-10}$ s^{-1} for HgCl, which is negligibly slow.

[f] We assume the same solubility for all HgXY species (X, Y ≡ Cl, Br, OH). In clouds and marine aerosols, $HgXY_{(aq)}$ converts to $HgCl_2$ due to the abundance of Cl^- (Hedgecock and Pirrone, 2001).

[g] We use a rate coefficient of 9×10^{-14} cm^3 molecule^{-1} s^{-1} (Pal and Ariya, 2004) in a sensitivity simulation (see Section 3.4).

10 m at which wind speeds were measured. The roughness length (z_0) and friction velocity (u_*) are calculated from the observed wind speed at 10 m ($u(z)$) by iteratively solving the system of equations (Stull, 1988, p. 377, 381):

$$z_0 = \alpha_C \frac{u_*^2}{g} \tag{3.5}$$

$$u_* = \frac{k\,u(z)}{\ln(z/z_0)} \tag{3.6}$$

where $\alpha_C = 0.016$ is the Charnock constant and $g = 9.8$ m s^{-2} is the gravitational acceleration.

We find v_d = 0.4–1.4 cm s^{-1} for the different data sets (Table 3.1). Combined with a typical MBL depth Z = 750 m, these deposition rates imply a RGM lifetime of 15–50 h against dry deposition. This is too slow to explain the rapid decrease observed in the afternoon and evening hours (Figure 3.1). A more important pathway for RGM loss may be uptake by sea-salt aerosols followed by aerosol deposition. We assume that all Hg^{II} species have the same solubility as $HgCl_2$. Once dissolved in aqueous aerosols or cloud droplets, Hg^{II} species convert to $HgCl_2$ due to the abundance of Cl^- (Hedgecock and Pirrone, 2001). Complexation of $HgCl_{2(aq)}$ to $HgCl_3^-$ and $HgCl_4^{2-}$ preferentially fractionates $HgCl_2$ into the sea-salt aerosol (Table 3.2) (Hedgecock and Pirrone, 2001). The equilibrium partitioning depends on the sea-salt aerosol chloride concentration, which is a function of the water

vapor saturation ratio (S):

$$\left[\mathrm{Cl}^-\right] = \frac{\rho_{\mathrm{SS}} f_{\mathrm{Cl}}}{M_{\mathrm{Cl}}} \left(\frac{1-S}{2-S}\right) \left(\frac{3.7}{4}\right)^3, \tag{3.7}$$

where M_{Cl} = 35.5 g mol^{-1} is the atomic weight of Cl, ρ_{SS} = 2200 kg m^{-3} is the density of dry sea salt, and f_{Cl} = 0.55 is the mass fraction of Cl in dry sea salt. This formula follows from an empirical expression for sea-salt aerosol growth relative to its dry radius (r_{dry}) (Lewis and Schwartz, 2006):

$$r = r_{\mathrm{dry}} \frac{4}{3.7} \left(\frac{2-S}{1-S}\right)^{1/3}. \tag{3.8}$$

The relation holds over $0.45 < S < 0.99$ which spans the range found in the MBL. For typical marine conditions of S = 0.8 and sea-salt aerosol liquid water content $L = 1 \times 10^{-10}\,\mathrm{m}^3_{\mathrm{water}}\,\mathrm{m}^{-3}_{\mathrm{air}}$, it follows that [Cl$^-$] = 4.5 M and 85% of total Hg$^{\mathrm{II}}$ is dissolved in sea-salt aerosol at equilibrium.

Because of the short sea-salt aerosol lifetime, one cannot assume RGM to be in equilibrium with the aerosol; RGM uptake is in fact limited by mass transfer. We find that this limitation slows down RGM loss by a factor of 1.5–3 relative to assuming equilibrium. Let c_a (mol m^{-3}) denote the aqueous-phase concentration of $\mathrm{Hg}^{\mathrm{II}}_{(\mathrm{aq})} \equiv \mathrm{HgCl}_{2(\mathrm{aq})} + \mathrm{HgCl}_3^- + \mathrm{HgCl}_4^{2-}$, and let H be the dimensionless effective Henrys law constant for $\mathrm{HgCl}_{2(\mathrm{aq})}$ accounting for the polychloride complexes. The net uptake of Hg$^{\mathrm{II}}$ by the aerosol is given

by

$$J = L k_{\mathrm{mt}} \left(c - \frac{c_a}{H} \right). \tag{3.9}$$

where k_{mt} is a mass transfer coefficient to the aerosol. For a monodisperse aerosol with number concentration N (m^{-3}) of particles of radius r, k_{mt} can be approximated by (Sander, 1999)

$$k_{\mathrm{mt}} = \frac{4\pi r^2}{L} \left(\frac{r}{D_g} + \frac{4}{v\alpha} \right)^{-1} N, \tag{3.10}$$

where D_g = 0.1 $\mathrm{cm}^2\ \mathrm{s}^{-1}$ is the diffusivity of RGM in air, $v = 1.5 \times 10^4$ $\mathrm{cm\ s}^{-1}$ is the mean molecular speed, and α = 0.5 is the assumed accommodation coefficient for $HgCl_2$. Results are insensitive to α in the range 0.1–1 typical of highly soluble gases.

We calculate RGM uptake by sea-salt aerosol by considering m = 5 dry aerosol size classes with radius divisions at 1, 3.2, 5.4, 7.6, 9.8, and 12 μm. Through sensitivity tests we found that smaller, submicron aerosols are insignificant sinks of RGM because of their small liquid water content while aerosols larger than 12 μm are also insignificant sinks because of their small number and short atmospheric residence time. For each size class, we calculate the number concentration by integrating over the steady-state aerosol number distribution governed by the balance between aerosol production (Lewis and Schwartz, 2004, p. 321 lognormal approximation) and loss by dry deposition (Zhang et al., 2001). For simulations over the Mediterranean Hedgecock et al. (2005) assumed fixed $L = 3 \times 10^{-11}$ $\mathrm{m}^3_{\mathrm{water}}\ \mathrm{m}^{-3}_{\mathrm{air}}$ and an aerosol residence time of 3 days. Using the wind speed from that study (3.8 $\mathrm{m\ s}^{-1}$) and S = 0.8, we obtain similar values of $L = 4.7 \times 10^{-11}$ $\mathrm{m}^3_{\mathrm{water}}\ \mathrm{m}^{-3}_{\mathrm{air}}$

and a residence time of 1.8 days averaged over all size classes. The total aerosol uptake in Equation 3.1 is a sum over the fluxes for each size class: $J = \sum_{i=1}^{m} J_i$.

In addition to Equation 3.1, the model calculates the sea-salt aerosol concentration:

$$\frac{dc_{a,i}}{dt} = \frac{J_i}{L_i} - v_{d,i}\frac{c_{a,i}}{Z}. \tag{3.11}$$

Here $c_{a,i}$, L_i, and $v_{d,i}$ are the $\mathrm{Hg}^{\mathrm{II}}_{(\mathrm{aq})}$ concentration, liquid water content, and aerosol deposition velocity for the i^{th} size class. This equation implicitly assumes that all sea-salt aerosols deposit to the ocean and none enter the free troposphere. The bulk aerosol concentration (c_a) in Equation 3.9 is the volume-weighted mean over the m size classes. We integrate the moderately-stiff system of Equations 3.1 and 3.11, using the MATLAB ode15s algorithm, for 6 days to reach diurnal steady state (i.e., identical diurnal cycles from one day to the next) and analyze the last day.

As a test of the above treatment of aerosol uptake and dry deposition, we simulated nighttime RGM under a range of wind speeds for the different data sets of Table 3.1 while holding other model parameters constant. Figure 3.2 shows consistency with the observed decline of nighttime RGM with wind speed. While both dry deposition and sea-salt aerosol uptake increase with wind speed, aerosol uptake explains proportionally more loss with faster winds. In addition to wind speed, relative humidity also affects uptake, but the present data sets all have humidities near 80%. Uptake is strongest at low relative humidity when the chloride concentration is greatest, despite the lesser aerosol liquid water content.

Figure 3.3 shows the assumed relative diurnal profiles of Br, Cl and OH while Table 3.1 gives the 24-h mean concentrations. OH concentrations are monthly mean values from the GEOS-Chem model (Park et al., 2004). For Cl we assume a 24-h mean concentration of 1.5×10^4 atoms cm^{-3}, typical of values previously inferred for the MBL (Singh et al., 1996; Wingenter et al., 2005); this makes Cl only a minor oxidant of Hg^0, as discussed below. For Br we adjust the 24-h concentration to best match the RGM diurnal amplitude, then calculate the associated BrO concentration from photochemical steady state (Platt and Janssen, 1995). We find daytime mean concentrations 0.6–1.2 ppt BrO are sufficient to explain the diurnal cycle in most conditions but we need to assume higher Br concentrations for the Atlantic, corresponding to 5.2 ppt BrO, and this is discussed below.

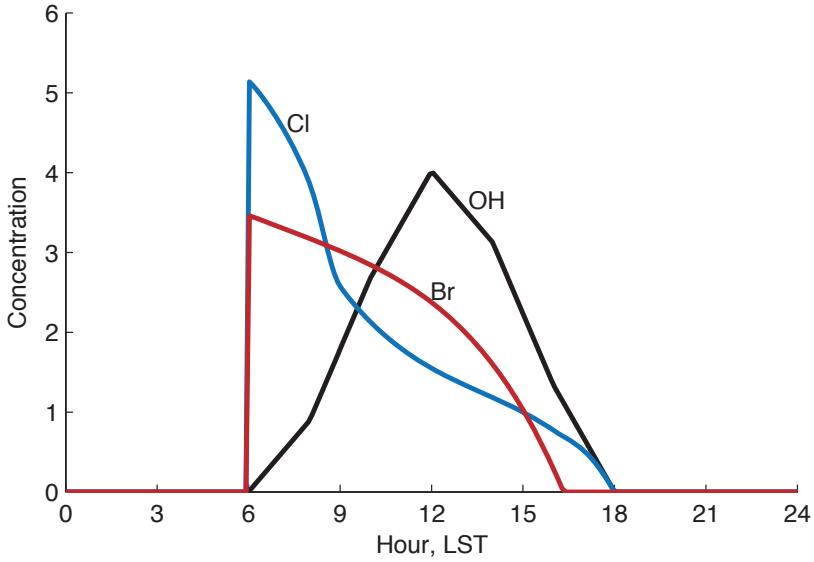

Figure 3.3: Diurnal profiles of MBL oxidants normalized to a 24-h mean of 1. [OH] (black) from Brasseur et al. (1999); [Br] (red) and [Cl] (blue) from Pszenny et al. (2004). Table 3.1 gives the 24-h model mean concentrations of oxidants for each data set.

Observations of RGM concentrations at mountain sites and from aircraft show an increase from the boundary layer to the free troposphere (Swartzendruber et al., 2006; Sill-

man et al., 2007). An implication is that entrainment from above could be a significant source of RGM to the MBL. The GEOS-Chem global simulation (Selin et al., 2007) gives Hg^{II} concentrations (RGM + particulate Hg^{II}) in the range 20–50 pg m^{-3} in the lower free troposphere over the regions examined here. If all of that Hg^{II} were RGM our model would overestimate mean MBL RGM concentrations as well as underestimate the relative amplitudes of diurnal cycles. We find a better match in our box model by entraining free tropospheric RGM concentrations in the range 10–20 pg m^{-3} as given in Table 3.1. These values are within the wide range of the few free tropospheric observations (Swartzendruber et al., 2006; Sillman et al., 2007), and could be accommodated in the GEOS-Chem model if half of Hg^{II} were in particulate form.

3.4 Model RGM diurnal cycles and budget

Figure 3.1 shows simulations of RGM for each observed region. The model reproduces major features of all RGM data sets: nighttime minimum, early morning rise, and midday peak before 13 LST. The peak-to-peak diurnal amplitudes in the model are 0.4–3.5 times the 24-h mean, as compared to 1–3 in the field data, indicating that the model RGM lifetime is consistent with observations. The consistency in 24-h mean concentrations reflects the choice of entrained RGM concentration (Section 3.3). At Okinawa, the simulated mean exceeds measurements by a factor of 2. Since less entrainment would imply decreasing RGM with altitude and the relative diurnal cycle is underestimated by a factor of 2, we believe that the RGM sinks are underestimated. Sea-salt aerosols generated in the surf

zone may explain the discrepancy.

We find that the RGM observations are most consistent with $2-9\times10^5$ atoms Br cm^{-3} (24-h mean) over the midlatitude and subtropical Pacific and at Okinawa (Table 3.1). Using photochemical steady state equations and O_3 measurements, the corresponding peak BrO concentrations are 0.6 ppt in the Pacific midlatitudes, 0.8 ppt in the Pacific subtropics, and 1.2 ppt at Okinawa. These are within the large range of BrO observations in the MBL and consistent with higher BrO in coastal zones (Leser et al., 2003).

Simulations of the Atlantic data reproduce the relative diurnal amplitude (3.5 in the model vs. 3 in observations) but the maximum is too early in the day. Matching the diurnal amplitude requires 4.3×10^6 atoms Br cm^{-3} (24-h mean), corresponding to 5.2 ppt BrO at sunrise. While there are few observations exceeding 2 ppt BrO in the remote MBL (Leser et al., 2003), the strong winds of the Atlantic cruise should have generated abundant sea-salt aerosols that might support such high Br levels. The strong winds also shorten the RGM lifetime to under 1 hour (Table 3.1), so that the RGM diurnal cycle follows that of its Br-driven source (Figure 3.3). This implies in turn a Hg^0 loss of 0.15 ng m^{-3} d^{-1} which should induce a diurnal cycle in Hg^0 concentrations but the observations show no such cycle. The high-wind conditions of the Atlantic cruise may challenge the steady-state assumption used in the model.

Sea-salt aerosols contain 80-90% of the total MBL Hg^{II} in the model. That is 25–45 pg Hg^{II} m^{-3} under most conditions. The simulation of the Atlantic data has up to 100 pg Hg^{II} m^{-3} or 95% of Hg^{II} in aerosols. These values compare well with measurements of

5–40 pg Hg^{II} m^{-3} (mean 20 pg m^{-3}) in coarse marine aerosol in Florida (Malcolm et al., 2003). Measurements in Alabama found somewhat lower values, 13 pg Hg^{II} m^{-3}, in total aerosol samples from airmasses originating over the Gulf of Mexico (Engle et al., 2008). Jaffe et al. (2005) reported only 3 pg m^{-3} of particulate Hg from the Okinawa site but their instrument excluded coarse aerosols and hence most sea-salt aerosol mass.

Figure 3.4 gives steady-state 24-h average budgets of RGM sources and sinks in the model MBL for the Pacific and Okinawa cases. We do not present the Atlantic case because the model does not fit these observations well. From Figure 3.4 we see that Hg^0+Br is the largest source of RGM, supplying 35–60%. Subsidence from the free troposphere is the next largest budget term, accounting for 25–40% of RGM in the MBL. Hg^0+O_3 provides most of the remaining chemical source (5–20%). Hg^0+Cl plays a minor role (3–7%), but it could be larger if Hg^0+Cl kinetics are faster than assumed or if Cl concentrations are greater; this would imply a somewhat smaller contribution from Hg^0+Br.

One the sink side, 80–90% of MBL RGM enters the ocean. Uptake into sea-salt aerosols and their subsequent deposition contributes 65–80% of the total RGM loss for the Pacific cruise and Okinawa, while direct dry deposition of RGM contributes 10–15%. For the higher wind speeds that were observed in the Atlantic subtropics, the fraction of RGM lost through sea-salt aerosols rises to 90%. The RGM lifetimes range from 50 min (Atlantic subtropics) to 8 h (Okinawa).

Ventilation to the free troposphere provides a sink for 10–20% of RGM in the MBL, partly compensating for entrainment. An entrainment velocity of 0.5 cm s^{-1} at the top of

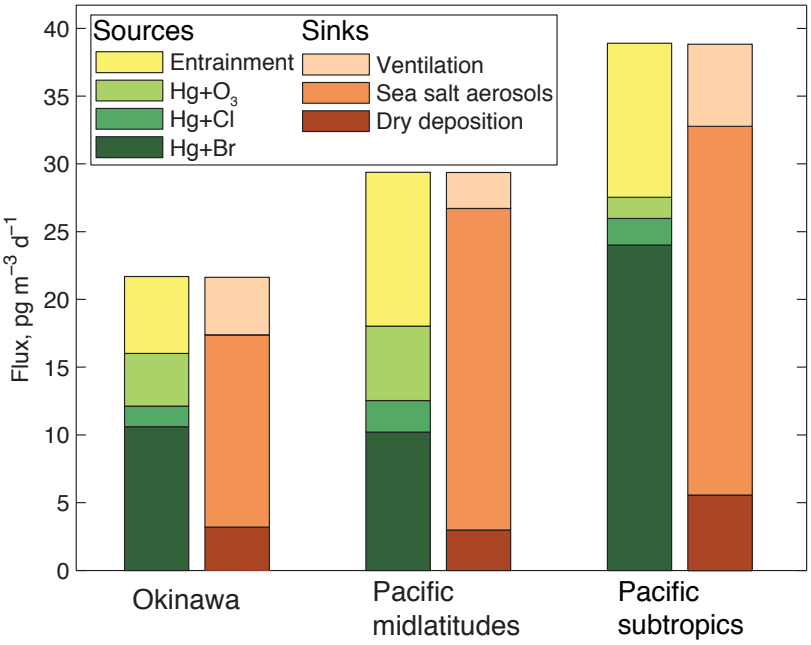

Figure 3.4: Model budgets of RGM sources and sinks in the marine boundary layer. Values are 24-h averages at steady state.

a 750 m thick boundary layer gives a 40 h residence time for air in the MBL. Combined with the ∼100 d chemical lifetime of Hg^0 under most conditions, this implies that no more than 3% of Hg^0 emitted into the MBL is oxidized before escaping to the free troposphere above. A corollary is that most of the Hg^{II} formed within the MBL has passed through the free troposphere as Hg^0. Mercury deposition to the ocean is thus mainly derived from the global mercury pool, rather than from marine emissions in a closed MBL cycle.

The total chemical production of RGM in the model is 15–28 pg m^{-3} d^{-1}, excluding the Atlantic. This is less than 2% loss of Hg^0 per day and below the 4–8 pg m^{-3} h^{-1} limit which would produce an observable diurnal cycle. Thus our model is consistent with the observed absence of diurnal Hg^0 variation without invoking a daytime Hg^0 source to compensate for the photochemical Hg^0 sink.

As mentioned in the Introduction, there are large uncertainties regarding gas-phase Hg chemistry, with most previous studies assuming OH and O_3 to be the major Hg^0 oxidants. Figure 3.1 shows the diurnal cycle of RGM that would result from a fast Hg^0+OH reaction (Pal and Ariya, 2004) plus Hg^0+O_3 and without Hg+halogen reactions. In this model RGM rises significantly only after 9 LST, due to the slow morning rise of OH (Nowak et al., 2001). In contrast, RGM simulated with halogen oxidants increases at sunrise, as it does in the observations. The RGM peak due to Hg^0+OH (14–15 LST) is delayed several hours relative to the observations and base simulation. Only when the apparent RGM lifetime is $\sim$1 h or less, as in the subtropical Atlantic data, is the Hg^0+OH reaction consistent with the observed time of peak RGM. But reproducing the observed diurnal amplitude in the Atlantic data with the Hg^0+OH reaction still requires large additional photochemical RGM sources. Due to the deficiencies in the Atlantic simulation with oxidation by either OH or Br (described above), the Atlantic data alone do not resolve the major oxidant. Nevertheless, the majority of available RGM data are more consistent with Hg^0 oxidation by Br, due to the earlier onset of bromine photochemistry. These tests cannot entirely reject the Hg^0+OH reaction from a model that also includes Hg+halogen reactions, but any significant contribution from OH would cause simulated RGM concentrations to lag behind the data.

While we have included the gas-phase Hg^0+O_3 reaction (Hall, 1995) in our simulations, several investigators have challenged its mechanism or atmospheric relevance (Shepler and Peterson, 2003; Calvert and Lindberg, 2005; Hynes et al., 2008). This reaction is a small

source of MBL RGM in our model (5–20%), and it has little diurnal variability, so its contribution could be replaced with a larger entrainment flux from the free troposphere. Such an increase would in fact better fit the observed and model values of RGM concentrations in the free troposphere.

3.5 Conclusions

We have analyzed atmospheric observations of reactive gaseous mercury (RGM) from Pacific and Atlantic cruises and from Okinawa in terms of mercury chemistry and deposition in the marine atmosphere. The dominant feature of the observations is a consistent diurnal cycle of concentrations with midday maximum, nighttime minimum, sharp increase after sunrise, and sharp decrease in afternoon. The early-morning rise and midday peak implicate a RGM source from Hg^0 oxidation by halogen atoms. The relative diurnal amplitude implies a RGM lifetime of only a few hours. Nighttime RGM is anticorrelated with wind speed, pointing to a fast deposition sink. In contrast to RGM, Hg^0 shows no significant diurnal cycle in the observations.

We developed a box model for the marine boundary layer (MBL) to examine the consistency between the RGM data and current understanding of RGM sources and sinks, assuming that all gas-phase Hg^{II} species are measured as RGM. After choosing concentrations of Br and free-tropospheric RGM within observational constraints to best match the amplitude and mean of the RGM diurnal cycle, we find that the observed cycle is consistent with a major RGM source from oxidation of Hg^0 by Br atoms. The implied MBL

BrO concentrations are in the range 0.6–1.2 ppt, consistent with available data, although simulation of the Altantic cruise data requires 5 ppt BrO. Oxidation of Hg^0 by Cl atoms and ozone is much smaller. A sensitivity simulation with Hg^0 oxidation mainly by OH generates a later rise and peak of RGM than observations, suggesting that the reaction is unimportant. The dominance of Br as a Hg^0 oxidant in the MBL was previously reported in box model calculations by Hedgecock et al. (2004; 2005), using older kinetic data for the Hg^0+Br reaction (Ariya et al., 2002) that implied much faster oxidation than the more recent data used here (Goodsite et al., 2004). This resulted in daytime Hg^0 depletion inconsistent with observations unless a compensating diurnal cycle in oceanic emission was assumed. The slower rates used here yield a Hg^0 lifetime $\sim$100 d in the MBL, consistent with the observed lack of Hg^0 diurnal variation.

Loss of RGM by dry deposition is too slow to account for the rapid decrease of RGM observed in the afternoon and evening hours. We find instead that the major loss pathway for RGM is uptake into sea-salt aerosols followed by aerosol deposition. We calculate the uptake rate with a physical mechanism accounting for sea-spray emission, aerosol deposition, aerosol hygroscopic growth and associated changes in concentration, and mass-transfer limitation. High concentrations present in sea-salt aerosols favor and complexes and enhance Hg^{II} solubility. Our model thus predicts that $>$80% of MBL Hg^{II} is present as sea-salt aerosol rather than RGM. The associated sea-salt aerosol concentrations of Hg^{II} are 25–45 pg m^{-3}, consistent with the few observations available. Uptake by sea-salt aerosols accounts for 65–80% of RGM loss from the MBL in our simulation, and enables us to

generally reproduce the observed phase and diurnal amplitude of the RGM observations. Considering direct dry deposition as well, 80–90% of RGM in the MBL deposits to the ocean.

We calculate a $\sim$100 d lifetime for Hg^0 in the MBL against oxidation to Hg^{II} in most conditions. Since ventilation of the MBL to the free troposphere takes place on a time scale $\sim$ 1 d, the long Hg^0 lifetime implies that Hg^0 emitted from the ocean is ventilated to the free troposphere rather than oxidized in the MBL and returned to the ocean in a closed system. A corollary is that RGM formed and deposited within the MBL derives primarily from Hg^0 transported in the free troposphere over long distances in the global mercury cycle.

Entrainment of RGM from the free troposphere in our model accounts for 25–40% of RGM in the MBL, second in importance to Hg^0 oxidation by Br atoms. Selin et al. (2008) previously proposed that subtropical subsidence of high-Hg^{II} air would be a major contributor to oceanic deposition of mercury. It provides a steady source of RGM to the MBL that our model requires to account for the observed magnitude of MBL concentrations and their relative diurnal amplitude. It is also consistent with the few RGM observations in the lower free troposphere.

Several key parameters and processes in our understanding of MBL mercury cycling have large uncertainties that require further study. Perhaps most important are measurements of BrO in the MBL with sub-ppt sensitivity, to test the hypothesis that Br is the dominant Hg^0 oxidant. Mercury observations under intermediate winds (6–10 m s^{-1}) are also necessary in light of our poor understanding of the RGM diurnal profile shape under

strong winds. Vertical profiles of Hg^{II} from the sea surface to the free troposphere, especially in the subtropical subsidence zones, would better constrain entrainment. Finally, concentrations in sea-salt aerosols should be measured to test the hypothesis that sea-salt aerosol deposition is the dominant pathway for mercury deposition to the ocean.

Bibliography

Ariya, P. A., Khalizov, A., and Gidas, A. (2002). Reactions of gaseous mercury with atomic and molecular halogens: Kinetics, product studies, and atmospheric implications. *J Phys Chem A*, 106(32):7310–7320.

Ariya, P. A., Skov, H., Grage, M. M. L., and Goodsite, M. E. (2008). Gaseous elemental mercury in the ambient atmosphere: Review of the application of theoretical calculations and experimental studies for determination of reaction coefficients and mechanisms with halogens and other reactants. *Adv Quantum Chem*, 55:43–55.

Balabanov, N., Shepler, B., and Peterson, K. (2005). Accurate global potential energy surface and reaction dynamics for the ground state of HgBr2. *J Phys Chem A*, 109(39):8765–8773.

Brasseur, G., Orlando, J., and Tyndall, G. (1999). *Atmospheric Chemistry and Global Change*. Oxford University Press.

Brooks, S., Saiz-Lopez, A., Skov, H., Lindberg, S., Plane, J., and Goodsite, M. (2006). The mass balance of mercury in the springtime Arctic environment. *Geophys Res Lett*, 33(13):L13812.

Calvert, J. and Lindberg, S. (2005). Mechanisms of mercury removal by O-3 and OH in the atmosphere. *Atmos Environ*, 39(18):3355–3367.

Clever, H., Johnson, S., and Derrick, M. (1985). The solubility of mercury and some sparingly soluble mercury salts in water and aqueous-electrolyte solutions. *Journal of Physical and Chemical Reference Data*, 14(3):631–681.

Cohen, M., Artz, R., Draxler, R., Miller, P., Poissant, L., Niemi, D., Ratte, D., Deslauriers, M., Duval, R., Laurin, R., Slotnick, J., Nettesheim, T., and McDonald, J. (2004). Modeling the atmospheric transport and deposition of mercury to the Great Lakes. *Environmental Research*, 95(3):247–265.

Donohoue, D., Bauer, D., Cossairt, B., and Hynes, A. (2006). Temperature and pressure dependent rate coefficients for the reaction of Hg with Br and the reaction of Br with Br: A pulsed laser photolysis-pulsed laser induced fluorescence study. *J Phys Chem A*, 110(21):6623–6632.

Donohoue, D., Bauer, D., and Hynes, A. (2005). Temperature and pressure dependent rate coefficients for the reaction of Hg with Cl and the reaction of Cl with Cl: A pulsed laser photolysis-pulsed laser induced fluorescence study. *J Phys Chem A*, 109(34):7732–7741.

Engle, M., Tate, M., Krabbenhoft, D., Kolker, A., Olson, M., Edgerton, E., DeWild, J., and McPherson, A. (2008). Characterization and cycling of atmospheric mercury along the central US Gulf Coast. *Applied Geochemistry*, 23(3):419–437.

Faloona, I., Lenschow, D., Campos, T., Stevens, B., van Zanten, M., Blomquist, B., Thornton, D., Bandy, A., and Gerber, H. (2005). Observations of entrainment in eastern pacific marine stratocumulus using three conserved scalars. *J Atmos Sci*, 62(9):3268–3285.

Goodsite, M., Plane, J., and Skov, H. (2004). A theoretical study of the oxidation of Hg-0 to HgBr2 in the troposphere. *Environ Sci Technol*, 38(6):1772–1776.

Hall, B. (1995). The gas phase oxidation of elemental mercury by ozone. *Water, Air, and Soil Pollution*, 80:301–315.

Hedgecock, I. and Pirrone, N. (2001). Mercury and photochemistry in the marine boundary layer-modelling studies suggest the in situ production of reactive gas phase mercury. *Atmos Environ*, 35(17):3055–3062.

Hedgecock, I. and Pirrone, N. (2004). Chasing quicksilver: Modeling the atmospheric lifetime of Hg-(g)(0) in the marine boundary layer at various latitudes. *Environ Sci Technol*, 38(1):69–76.

Hedgecock, I., Pirrone, N., Sprovieri, F., and Pesenti, E. (2003). Reactive gaseous mercury in the marine boundary layer: modelling and experimental evidence of its formation in the mediterranean region. *Atmos Environ*, 37:S41–S49.

Hedgecock, I., Pirrone, N., Trunfio, G., and Sprovieri, F. (2006). Integrated mercury cycling, transport, and air-water exchange (MECAWEx) model. *J Geophys Res*, 111(D20):D20302.

Hedgecock, I., Trunfio, G., Pirrone, N., and Sprovieri, F. (2005). Mercury chemistry in the MBL: Mediterranean case and sensitivity studies using the AMCOTS (Atmospheric Mercury Chemistry over the Sea) model. *Atmos Environ*, 39(38):7217–7230.

Hignett, P. (1991). Observations of diurnal variation in a cloud-capped marine boundary layer. *J Atmos Sci*, 48(12):1474–1482.

Holmes, C., Jacob, D., and Yang, X. (2006). Global lifetime of elemental mercury against oxidation by atomic bromine in the free troposphere. *Geophysical Research Letters*, 33(20):L20808.

Hynes, A., Donohoue, D., Goodsite, M., Hedgecock, I., Pirrone, N., and Mason, R. (2008). Our current understanding of major chemical and physical processes affecting mercury dynamics in the atmosphere and at air-water/terrestrial interfaces. In *Mercury Fate and Transport in the Global Atmosphere*. United Nations Environment Programme.

Jaffe, D., Prestbo, E., Swartzendruber, P., Weiss-Penzias, P., Kato, S., Takami, A., Hatakeyama, S., and Kajii, Y. (2005). Export of atmospheric mercury from Asia. *Atmos Environ*, 39(17):3029–3038.

Keene, W., Stutz, J., Pszenny, A., Maben, J., Fischer, E., Smith, A., von Glasow, R., Pechtl, S., Sive, B., and Varner, R. (2007). Inorganic chlorine and bromine in coastal New England air during summer. *J Geophys Res*, 112(D10).

Landis, M., Stevens, R., Schaedlich, F., and Prestbo, E. (2002). Development and characterization of an annular denuder methodology for the measurement of divalent inorganic reactive gaseous mercury in ambient air. *Environ Sci Technol*, 36(13):3000–3009.

Laurier, F. and Mason, R. (2007). Mercury concentration and speciation in the coastal and open ocean boundary layer. *J Geophys Res*, 112(D6):D06302.

Laurier, F., Mason, R., Whalin, L., and Kato, S. (2003). Reactive gaseous mercury formation in the North Pacific Ocean's marine boundary layer: A potential role of halogen chemistry. *J Geophys Res*, 108(D17):4529.

Leser, H., Honninger, G., and Platt, U. (2003). MAX-DOAS measurements of BrO and NO2 in the marine boundary layer. *Geophysical Research Letters*, 30(10):1537.

Lewis, E. and Schwartz, S. (2004). *Sea Salt Aerosol Production*. Number 152 in Geophysical Monograph Series. American Geophysical Union.

Lewis, E. and Schwartz, S. (2006). Comment on "size distribution of sea-salt emissions as a function of relative humidity". *Atmos Environ*, 40(3):588–590.

Lin, C., Pongprueksa, P., Lindberg, S., Pehkonen, S., Byun, D., and Jang, C. (2006). Scientific uncertainties in atmospheric mercury models I: Model science evaluation. *Atmos Environ*, 40(16):2911–2928.

Lindberg, S., Bullock, R., Ebinghaus, R., Engstrom, D., Feng, X., Fitzgerald, W., Pirrone, N., Prestbo, E., and Seigneur, C. (2007). A synthesis of progress and uncertainties in attributing the sources of mercury in deposition. *Ambio*, 36(1):19–32.

Lindqvist, O. and Rodhe, H. (1985). Atmospheric mercury - a review. *Tellus Series B*, 37(3):136–159.

Linstrom, P. and Mallard, W. (2005). NIST Chemistry WebBook, NIST Standard Reference Database Number 69. National Institute of Standards and Technology.

Malcolm, E., Keeler, G., and Landis, M. (2003). The effects of the coastal environment on the atmospheric mercury cycle. *J Geophys Res*, 108(D12).

Mason, R. and Sheu, G. (2002). Role of the ocean in the global mercury cycle. *Global Biogeochem. Cycles*, 16(4):1093.

Mergler, D., Anderson, H., Chan, L., Mahaffey, K., Murray, M., Sakamoto, M., and Stern, A. (2007). Methylmercury exposure and health effects in humans: A worldwide concern. *Ambio*, 36(1):3–11.

Nowak, J., Davis, D., Chen, G., Eisele, F., Mauldin, R., Tanner, D., Cantrell, C., Kosciuch, E., Bandy, A., Thornton, D., and Clarke, A. (2001). Airborne observations of DMSO, DMS, and OH at marine tropical latitudes. *Geophysical Research Letters*, 28(11):2201–2204.

Pal, B. and Ariya, P. A. (2004). Gas-phase HO··initiated reactions of elemental mercury: Kinetics, product studies, and atmospheric implications. *Environ Sci Technol*, 38(21):5555–5566.

Park, R., Jacob, D., Field, B., Yantosca, R., and Chin, M. (2004). Natural and transboundary pollution influences on sulfate-nitrate-ammonium aerosols in the United States: implications for policy. *J Geophys Res*, 109:D15204.

Petersen, G., Bloxam, R., Wong, S., Munthe, J., Kruger, O., Schmolke, S., and Kumar, A. (2001). A comprehensive eulerian modelling framework for airborne mercury species: model development and applications in Europe. *Atmos Environ*, 35(17):3063–3074.

Platt, U. and Janssen, C. (1995). Observation and role of the free radicals NO_3, ClO, BrO and IO in the troposphere. *Faraday Discussions*, 100:175–198.

Pszenny, A., Moldanov, J., Keene, W., Sander, R., Maben, J., Martinez, M., Crutzen, P., Perner, D., and Prinn, R. (2004). Halogen cycling and aerosol pH in the Hawaiian marine boundary layer. *Atmos Chem Phys*, 4:147–168.

Sander, R. (1999). Modeling atmospheric chemistry: Interactions between gas-phase species and liquid cloud/aerosol particles. *Surveys in Geophysics*, 20(1):1–31.

Seigneur, C., Vijayaraghavan, K., and Lohman, K. (2006). Atmospheric mercury chemistry: Sensitivity of global model simulations to chemical reactions. *J Geophys Res*, 111(D22).

Seinfeld, J. and Pandis, S. (2006). *Atmospheric Chemistry and Physics: From Air Pollution to Climate Change*. Wiley-Interscience.

Selin, N. E., Jacob, D. J., Park, R. J., Yantosca, R. M., Strode, S., Jaeglé, L., and Jaffe, D. (2007). Chemical cycling and deposition of atmospheric mercury: Global constraints from observations. *J Geophys Res*, 112(D2):1–14.

Selin, N. E., Jacob, D. J., Yantosca, R. M., Strode, S., Jaeglé, L., and Sunderland, E. M. (2008). Global 3-D land-ocean-atmosphere model for mercury: Present-day versus preindustrial cycles and anthropogenic enrichment factors for deposition. *Global Biogeochem. Cycles*, 22(2):1–13.

Shepler, B. and Peterson, K. (2003). Mercury monoxide: A systematic investigation of its ground electronic state. *J Phys Chem A*, 107(11):1783–1787.

Shia, R., Seigneur, C., Pai, P., Ko, M., and Sze, N. (1999). Global simulation of atmospheric mercury concentrations and deposition fluxes. *J Geophys Res*, 104(D19):23747–23760.

Sillman, S., Marsik, F. J., Al-Wali, K. I., Keeler, G. J., and Landis, M. S. (2007). Reactive mercury in the troposphere: Model formation and results for Florida, the northeastern United States, and the Atlantic Ocean. *J Geophys Res*, 112(D23):D23305.

Singh, H., Thakur, A., Chen, Y., and Kanakidou, M. (1996). Tetrachloroethylene as an indicator of low cl atom concentrations in the troposphere. *Geophysical Research Letters*, 23(12):1529–1532.

Strode, S., Jaegle, L., Jaffe, D., Swartzendruber, P., Selin, N., Holmes, C., and Yantosca, R. (2008). Trans-Pacific transport of mercury. *J Geophys Res*, 113:D15305.

Strode, S. A., Jaegle, L., Selin, N. E., Jacob, D. J., Park, R. J., Yantosca, R. M., Mason, R. P., and Slemr, F. (2007). Air-sea exchange in the global mercury cycle. *Global Biogeochem. Cycles*, 21(1):GB1017.

Stull, R. (1988). *An Introduction to Boundary Layer Meteorology*. Kluwer Academic.

Swartzendruber, P. C., Jaffe, D. A., Prestbo, E. M., Weiss-Penzias, P., Selin, N. E., Park, R., Jacob, D. J., Strode, S., and Jaegle, L. (2006). Observations of reactive gaseous mercury in the free troposphere at the Mount Bachelor Observatory. *J Geophys Res*, 111(D24):D24302.

Tackett, P., Cavender, A., Keil, A., Shepson, P., Bottenheim, J., Morin, S., Deary, J., Steffen, A., and Doerge, C. (2007). A study of the vertical scale of halogen chemistry in the Arctic troposphere during polar sunrise at Barrow, Alaska. *J Geophys Res*, 112(D7):D07306.

von Glasow, R., Sander, R., Bott, A., and Crutzen, P. (2002). Modeling halogen chemistry in the marine boundary layer - 1. cloud-free MBL. *J Geophys Res*, 107(D17):4341.

Wingenter, O., Sive, B., Blake, N., Blake, D., and Rowland, F. (2005). Atomic chlorine concentrations derived from ethane and hydroxyl measurements over the equatorial pacific ocean: Implication for dimethyl sulfide and bromine monoxide. *J Geophys Res*, 110(D20):D20308.

Zhang, L., Gong, S., Padro, J., and Barrie, L. (2001). A size-segregated particle dry deposition scheme for an atmospheric aerosol model. *Atmos Environ*, 35:549–560.

Chapter 4

Global atmospheric model for mercury including oxidation by bromine atoms

Abstract

We present a global atmospheric model for mercury (GEOS-Chem) in which atomic bromine is the sole oxidant of Hg^0. We compare this chemical mechanism against an alternative one with oxidation only by OH and ozone and test both mechanisms against observed concentrations and wet deposition. Our model also includes updated emissions (8600 Mg a^{-1}), improved scavenging by ice and snow, a new parameterization of Hg^{II} uptake and deposition through sea-salt aerosol, and a coupled snowpack emission model. Bromine concentrations here derive from atmospheric models constrained by source gas distributions and match satellite BrO columns. We find that the observed spatial distribution and seasonal cycle of total gaseous mercury (TGM) are equally consistent with either the bromine-only mechanism or the OH and O_3 mechanism, while mercury oxidation in summer subsidence events over Antarctica is more consistent with the bromine mechanism. Wet deposition measurements over the US are also consistent with the bromine mechanism, but require some additional bromine in the free troposphere, perhaps from sea-salt. The Arctic Hg^0 seasonal cycle suggests that 40% of Hg^{II}deposited to snow is retained at the surface, amounting to 100 Mg a^{-1} accumulation in the ocean and soil. Aircraft observations in Arctic spring find complete Hg^0 oxidation in the lower stratosphere that the model cannot reproduce, except possibly with oxidation by chlorine species in the winter vortex. Atmospheric reduction, which has no established mechanism, is not required to reproduce any major features of mercury observations.

4.1 Introduction

Mercury is a neurotoxic pollutant that is dispersed globally by atmospheric transport. Emission is mostly as elemental mercury (Hg^0). Atmospheric observations of Hg^0 imply an atmospheric lifetime of the order of a year (Lindberg et al., 2007). The oxidized product Hg^{II} is highly water soluble and thus deposits rapidly through precipitation and surface uptake. Understanding the global budget of atmospheric mercury and the source-receptor relationships for mercury deposition therefore requires global atmospheric transport models with accurate redox chemistry.

A fundamental limitation of current models is the uncertainty in the atmospheric chemistry of mercury (Lin et al., 2006; Ariya et al., 2008). Atmospheric observations imply that oxidation of Hg^0 to Hg^{II} must be photochemical (Shia et al., 1999; Selin et al., 2007). Models generally assume that gas-phase OH and ozone are the main oxidants, and also include aqueous-phase reduction of Hg^{II} to Hg^0 that competes with deposition as a sink for Hg^{II} (Bergan and Rodhe, 2001; Petersen et al., 2001; Cohen et al., 2004; Lin et al., 2006; Seigneur et al., 2006; Selin et al., 2007; Pongprueksa et al., 2008). However, recent work suggests that oxidation of Hg^0 by OH and O_3 is too slow to be of atmospheric relevance (Calvert and Lindberg, 2005; Hynes et al., 2008). Present-day measurement techniques cannot determine the molecular identity of atmospheric Hg^{II} oxidation products, but instead quantify all gas-phase Hg^{II} as reactive gaseous mercury (RGM). There is also no accepted kinetics or mechanism for Hg^{II} atmospheric reduction (Ariya et al., 2008; Hynes et al., 2008).

Holmes et al. (2006) proposed that gas-phase Br atoms might be the dominant global oxidant of Hg^0, with most of the oxidation taking place in the free troposphere. Several pieces of evidence support this idea. Oxidation of Hg^0 by Br is thought to explain the mercury depletion events (MDEs) in polar spring (Goodsite et al., 2004; Simpson et al., 2007; Steffen et al., 2008). Diurnal patterns of Hg^{II} in the marine boundary layer are consistent with oxidation by Br (Hedgecock et al., 2005; Holmes et al., 2009). Column measurements of BrO suggest a background concentration of 0.5-2 ppt in the free troposphere (Pundt et al., 2002; Van Roozendael et al., 2002; Sinnhuber et al., 2005) that could be accounted for by photolysis and oxidation of bromocarbons (Yang et al., 2005). Br atom concentrations deduced from photochemical equilibrium with this background BrO could yield an Hg^0 atmospheric lifetime of less than a year (Holmes et al., 2006). The lower stratosphere also contains elevated BrO (Salawitch et al., 2005), which might explain the rapid depletion of Hg^0 observed above the tropopause (Talbot et al., 2008).

Constructing a plausible global model of Hg+Br chemistry is challenging because of the large range of reported Hg+Br kinetics (reviewed by Holmes et al., 2006; Hynes et al., 2008; Ariya et al., 2008) and because of uncertainties in the concentrations of atmospheric Br. Gaseous inorganic bromine (Br_y) originates from atmospheric degradation of bromocarbons and debromination of sea-salt aerosols (Yang et al., 2005; Pszenny et al., 2004; von Glasow et al., 2002). Short-lived bromocarbons including $CHBr_3$ and CH_2Br_2 emitted by the ocean, and CH_3Br of both biogenic and anthropogenic origin, are thought to dominate the supply of Br_y in the free troposphere and lower stratosphere, while sea salt dominates

in the marine boundary layer (MBL) (Yang et al., 2005). Br_y cycles between radical forms (Br and BrO) and non-radical reservoir species (HOBr, HBr, $BrNO_3$, $BrNO_2$, and Br_2) (Pszenny et al., 2004). Br and BrO are in fast photochemical equilibrium during daytime and disappear into the reservoir species at night. Heterogeneous reactions of HOBr, HBr, and $BrNO_3$ on aerosols could also be important for maintaining radical concentrations (von Glasow et al., 2004; Yang et al., 2005). Br_y is eventually removed from the atmosphere by wet and dry deposition.

Three previous global mercury model studies have included Br as an Hg^0 oxidant in addition to OH and O_3 (Ariya et al., 2004; Seigneur and Lohman, 2008; Dastoor et al., 2008). The studies of Ariya et al. (2004) and Dastoor et al. (2008) focused on simulation of Arctic MDEs. They showed success in reproducing Hg^0 observations at Arctic sites, and concluded that MDEs cause net deposition throughout the Arctic, even after accounting for reemission of Hg^0 from the snowpack. Seigneur and Lohman (2008) evaluated the sensitivity of the simulated interhemispheric and vertical gradients of Hg^0 to the Hg+Br reaction kinetics. Their simulated mean surface Hg^0 concentrations changed by 20-40% across the range of the kinetic data (Ariya et al., 2002; Donohoue et al., 2006), with the best results obtained with the slow kinetics. In contrast, Dastoor et al. (2008) reported that the fast kinetics gave a better simulation of Hg^0 in the Arctic at Alert, Canada. Seigneur and Lohman (2008) also presented a sensitivity test in which Br was the sole oxidant of Hg^0. This showed an unrealistic meridional distribution of Hg^0 with a peak in the tropics and minima at the polesa pattern due to the satellite-derived distribution of tropospheric

BrO that they used to derive their global Br distribution.

Here we use the GEOS-Chem global chemical transport model (Selin et al., 2008) to evaluate whether a model with Br as the sole Hg^0 oxidant can in fact be consistent with atmospheric observations. The above model studies derived their tropospheric bromine concentrations from satellite observations of BrO columns (Chance, 1998; Burrows et al., 1999), but recent observations from the ARCTAS aircraft campaign in the Arctic have shown that previous inferences of tropospheric BrO from the satellite column data are seriously flawed (Salawitch et al., 2009). Here we use a combination of field measurements and process-based models to estimate the distribution of Br from the surface to the stratosphere. We also describe several other improvements to the GEOS-Chem mercury model including updated anthropogenic emissions, mechanistic uptake by sea-salt aerosols, scavenging by snow and ice, and a coupled snowpack reservoir. We evaluate the ability of this new model version to reproduce atmospheric observations through comparisons with multiple data sets.

4.2 Model description

The previous version of the GEOS-Chem atmosphere-ocean-land mercury model (v7.04) was described by Selin et al. (2008). The model includes a global 3-D atmosphere (here $4^\circ \times 5^\circ$ horizontal resolution, 55 vertical levels, hourly time steps) coupled to 2-D surface ocean and soil reservoirs. The atmospheric component is driven by assimilated meteorological data from the Goddard Earth Observing System (GEOS) of the NASA Global Mod-

eling and Assimilation Office (GMAO). It includes three transported species: Hg^0, Hg^{II}, and inert, nonvolatile particulate mercury (Hg^P). The surface ocean component (Strode et al., 2007) includes three species: Hg^0, reactive dissolved Hg^{II}, and inert particle-bound Hg^P. These ocean species undergo chemical interconversion and vertical exchange with the atmosphere and with a deep ocean reservoir of fixed mercury concentrations. Horizontal transport in the ocean is neglected. Natural soil mercury concentrations are specified on the $4^\circ \times 5^\circ$ grid by steady state of emissions and deposition in the preindustrial atmosphere (Selin et al., 2008). They are augmented for present-day on the basis of the modeled deposition patterns of anthropogenic mercury.

In the present model we have updated the emissions, atmospheric chemistry, and deposition modules used by Selin et al. (2008). We elaborate on these improvements below. We also updated the transport component by using meteorological input from the GEOS-5 assimilation data, which have $0.5^\circ \times 0.67^\circ$ horizontal resolution and 72 vertical layers. As before, we degrade the horizontal resolution to $4^\circ \times 5^\circ$ for computational expediency. Tracer transport algorithms are from the current GEOS-Chem version (8.02.03), which includes improved advection in the tropopause region (MacKenzie, 2009) and a non-local parameterization of boundary layer mixing (Lin and McElroy, 2010). Figure 4.1 presents our updated global mercury budget, which we will discuss in Section 4.4.

4.2.1 Emissions

Selin et al. (2008) previously used the GEIA anthropogenic emissions for 2000 (Pacyna

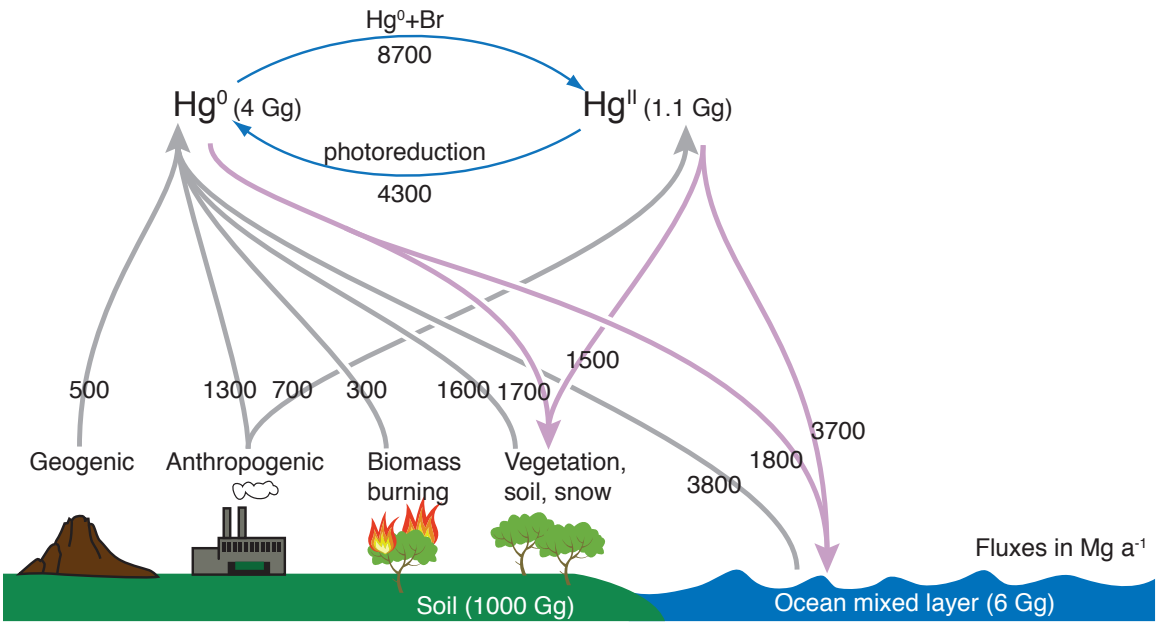

Figure 4.1: Global budget of atmospheric mercury derived from this work. Hg^{II} here includes gaseous and particulate forms, plus a negligible contribution (2 Mg) from inert particulate mercury.

et al., 2006) but found that they had to increase Hg^0 emissions globally by 30% (by 50% in China) to 3400 Mg a^{-1} total Hg in order to accommodate atmospheric observations. Those emissions exceed the 2200-2600 Mg a^{-1} range of recent estimates and are likely too high (Mason and Sheu, 2002; Pacyna et al., 2006; Streets et al., 2009; Pirrone et al., 2010). Here we use the Streets et al. (2009) global inventory for 2006 partitioned into six regions; emissions within each region follow the GEIA distribution. Emissions from artisanal gold mining are 450 Mg a^{-1} following Selin et al. (2008). Our anthropogenic emissions thus total 1300 Mg a^{-1} Hg^0, 650 Mg a^{-1} Hg^{II}, and 100 Mg a^{-1} Hg^P. While these are 30% lower than in Selin et al. (2008), our simulation remains consistent with the observed Hg^0 concentrations (as we will show below) because changes in the redox chemistry prolong the Hg^0 lifetime.

The soil emissions specified by Selin et al. (2008) were an exponential function of both soil temperature and solar radiation, producing a strong summer peak. With the smaller anthropogenic emissions and slower oxidation in the present model, these emissions would result in a summer Hg^0 maximum at northern midlatitudes that is at odds with observations (Selin et al., 2007). Here we specify soil emission E as a function of solar radiation following Zhang et al. (2001),

$$E = \beta C_s \exp(\alpha R_g), \tag{4.1}$$

where C_s is the soil mercury concentration (g g^{-1}), R_g is the solar radiation flux at the ground, and $\alpha = 1.1 \times 10^3$ m^2 W^{-1}. The scaling factor β = 0.02 g m^{-2} h^{-1} is derived here from global mass balance in the preindustrial period, as described by Selin et al. (2008). With this change, simulated TGM concentrations follow the observed seasonal cycle, but total present-day soil emissions, 1100 Mg a^{-1}, are unchanged from Selin et al. (2008).

As in Selin et al. (2008), soil and vegetation emit an additional 260 Mg a^{-1} through rapid photoreduction of deposited Hg^{II}. Biomass burning emits 300 Mg a^{-1} following the distribution of biomass burning CO, using a new Hg/CO emission ratio of 100 mol mol^{-1}, as discussed below. The model no longer includes emissions through plant transpiration because of field evidence that this process is unimportant (Gustin et al., 2004).

Arctic field studies find large Hg^0 emissions from sunlit snowpacks in spring and summer after MDEs cause surface mercury enhancements (Cobbett et al., 2007; Steffen et al., 2008, and references therein). Some mercury may be retained in ecosystems during snowmelt (Dommergue et al., 2003; Brooks et al., 2006; Johnson et al., 2008), but low Hg

concentrations in late-season snow and meltwater suggest that most of the MDE-deposited mercury returns to the atmosphere (Kirk et al., 2006). We add a snowpack reservoir on the $4^\circ \times 5^\circ$ grid that accumulates mercury deposition and releases it as Hg^0 under sunlit conditions. The reservoir lifetime is 180 d, decreasing to 21 d when $T > 270$ K to fit observations by Fain et al. (2007; 2008) that re-emission accelerates sharply when melting begins. This simple parameterization reproduces the seasonal cycle of atmospheric Hg^0 at Arctic sites as will be shown in Section 4.3.2. We find that 60% of mercury deposited to snow is eventually reemitted and 40% enters the underlying ocean or soil. Global snow emissions are 230 Mg a^{-1}.

Figure 4.1 summarizes model emissions. Net ocean emissions respond dynamically to changes in emissions and chemistry and are now 2000 Mg a^{-1}, which is 40% smaller than the earlier model and closer to central estimates from other studies (Lamborg et al., 2002; Mason and Sheu, 2002; Sunderland and Mason, 2007; Mason, 2008). Global mercury emissions are 8600 Mg a^{-1} if we include gross ocean Hg^0 emissions or 6800 Mg a^{-1} if we include only net ocean emission.

4.2.2 Chemistry

A major update in this work is to oxidize Hg^0 by Br atoms instead of by ozone and OH. Table 4.1 lists the reactions involved. Atomic bromine initiates Hg^0 oxidation in the gas phase following a mechanism described by Goodsite et al. (2004). The unstable product HgBr may either dissociate or react with Br or OH to form Hg^{II}. We use kinetic coefficients

from Donohoue et al. (2006), Goodsite et al. (2004) and Balabanov et al. (2005), which are consistent with RGM observations in the marine boundary layer (Holmes et al., 2009). These coefficients are at the low end of the published range (Holmes et al., 2006) and are similar to the ones chosen by Seigneur and Lohman (2008) to fit observed vertical Hg^0 gradients. OH concentrations for the $HgBr + OH \rightarrow HgBrOH$ reaction are archived from a GEOS-Chem full-chemistry simulation (Park et al., 2004).

Global bromine concentrations are specified on the model grid for each by combining estimates of the contributions from its major precursors: biogenic bromocarbons, halons, and sea-salt aerosol bromide. For the troposphere and lower stratosphere, we use archived Br from the p-TOMCAT model with biogenic bromocarbon and methyl bromide source gases (Yang et al., 2005). In the middle stratosphere and above, where halons decompose, we use archived Br from the NASA Global Modeling Initiative (GMI) Aura4 model with halon and methyl bromide source gases (Strahan et al., 2007). These model estimates are constrained by observations of the bromocarbon source gases (e.g. Douglass et al., 2004; WMO, 2007; Warwick et al., 2007) and standard gas-phase chemistry of Br_y (Sander et al., 2006). They may be lower limits because we do not account for ventilation of MBL air containing Br_y from sea-salt aerosol (Yang et al., 2005) or heterogeneous reactions of Br_y on aerosols releasing Br radicals (Yang et al., 2005; von Glasow et al., 2004). For the MBL, we assume a uniform daytime concentration of 1 ppt BrO, consistent with the few observations available (Leser et al., 2003; Saiz-Lopez et al., 2004; Martin et al., 2009; O'Brien et al., 2009) and with the observed diurnal cycle of RGM (Holmes et al., 2009).

We calculate the associated Br concentrations from photochemical steady state (Platt and Janssen, 1995),

$$\frac{[\mathrm{Br}]}{[\mathrm{BrO}]} = \frac{J_{\mathrm{BrO}} + k_1[\mathrm{NO}]}{k_2[\mathrm{O_3}]}, \tag{4.2}$$

where J_{BrO} is the BrO photolysis frequency, $k_1 = 2.1 \times 10^{-11}$ cm^3 molecule^{-1} s^{-1} and $k_2 = 1.2 \times 10^{-12}$ cm^3 molecule^{-1} s^{-1} are the rate coefficients for the $\mathrm{BrO} + \mathrm{NO} \rightarrow \mathrm{Br} + \mathrm{NO_2}$ and $\mathrm{Br} + \mathrm{O_3} \rightarrow \mathrm{BrO} + \mathrm{O_2}$ reactions respectively (Platt and Janssen, 1995), [NO] = 10 ppt is assumed, and [O_3] and mean daytime J_{BrO} are archived from GEOS-Chem full-chemistry simulations (Park et al., 2004; Parrella, 2010). We impose a diurnal cycle for Br as given by Holmes et al. (2009).

Springtime photochemistry of sea salt on sea ice can produce unusually high Br concentrations in the polar boundary layer in spring, resulting in fast oxidation of mercury and ozone (Simpson et al., 2007). BrO concentrations during these episodes are typically 5-15 ppt (Steffen et al., 2008). Here we specify 5 ppt BrO in the Arctic (Antarctic) boundary layer during March-May (August-October) over regions with sea ice, temperatures below 268 K, and sunlight. We calculate the associated Br concentration in steady state as above, assuming that O_3 is depleted to 5 ppb.

Figure 4.2 shows the resulting GEOS-Chem Br mixing ratios for the months of January and July. We also show BrO for reference although the model does not use it. Br and BrO have have a strong photochemically driven seasonal cycle in the extratropics. Concentrations increase with altitude due to photochemical production. Minima in the tropical lower troposphere reflect wet deposition of soluble inorganic bromine species. Br concen-

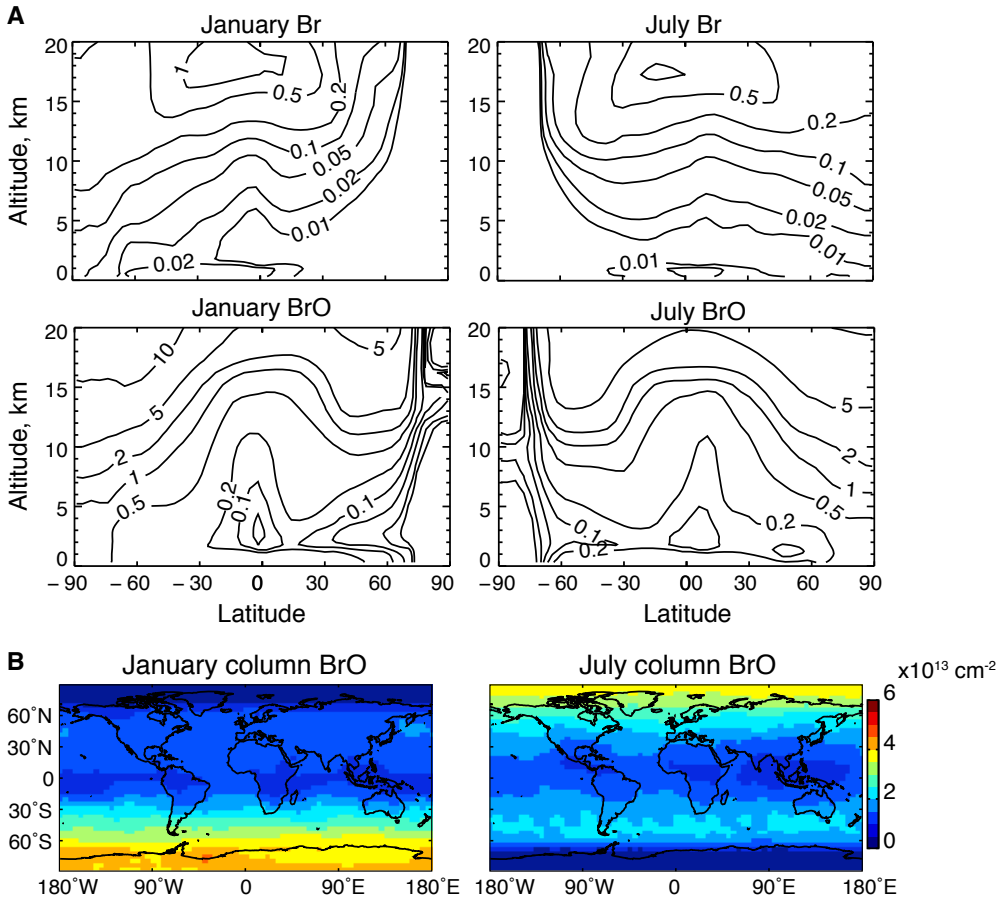

Figure 4.2: (A) Zonal mean Br and BrO mixing ratios (ppt) and (B) BrO columns for January and July.

trations peak at the tropical tropopause due to strong radiation and relatively low ozone, but otherwise show little latitudinal variation in the summer hemisphere. Monthly mean BrO columns range from 1×10^{13} cm^{-2} in the tropics up to 4×10^{13} cm^{-2} at the summer pole, which agrees well with values and latitudinal trends observed from satellites (Chance, 1998; Richter et al., 2002; Sioris et al., 2006), after we account for the two-fold difference between 24-h averages shown here and the daytime concentrations detected from space.

From these Br concentration fields and the mechanism in Table 4.1 we obtain a global

Table 4.1: Redox mechanism for mercury in GEOS-Chem

Reaction[a]	Rate coefficient[b]	Reference[c]
$Hg^0 + Br + M \rightarrow HgBr + M$	$1.5 \times 10^{-32}(T/298)^{-1.86}$ [M]	(1)
$HgBr \xrightarrow{M} Hg^0 + Br$	$3.9 \times 10^9 \exp(-8357/T)(T/298)^{0.51}$	d
$HgBr + Br \xrightarrow{M} HgBr_2$	$2.5 \times 10^{-10}(T/298)^{-0.57}$	(2)
$HgBr + OH \xrightarrow{M} HgBrOH$	$2.5 \times 10^{-10}(T/298)^{-0.57}$	(2)
$HgBr + Br \rightarrow Hg^0 + Br_2$	3.9×10^{-11}	(3)
$Hg^{II}_{(aq)} + h\nu \rightarrow Hg^0$	$4.5 \times 10^{-3} J_{NO_2}$	this study

[a] Species are gas-phase except where (aq) indicates aqueous-phase.
[b] Rate coefficients units are cm^3 molecule^{-1} s^{-1}, except for photolysis which has units of s^{-1}. T is temperature in K. [M] is the number density of air in molecules cm^{-3}. J_{NO_2} is the NO_2 photolysis frequency in s^{-1}.
[c] (1) Donohoue et al. (2006); (3) Goodsite et al. (2004); (3) Balabanov et al. (2005)
[d] Derived from the temperature-dependent reaction free energy ($\Delta G = 56.5$ kJ mol^{-1} at 298 K) for $Hg^0 + Br \rightarrow HgBr$ (Goodsite et al., 2004) and the above rate coefficient for the forward reaction.

Hg^0 chemical lifetime of 6 months, with most of the oxidation taking place in the free troposphere. We find that HgBrOH is the major product, but it and other Hg^{II} species are expected to undergo ion exchange in cloud and aerosol water to produce $HgCl_2$ primarily (Hedgecock and Pirrone, 2001; Lin et al., 2006). Subsequent deposition of Hg^{II} depends on its gas/aerosol partitioning, for which observations show considerable variability (Jaffe et al., 2005; Caldwell et al., 2006; Liu et al., 2007; Valente et al., 2007; Cobbett et al., 2007; Weiss-Penzias et al., 2009). This partitioning is expected to depend on temperature, aerosol load, and aerosol composition (Lin et al., 2006; Rutter and Schauer, 2007a,b) but the dependence is not well quantified. Here we assume 50/50 partitioning of Hg^{II} between the gas and aerosol phase for the purpose of calculating Hg^{II} deposition as described in the following sub-sections. Our initial simulation without reduction of Hg^{II} produced mean Hg^0 surface concentrations that were smaller than observed. Early global models for mercury included aqueous reduction of Hg^{II} by HO_2 and SO_3^-, but these are now thought to be negligibly slow (Van Loon et al., 2000; Gårdfeldt and Jonsson, 2003). More recent mod-

els have hypothesized gaseous or aqueous reactions and tuned the kinetics to match the Hg^0 observations (Selin et al., 2007; Pongprueksa et al., 2008). Laboratory studies have reported fast UV photoreduction of aqueous $HgCl_2$ in the presence of organic acids (Pehkonen and Lin, 1998; Ababneh et al., 2006; Si and Ariya, 2008). We assume Hg^{II} reduction in liquid water clouds to be proportional to the NO_2 photolysis frequency, archived from a GEOS-Chem full-chemistry simulation (Mao et al., 2010b), and adjust the reduction rate to best match the global mean surface Hg^0 measurements. The best fit yields a Hg^{II} global tropospheric lifetime of 1.7 months against reduction. After including reduction, we calculate a global atmospheric lifetime of 9 months for mercury. We will also discuss results from a sensitivity simulation without Hg^{II} reduction and instead decreasing the overall rate of $Hg^0 + Br + X \rightarrow\rightarrow Hg^{II}$ (X $\equiv$ Br, OH) reaction by 60% to yield the same atmospheric lifetime of mercury as in the standard simulation. This decrease in oxidation lies within the range of theory-derived kinetic coefficients for $HgBr + X \rightarrow HgBrX$ (Goodsite et al., 2004; Balabanov et al., 2005) or could be accommodated by smaller atomic Br concentrations.

An important objective of this study is to evaluate the ability of GEOS-Chem to fit observations using Br as the sole Hg^0 oxidant instead of OH and ozone. We will compare results from a simulation with Br chemistry (the "Hg+Br model) versus one with OH and ozone chemistry ("Hg+OH/O_3 model). For the latter we follow the kinetics of Sommar et al. (2001) and Hall (1995), as used by Selin et al. (2007), with OH and ozone concentrations specified from a full-chemistry GEOS-Chem simulation. The resulting oxidation of Hg^0 is faster than by Br and takes place at lower altitudes where Hg^{II} deposits faster, so we

compensate by increasing the reduction rate 4 fold. The Hg^0 lifetime in that simulation is 3.5 months with OH contributing 80% of the sink.

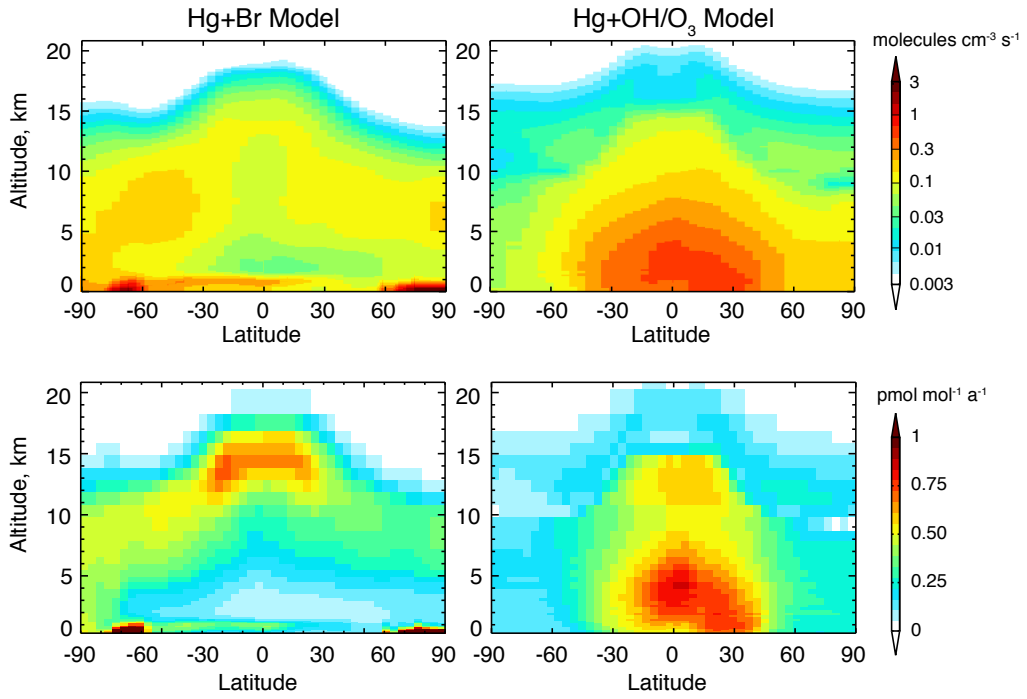

Figure 4.3: Annual zonal mean distribution of the Hg^0 oxidation rate under the Hg+Br and $Hg+OH/O_3$ chemical mechanisms.

Figure 4.3 shows the zonal distribution of oxidation and reduction in the base Hg+Br model and in the $Hg+OH/O_3$ sensitivity simulation. Oxidation by bromine is fast in the MBL where Br number density is largest, but most of the global oxidation occurs in the free troposphere due to low temperatures and increasing Br mixing ratios with altitude (Holmes et al., 2006). Oxidation is also fast in the stratosphere but most mercury there is already Hg^{II}. The southern hemisphere has slightly faster oxidation than the northern hemisphere because of the oceanic source of bromocarbons and the low temperatures over Antarctica. Springtime bromine explosions drive secondary oxidation maxima in the polar boundary

layers. Oxidation by OH and O_3 follows the general distribution of OH concentrations, with a maximum in the lower tropical troposphere and symmetry about the equator. Reduction of Hg^{II} (not shown) peaks at 1-2 km altitude, where cloud liquid water is high, and no reduction occurs above 10 km where clouds are entirely ice.

4.2.3 Sea-salt aerosol as a sink for mercury

Building on earlier work by Hedgecock and Pirrone (2001) and Selin et al. (2007), we previously suggested that uptake of Hg^{II} by sea-salt aerosols as $HgCl_4^{2-}$ is the dominant sink for Hg^{II} in the marine boundary layer and the major source of mercury to the surface ocean (Holmes et al., 2009). We calculated the Hg^{II} uptake rate and subsequent deposition flux (F_{dep}) in a box model of the marine boundary layer (MBL) on the basis of the local 10-m wind speed (u_{10}), relative humidity (saturation ratio S) and mixing depth (H). Fast winds enhance uptake through increased sea spray, while low relative humidity increases $[Cl^-]$ within the sea-salt aerosol and hence promotes formation of $HgCl_4^{2-}$. We accounted for mass-transport limitations at the gas-particle interface over the sea-salt aerosol size distribution. Here we parameterize the results from this MBL box model for implementation in GEOS-Chem as a first-order rate coefficient (k) for Hg^{II} net uptake and subsequent deposition,

$$F_{dep} = k(u_{10}, S)\, H\, [Hg^{II}]. \tag{4.3}$$

Figure 4.4 shows $k(u_{10}, S)$ simulated in the box model with full physics over the range of conditions expected in the marine atmosphere (Holmes et al., 2009). We fit k to the

following form:

$$k(u_{10},S) = a_0\,[1-\exp\,(a_1(1-S))]\exp\left(a_2\,u_{10}+a_3\,u_{10}^{1/2}+a_4\,u_{10}^{3/2}\right) \tag{4.4}$$

with coefficients $a_0 = 1\times10^{-10}$ s^{-1}, $a_1 = -59.91$, $a_2 = -1.935$ s m^{-1}, $a_3 = 9.009$ s$^{1/2}$ m$^{-1/2}$, and $a_4 = 0.1477$ s$^{3/2}$ m$^{-3/2}$. This simplified model closely fits the 24-h mean loss rate in the full-physics model ($r^2 = 0.97$) over the parameter range $0.7 \le S \le 0.99$ and $0.1 \le u_{10} \le 20$ m s^{-1}.

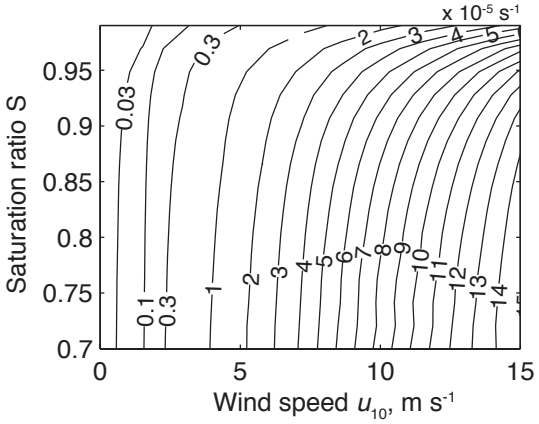

Figure 4.4: Rate coefficient k, (10^{-5} s^{-1}) for gaseous Hg^{II} uptake and deposition by sea-salt aerosols as simulated by the marine boundary layer model of Holmes et al. (2009) as a function of 10-m wind speed (u_{10}) and water vapor saturation ratio (S). For each (u_{10}, S) pair we conducted 40 Monte Carlo simulations with other box model parameters varying over their likely ranges.

4.2.4 Other deposition processes

GEOS-Chem includes wet scavenging of Hg^{II} and Hg^{P} following the scheme of Liu et al. (2001), and dry deposition of Hg^{0}, Hg^{II}, and Hg^{P} following the resistance-in-series scheme of Wesely (1989). Selin and Jacob (2008) describe how these schemes apply to mercury in

the previous version of the model. They assumed Hg^{II} to be gaseous $HgCl_2$ for the purpose of computing deposition; the Henry's law solubility constant of $HgCl_2$ is 1.4×10^6 M atm^{-1} (Lindqvist and Rodhe, 1985), sufficiently high for near-100% scavenging in clouds and fast dry deposition limited by aerodynamic resistance. Here we assume 50/50 partitioning of Hg^{II} between the gas and aerosol phase, which increases the lifetime of Hg^{II} against dry deposition as compared to the previous model version.

Selin et al. (2008) assumed no scavenging of Hg^{II} in cold (frozen) clouds and snow, and a zero retention efficiency of Hg^{II} upon cloud freezing, in order to reproduce the observations of low wet deposition fluxes of mercury at northern U.S. sites in winter (Selin and Jacob, 2008). However, observations by Douglas et al. (2008) indicate high mercury concentrations in rime ice, implying high retention efficiency. Therefore we now assume that supercooled water in mixed-phase clouds retains all Hg^{II} and Hg^{P} during freezing. Douglas et al. (2008) and Johnson et al. (2008) found by contrast very low Hg concentrations in ice grown from the vapor phase, so we still assume no mercury scavenging by cloud ice. Below-cloud scavenging by snow is included only for aerosol Hg^{II} and Hg^{P}, with the same efficiency as by rain (Murakami et al., 1983; Feng, 2009). Sigler et al. (2009) found that snowfall has little effect on ambient RGM, so we do not include below-cloud scavenging of gaseous Hg^{II} by snow. Adding low-temperature scavenging as described above increases deposition at high latitudes, but also allows low-latitude convective rainfall to scavenge from higher altitudes.

4.3 Model evaluation

We test here whether the "Hg+Br model (simulation with Hg^0 oxidation initiated by Br only) can reproduce the general patterns seen in atmospheric observations, and compare these results to the "Hg+OH/O_3 model (simulation with Hg^0 oxidation by OH and O_3). All simulations are initialized over 15 years of repeated present-day meteorological data to reach annual steady state in the stratosphere. We then analyze model results averaged over 2006-2008 and compare to observed concentrations and wet deposition.

4.3.1 Global distribution of mercury

Figure 4.5 shows annual mean observed surface concentrations of total gaseous mercury (TGM $\equiv$ Hg^0 + RGM) compared to the Hg+Br model. TGM in the model is calculated as Hg^0 + 0.5 Hg^{II}. The measurements include annual means at 39 land stations during 2000-2008, plus data from ship cruises (Lamborg et al., 1999; Temme et al., 2003; Laurier and Mason, 2007; Soerensen et al., 2010a). Interannual variability of TGM is small (Mao et al., 2008; Peterson et al., 2009) and is therefore expected to be a small source of error in the comparison. The model reproduces the spatial variability in the annual mean data at the 39 land sites ($r^2 = 0.88$). The mean and standard deviation for the ensemble of sites is 209 $\pm$ 112 ppq in the observations and 185 $\pm$ 58 ppq in the model. The model is unbiased with respect to sites in Europe and North America. The match to observations is similar in the Hg+OH/O_3 model (189 $\pm$ 56 ppq, r^2 = 0.87) because anthropogenic emissions strongly influence the TGM concentrations at the land sites.

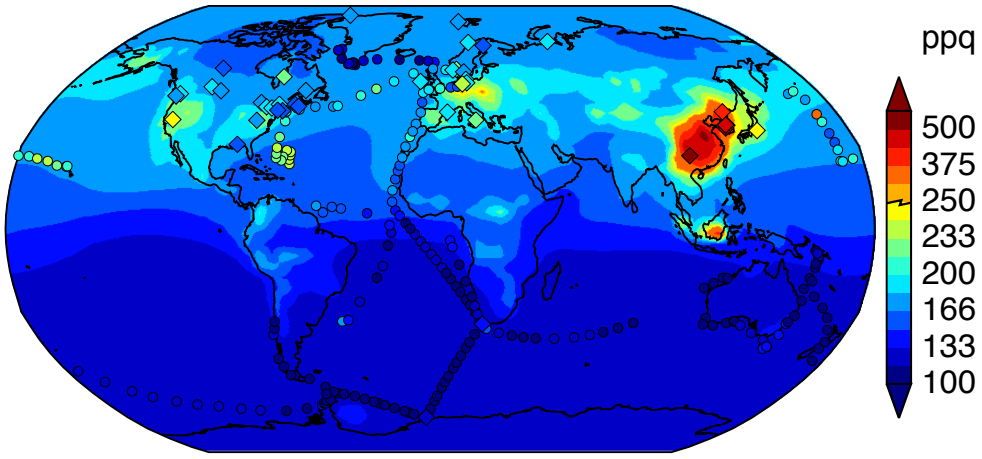

Figure 4.5: Global distribution of total gaseous mercury (TGM) concentrations in surface air. Model values (background) are annual means for 2006-2008. Data for land stations (diamonds) are annual means for available years during 2000-2008 and all other observations from ship cruises (circles) are averaged over 1° latitude bins. Observations include those used by Selin et al. (2007), plus additional sites in Europe (Steffen et al., 2005, EMEP 2009), North America (Steffen et al., 2005; Yatavelli et al., 2006; Stamenkovic et al., 2007; Temme et al., 2007; Choi et al., 2008; Sigler et al., 2009, E. Edgerton pers. comm.), East Asia (Nguyen et al., 2007; Sakata and Asakura, 2007; Feng et al., 2008; Wan et al., 2009, Y-J Han pers. comm.) and the Galathea cruise (Soerensen et al., 2010a). Note the change in linear color scale at 250 ppq.

A prominent deficiency in the model, previously identified by Selin et al. (2007), is that it does not reproduce the high concentrations observed over the North Atlantic and Pacific from ship cruises. These could be due to upwelling of elevated sub-surface ocean mercury, possibly reflecting the legacy of past anthropogenic emissions (Soerensen et al., 2010b).

The Hg+Br and Hg+OH/O_3 models diverge in their surface TGM predictions for the southern hemisphere because of the different oxidant distributions (Figures 4.2 and 4.3). The Hg+Br model predicts 120 ppq TGM throughout the southern mid-latitudes versus 150 ppq in the Hg+OH/O_3 model. The Hg+Br model closely matches the mean concentration observed on the Antarctic coast, while the data from Cape Point, South Africa lie evenly between the two models. Transient measurements from ships encompass a wider

range 110-160 ppq, so both oxidation mechanisms are consistent with the current southern hemisphere data, but more measurements here could help constrain the oxidants.

Our results differ markedly from the model of Seigneur and Lohman (2008), which predicted peak Hg^0 in the tropics and unrealistically low concentrations in the extra-tropics when Br was the sole oxidant. Seigneur and Lohman inferred Br concentrations from the GOME BrO columns, imposing vertical distributions and Br/BrO ratios from the p-TOMCAT CTM (Yang et al., 2005). That CTM does not include halons and would therefore greatly underestimate the contribution of the stratosphere to the BrO column. Considering that the stratospheric contribution drives the BrO column increase with latitude (Figure 4.2), this method would particularly overestimate tropospheric Br and tropospheric Hg^0 oxidation at high latitudes.

4.3.2 Seasonal cycle at surface sites

Figure 4.6 compares simulated and observed seasonal cycles of TGM at surface sites. Northern midlatitudes sites show on average a late summer minimum in both observations and model. Bergan and Rodhe (2001) and Selin et al. (2007) attributed this seasonal cycle to the photochemical sink from OH. However, the seasonal variation of soil emission (peaking in summer) can offset the chemical sink and suppress this seasonal minimum (Selin et al., 2008). In our model, the summer maximum of Br (Figure 4.6) drives a late summer minimum for TGM, and our updated soil emission parameterization (Equation 4.1) has a weaker seasonal dependence than that used by Selin et al. (2008).

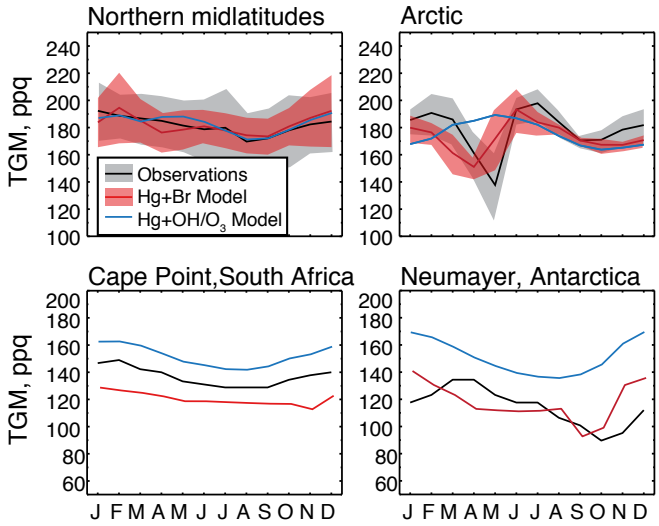

Figure 4.6: Mean seasonal variation of total gaseous mercury (TGM) at Arctic, northern midlatitude, and southern hemisphere sites. The northern midlatitude panel shows an average over 15 sites where monthly mean data are available, including the sites from Selin et al. (2007) plus Andoya and Birkenes in Norway (EMEP 2009), Kuujjuarapik, Canada (Steffen et al., 2005), Athens, Ohio and Pensacola, Florida in the US (Yatavelli et al., 2006, E. Edgerton pers. comm.). The Arctic panel is an average over 3 sites: Alert, Canada, Zeppelin, Norway, and Amderma Russia (Steffen et al., 2005, EMEP 2009). Shaded areas show standard deviation among sites for observations and for the Hg+Br model.

At Cape Point (South Africa), the only site with monthly data in the southern hemisphere outside Antarctica, TGM is highest in summer (December-February), opposite to the northern hemisphere. Our model has little seasonal variation at that sites, which is still an improvement over the earlier model which had opposite seasonality to observations due to the larger anthropogenic emissions that obscured the dip in ocean emissions during austral winter.

Observations at Arctic sites and at the Neumayer Antarctic site show a springtime minimum driven by MDEs and a summertime maximum driven by re-emission from the snowpack (Steffen et al., 2005; Cobbett et al., 2007). The Hg+Br model can reproduce this

seasonal variation but not the Hg + OH/O_3 model, which does not include MDEs. We find that atmospheric concentrations are consistent with re-emission of 60% of Hg deposited to the snowpack during springtime and 40% net deposition to the ocean and soil. Higher re-emission fractions cause excessive summertime summertime Hg^0 concentrations in the model and overestimate the annual mean. The ocean and soil within the Arctic Circle receives 110 Mg a^{-1} net deposition in the Hg+Br model versus 60 Mg a^{-1} in the Hg+OH/O_3 model without MDEs. Dastoor et al. (2008) estimates a similar re-emission fraction, but 40% larger deposition fluxes and hence 40% larger net transfer to the surface.

4.3.3 Testing oxidation chemistry through Antarctic subsidence events

Observations at Antarctic sites show frequent summertime events of depleted Hg^0 and enhanced RGM together with elevated ozone (Sprovieri et al., 2002; Temme et al., 2003; Aspmo and Berg, 2009). These differ from springtime depletion events in that O_3 is anti-correlated with Hg^0. From four events in the published Neumayer and Terra Nova Bay data (Sprovieri et al., 2002; Temme et al., 2003), we estimate ranges of -6.0– -11.5 for $\Delta Hg^0/\Delta O_3$ and 1.5–4.0 for $\Delta RGM/\Delta O_3$. Aspmo and Berg (2009) used back-trajectories to identify the mid-troposphere as the source region for such events. Brooks et al. (2008) also found that subsiding air at the South Pole contains elevated Hg^{II}. Holmes et al. (2006) previously cited these summer Antarctic events as qualitative evidence for Hg+Br chemistry. These observations provide a sensitive test for Hg^0 oxidation chemistry in the model because the cold, dry Antarctic atmosphere minimizes the confounding effect of aqueous

reduction. In addition, Br is an effective Hg^0 oxidant over Antarctica in summer (Figure 4.3) while OH is ineffective.

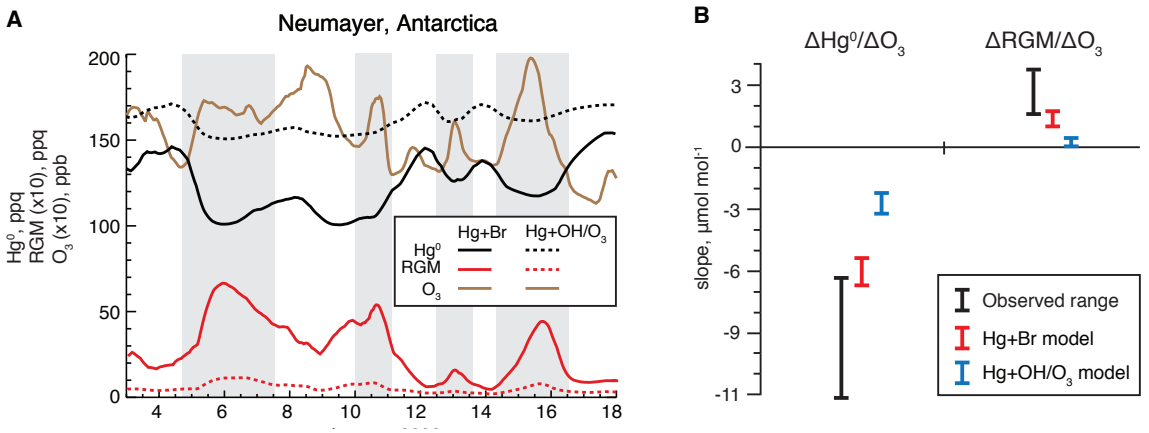

Figure 4.7: (A) Time series of Hg^0, RGM and O_3 simulated at Neumayer Station, Antarctica in the Hg+Br and Hg+OH/O_3 models. Shaded regions show summertime subsidence events. (B) $\Delta Hg^0/\Delta O_3$ and $\Delta RGM/\Delta O_3$ ratios observed and modeled at Neumayer during January-February. Observed ratios were calculated from data reported by Temme et al. (2003). Modeled ranges are 95% confidence intervals for standard major axis slope from the bootstrap method.

Figure 4.7 shows simulated Hg^0 and RGM at Neumayer station for January 2008, and O_3 from a GEOS-Chem full-chemistry simulation at the same time and location (Mao et al., 2010b). The model time series shows several subsidence events with enhanced O_3 and RGM, and depleted Hg^0. These events last 1-3 days, as found by Temme et al. (2003). We derive the model $\Delta Hg^0/\Delta O_3$ and $\Delta RGM/\Delta O_3$ ratios shown in Figure 4.7B from a standard major axis fit to the January time series. Due to the fast Hg+Br reaction over Antarctica seen in Figure 4.3, this oxidation mechanism predicts much greater RGM enhancements in the subsidence events than the Hg+OH/O_3 mechanism, and it is more consistent with observations.

4.3.4 Wet deposition

Figure 4.8 compares the Hg+Br model with annual wet deposition measurements from the Mercury Deposition Network (MDN, National Atmospheric Deposition Program, 2009) over North America and the European Monitoring and Evaluation Programme (EMEP, data courtesy of O. Travnikov) over Europe. These networks collect weekly (MDN) or monthly (EMEP) integrated samples of precipitation and wet deposition and comparisons here use sites with at least 75% of annual data present during the simulated years. We also require fewer than 5 consecutive missing samples for MDN. Both MDN and EMEP have been used extensively to test atmospheric mercury models (e.g. Selin et al., 2008; Bullock et al., 2009; Gusev et al., 2009) and to evaluate the impact of Hg emission reductions (e.g. Butler et al., 2008; Wangberg et al., 2007; Pacyna et al., 2009; Prestbo and Gay, 2009). Wet deposition is very similar in the Hg+OH/O_3 model except where discussed below.

The model predicts the highest wet deposition in the coal-burning regions of Europe and North America, reflecting near-field deposition of emitted Hg^{II} and Hg^{P}. Observations over Europe are elevated in industrialized central region and show a poleward decrease in deposition with similar magnitude to the model. Over the Eastern US, the observations likewise show high deposition stretching from Texas to the Mid-Atlantic states, where anthropogenic mercury emissions are largest. At the northern end of this band the model exceeds observations, regardless of oxidant. The models positive bias occurs mainly in winter and can be eliminated by suppressing cold scavenging, as found by Selin and Jacob (2008). But observations indicate that such scavenging occurs (Douglas et al., 2008),

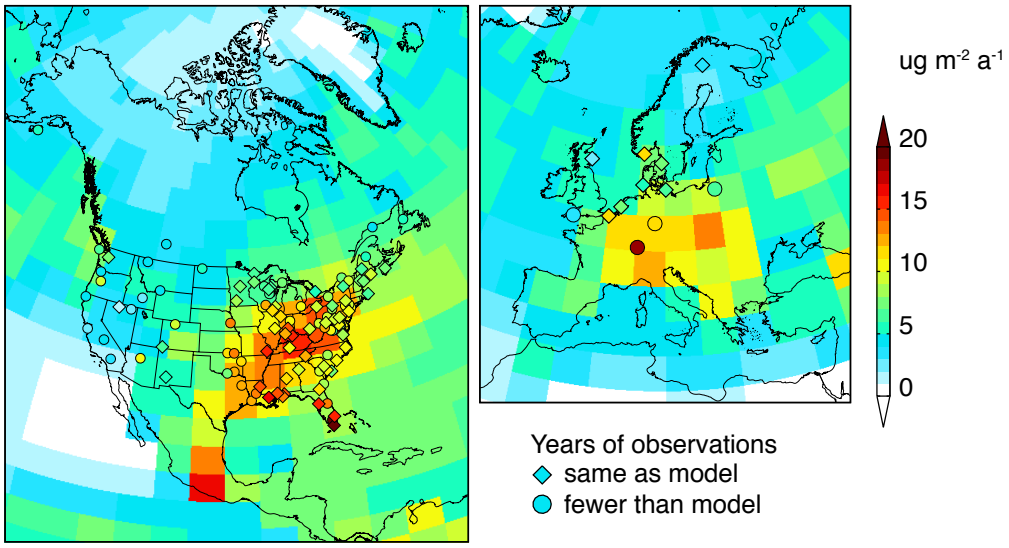

Figure 4.8: Annual mercury wet deposition over North America during 2006-2008 and Europe during 2006-2007 from the Hg+Br model. Overlaid points show observations for the same years from the Mercury Deposition Network (MDN) over North America and from the European Monitoring and Evaluation Programme (EMEP) over Europe.

and suppressing cold scavenging in the model causes 40% underestimates of deposition in Alaska, Alberta and Finland. Fast reduction may compete with near-field deposition as the fate of Hg^{II} emissions. We assume in the model that reduction is photochemical and therefore ineffective in winter, but Edgerton et al. (2006) have observed Hg^{II} reduction in coal-fired power plant plumes in all seasons. Reduction in plumes may decrease wet deposition over the Mid-Atlantic and Midwest emission regions (Lohman et al., 2006; Vijayaraghavan et al., 2008) and will be addressed in future work.

Sites around the Gulf of Mexico report the highest mercury wet deposition in North America, even though regional mercury emissions are lower than in the Northeast US. Convective scavenging of mercury from the free troposphere likely causes this regional feature

(Guentzel et al., 2001; Selin et al., 2008). The Hg+Br model underpredicts wet deposition here by 50%. While the Hg+OH/O_3 model is closer to observations in the northern Gulf region, it is still 40% lower than MDN sites in south Florida. On a monthly basis, both models overlap the observed wet deposition range in the Gulf region during November-May, but only the Hg+OH/O_3 model has a strong deposition peak during the wet summer months, which accounts for its better comparison with the annual mean. During these months OH provides a vigorous subtropical Hg^{II} source available for scavenging in the Hg+OH/O_3 model, while there is little Br present in the Hg+Br model. Since Br concentration used here are likely lower limits on the atmospheric abundance (see Section 4.2.2), we test whether larger concentrations in the subtropics—within the observational constraints on BrO—could supply enough Hg^{II} to match the summer wet deposition. Larger Br and BrO concentrations in the boundary layer and lower free troposphere would be consistent with the RGM diurnal cycle in the subtropical Atlantic (Holmes et al., 2009) and with sea-salt Br_y ventilated from the MBL (Yang et al., 2005). In a sensitivity test, we add 0.5 ppt BrO below 4 km altitude in the subtropical marine atmosphere, and apply the seasonality of bromine release from sea-salt aerosols (Sander et al., 2003). With this change, summertime wet deposition in the Hg+Br model reaches the lower end of observed wet deposition over the Gulf of Mexico with little change elsewhere. Equivalent Hg^0 oxidation could occur at lower BrO levels if several ppt IO is present, which would increase the [Br]/[BrO] beyond Equation 4.2 (Calvert and Lindberg, 2004), although this would likely affect Hg cycling globally.

4.3.5 Aircraft measurements

Figure 4.9 shows mean vertical profiles measured from aircraft by Robert Talbot's group (University of New Hampshire) during the INTEX-B (Singh et al., 2009) and ARCTAS (Jacob et al., 2010) campaigns over North America and the Pacific and Arctic Oceans. Due to uncertain inlet loss of RGM, the measurements include Hg^0 plus some fraction of gaseous Hg^{II} (Talbot et al., 2007, 2008; Mao et al., 2010a). This provides an upper limit for Hg^0 and a lower limit for TGM, and we refer to it here as Hg^{0*}. We increase the INTEX-B measurements by 40% based on an in-flight intercomparison (Swartzendruber et al., 2008). The aircraft data are still ∼10% lower on average than the model, but we focus this analysis on the shape of the vertical profile rather than the absolute values, since the model is unbiased relative to observations at surface sites (Section 4.3.1).

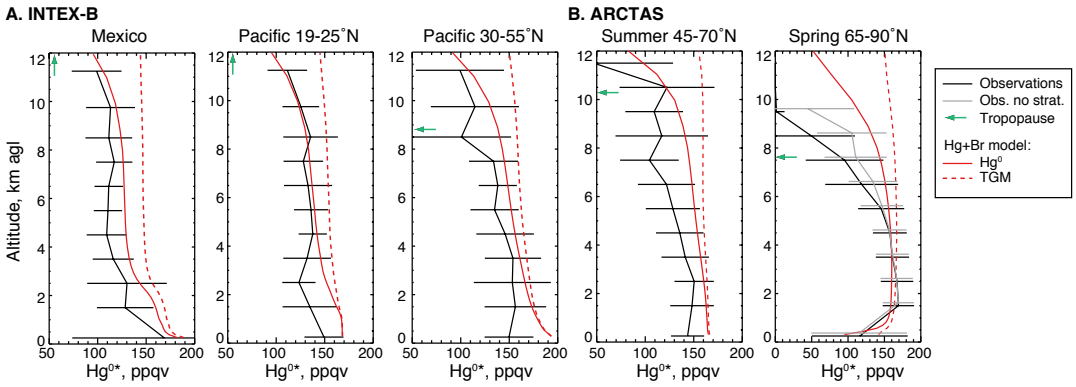

Figure 4.9: Mean vertical profiles and standard deviations of mercury measured by aircraft and compared to model. (A) INTEX-B over Mexico during April 2006 and over the central Pacific Ocean during April-May 2006 (Talbot et al., 2008; Singh et al., 2009). We correct a low bias of 40% in the observations based on an in-flight intercomparison (Swartzendruber et al., 2008). (B) ARCTAS flights in summer 2008 (45-70°N) and spring 2008 (65-90°N) (Jacob et al., 2010; Mao et al., 2010a). Arrows show observed mean tropopause ($O_3 > 100$ ppb). Model results show monthly mean mixing ratios of Hg^0 and TGM simulated over each flight region with the Hg+Br model. Altitudes are above ground level. Note the different horizontal scale in the right panel.

Boundary layer enhancements in the vertical profiles are similar to the model profiles over Mexico, where the aircraft flew mainly near Mexico City and coastal urban areas (Singh et al., 2009), showing consistency with the anthropogenic emission inventory. Marine emissions also drive a small surface enhancement in the subtropical Pacific Ocean that also appears in the model, diluted through a well-mixed 1.5 km deep boundary layer. Conversely, the mid-latitude observations taken in May 2006 over the Pacific show no signs of marine emissions. The model, however, predicts net Hg^0 emissions similar to those observed in the flight region by Laurier et al. (2003) in May 2002 (25 μg m^{-2} d^{-1}), and such large emissions force a surface enhancement that is inconsistent with the aircraft profile. Summer ocean emissions are expected to be much smaller due to slower winds (Soerensen et al., 2010b), so errors in the underlying meteorology may explain the profile discrepancy.

At the highest flight altitudes the observations and model show greater oxidation at high latitudes. This is because Hg^{II} dominates atmospheric mercury in the stratosphere (Selin et al., 2007) and the tropopause descends poleward. In subtropical regions over Mexico and the Pacific Ocean there is no Hg^{0*} decrease in the free troposphere up to 11 km and the slight oxidation in upper levels of the model is within the observed range. Flights in the Pacific midlatitudes and around summer ARCTAS found lower Hg^{0*} at the same altitudes and the model reflects this, but the difference is minimized because these flights occurred in May and July when the tropopause is higher than during the low latitude flights in March and April.

Observations show a much steeper decrease of mercury above the tropopause in the

springtime ARCTAS region than elsewhere. While the model predicts more oxidation in this profile than the others, the observed magnitude is much greater. Complete Hg^{0*} depletions were common during ARCTAS in stratospheric air with $O_3 > 100$ ppb and Hg was rarely detectable when O_3 exceeded 200 ppb, suggesting that oxidation increases abruptly above the tropopause (Talbot et al., 2007; Kim et al., 2009). We test whether additional Br could be responsible by doubling it to levels corresponding to BrO ∼4 ppt above the local instantaneous tropopause in the model. Simulated Hg^0 decreased only 10 ppq at 10 km. Much higher bromine concentrations are unlikely based on satellite observations (Chance, 1998) and constraints on the stratospheric bromine budget (Liang et al., 2010). In another sensitivity test, we added $Hg^0 + BrO \rightarrow Hg^{II}$ to the model ($k_{Hg+BrO} = 10^{-14}$ cm^3 $molecule^{-1}$ s^{-1} Raofie and Ariya, 2004), but this reaction enhanced Hg^0 oxidation throughout the column rather than in the stratosphere primarily.

Other oxidants in the polar stratosphere might include Cl, Cl_2, and BrCl generated from polar aerosol chemistry in the wintertime stratosphere. These oxidation reactions are fast (Ariya et al., 2002; Donohoue et al., 2005) but limited by the low oxidant concentrations. The GMI Aura model predicts mean values of ∼1 ppt ClO in the lowermost stratosphere during spring ARCTAS, corresponding to 0.5 ppq Cl and up to 100 ppt Cl_2 and 30 ppt BrCl (Strahan et al., 2007). Based on the available kinetic data (mainly 298 K), the resulting lifetime of Hg^0 would be exceed 1 year, too long to account for Hg^0 depletion. However, Thornton et al. (2003) observed much greater chlorine activation (∼10 ppt ClO) in the Arctic winter stratosphere than predicted by the GMI model. At these levels, Cl, Cl_2 and

BrCl could become important Hg^0 oxidants.

ARCTAS flights in spring frequently sampled MDEs over the Arctic Ocean, and hydrocarbon measurements aboard the aircraft are consistent with bromine-driven oxidation (Mao et al., 2010a; Kim et al., 2009). The Hg+Br model closely matches the observed mean boundary layer depletion and its shallow vertical extent ($<$ 1 km). Above 2 km the model and observations are typical of mean springtime values for the northern hemisphere.

The Hg+OH/O_3 model predicts very similar vertical profiles to the Hg+Br model in the INTEX-B and ARCTAS flight regions except for MDEs (not shown). Profile measurements in the tropics, however, could distinguish between the oxidation mechanisms. Peak OH concentrations at 3-5 km cause fast Hg^0 oxidation in the OH/O_3 model, while tropical rainfall efficiently scavenges inorganic bromine, suppressing Hg^0 oxidation by Br. The largest differences in the model appear in the wet season over Indonesia where Hg^{II} is 1-3 ppq throughout the troposphere in the Hg+OH/O_3 model, but always $<$ 0.5 ppq in the Hg+Br model.

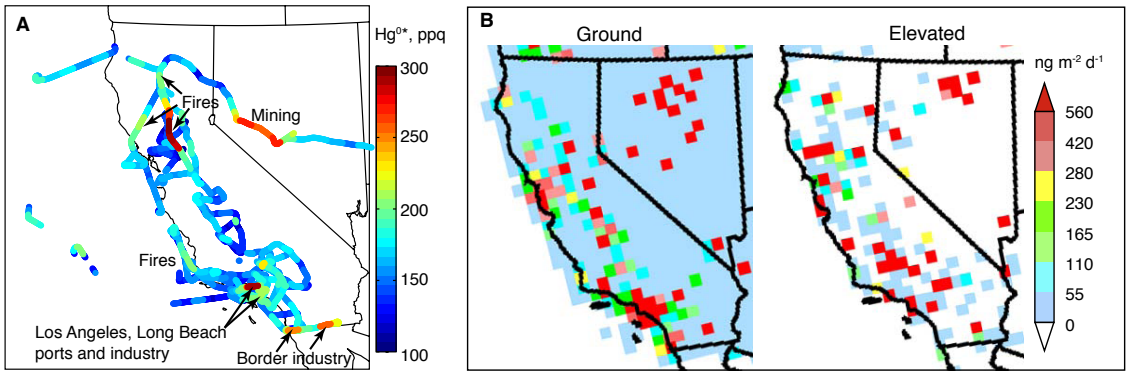

Figure 4.10: (A) Mercury distribution in the boundary layer (<2 km agl) during ARCTAS flights (June 2009). Sources are identified through correlations with other species (CO, O_3, CH_3CN, HCN). (B) EPA anthropogenic emission inventory for 2001 for all mercury species (EPA 2008).

The ARCTAS flights over California (Jacob et al., 2010) provided a first opportunity for detailed boundary layer mapping of a continental source region. These data have not been reported before. Figure 4.10 shows the mercury measurements in the boundary layer ($<$ 2 km). Polluted conditions during these flights caused intermittent low bias in one of the two instrument channels, which we correct by removing the lower value of each consecutive measurement pair. Model results are too coarse to be usefully compared to these observations. The highest concentrations were in biomass burning plumes sampled in both northern and southern California. The three most concentrated plumes had Hg/CO enhancement ratios of 90-130 nmol mol^{-1} and the mean enhancement ratio for all fire plumes (identified by $CH_3CN > 0.25$ ppt) was 80 nmol mol^{-1}. Weiss-Penzias et al. (2007) and Finley et al. (2009) found similar Hg/CO enhancements (136 $\pm$ 60 nmol mol^{-1}) in the Pacific Northwest during summers 2004-5, and Talbot and Mao (2009) found 60 nmol mol^{-1} during summer ARCTAS flights, which are similar to ratios of 70-240 nmol mol^{-1} observed worldwide (Ebinghaus et al., 2007). Based on these measurements, we reduced the Hg/CO emission ratio for biomass burning in GEOS-Chem to 100 nmol mol^{-1} in this work (previously 210 nmol mol^{-1}), although the source is small on a global scale (Figure 4.1).

Apart from the fire plumes, the California observations show highest Hg^{0*} near industry and ports in Los Angeles and Long Beach. Typical concentrations exceeded 200 ppq throughout the Los Angeles basin, following a pattern that closely resembles the emission distribution in the EPA source inventory (EPA 2008). A fresh anthropogenic plume

with high SO2 encountered near the Mexico border does not correspond with any nearby sources in the inventory, suggesting that some industrial emissions in the border region are underestimated. Offshore marine airmasses contained up to 200 ppq Hg^{0*} as well as elevated dimethyl sulfide indicative of ocean emissions. Mercury levels also persisted above 220 ppq for 150 km on a flight over active and inactive mines in western Nevada. These elevated concentrations are typical for summertime at surface sites in Nevada and may result from a mix of mining operations and naturally Hg-enriched soils (Lyman and Gustin, 2008).

4.3.6 Is atmospheric reduction important?

Atmospheric models including Hg^0 oxidation by OH require atmospheric reduction of 4000-10000 Mg a^{-1} Hg^{II} to simulate observed mean surface TGM concentrations and dampen its seasonal cycle (Bergan and Rodhe, 2001; Lin et al., 2006; Seigneur et al., 2006; Selin et al., 2007). Selin et al. (2007) While several reductants are known (see review by Ariya et al., 2008), none have demonstrated global importance. The reported fast oxidation in fresh anthropogenic plumes (Edgerton et al., 2006) is a small contribution to the required global flux (50% reduction in plumes is 350 Mg a^{-1}). Therefore, if OH oxidizes Hg^0, there is an important missing reductant. We test whether atmospheric reduction is necessary within the Hg+Br model in a sensitivity test without atmospheric reduction, and 60% slower overall rate of $Hg^0 + Br + X \rightarrow\rightarrow Hg^{II}$ (X $\equiv$ Br, OH). Slower oxidation could be accommodated within the range of theory-derived kinetic coefficients for the rate-limiting

reaction: $HgBr + X \rightarrow HgBrX$ ($X \equiv$ Br, OH) (Goodsite et al., 2004; Balabanov et al., 2005), or by smaller Br concentrations. The Hg+Br model without reduction produces identical results to the Hg+Br model with reduction in all concentration and deposition comparison tests that we present here. Atmospheric reduction is therefore unnecessary to explain the major features of the global mercury cycle, if Br is the dominant oxidant of Hg^0.

4.4 Global mercury budget

Figure 4.1 shows the global atmospheric mercury budget derived from our updated Hg+Br simulation in GEOS-Chem. This may be compared with budgets based on earlier versions of the model and described by Selin et al. (2008). Emissions and deposition in our Hg+OH/O_3 simulation differ from the Figure by less than 10%. The masses of mercury species in the figure are for the full atmosphere. The troposphere accounts for 99% of total atmospheric Hg^0 but only 50% of Hg^{II}, reflecting the lack of Hg^{II} chemical or depositional loss in the stratosphere (Selin et al., 2007). The Hg^{II} burden in Figure 4.1 includes inert particulate mercury Hg^P but it contributes only 2 Mg. Nearly all redox fluxes occur in the troposphere, as seen in Figure 4.3.

Anthropogenic emissions here are 2050 Mg a^{-1} and total emissions are 8600 Mg a^{-1}, both within the literature range as described in Section 4.2.1. Although the original GEOS-Chem model of Selin et al. (2007) used similar anthropogenic emissions (2200 Mg a^{-1}), Selin et al. (2008) increased these to 3400 Mg a^{-1} to match observed TGM after adding Hg^0 dry deposition to the model. Our model matches observed TGM with smaller emis-

sions because faster reduction here gives a longer atmospheric mercury lifetime—9 vs. 6 months. Atmospheric reduction can be eliminated entirely in the Hg+Br model if the oxidation kinetic coefficients are reduced within their uncertainty, as described in Section 4.3.6. All estimates for TGM lifetime fall within the range of 0.3-1.5 years based on flux measurements (Mason and Sheu, 2002).

The model's terrestrial biosphere emits 1100 Mg a^{-1} from soils plus 260 Mg a^{-1} from prompt recycling of Hg^{II} deposited to vegetation (Selin et al., 2008) and 260 Mg a^{-1} from snow. The total is unchanged from the present-day soil and vegetation emissions from Selin et al. (2008), even though we eliminated mercury evapotranspiration, since it is constrained by preindustrial steady state. Mason (2008) extrapolated field flux measurements to estimate that terrestrial ecosystems emit 1650 Mg a^{-1} (range 860-3800 Mg a^{-1}) including primary geogenic sources but excluding biomass burning. In our model the corresponding emission is 2200 Mg a^{-1}, well within that range.

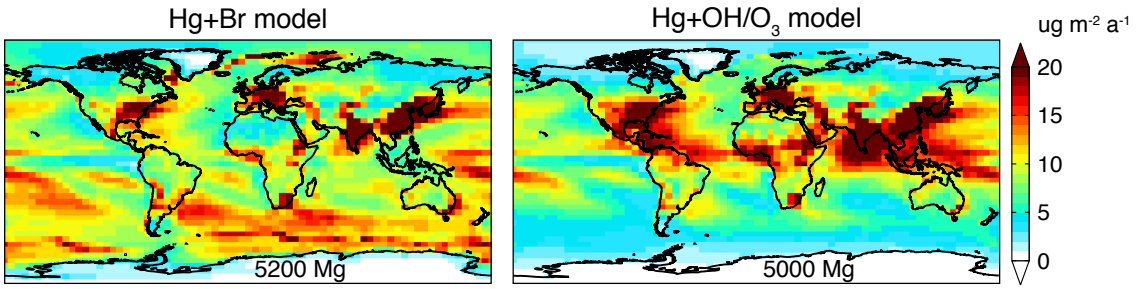

Figure 4.11: Annual deposition flux of Hg^{II} plus Hg^{P} in the Hg+Br and Hg+OH/O_3 models.

Most atmospheric mercury is removed as Hg^{II} (5200 Mg a^{-1}) and the spatial pattern of this deposition appears in Figure 4.11. Wet deposition accounts for 3000 Mg a^{-1} and dry deposition for 800 Mg a^{-1}. Sea-salt aerosols take up an additional 1400 Mg a^{-1} and

this accounts for >90% of Hg^{II} deposition over the oceans. Apart from industrial regions with Hg^{II} and Hg^{P} emissions, the largest dry and aerosol deposition occurs in subtropical subsidence zones that carry Hg^{II} from aloft, as found by Selin et al. (2008). We also predict enhanced Hg^{II} deposition along sea ice margins where Hg^{II} from mercury depletion events advects over open water. Hg^{0} dry deposition (not shown) is 3400 Mg a^{-1}, but emissions offset this so that oceans everywhere are net sources of atmospheric Hg^{0} and land regions are a small net sink (<100 Mg a^{-1}). The deep ocean in the model sequesters 1700 Mg a^{-1} from the atmosphere, similar to the previous GEOS-Chem model (2100 Mg a^{-1}) (Selin et al., 2008).

The Hg+OH/O_3 model generates a very different Hg^{II} deposition pattern from the Hg+Br model, as seen in Figure 4.11, mostly due to changes in wet deposition. With the Hg+OH/O_3 oxidation mechanism, deposition is largest in the tropics where [OH] is greatest and deep convective rain occurs frequently. The Hg+Br model has more significant Hg^{II} deposition in the mid-latitude storm tracks and Arctic due to the oxidation differences seen in Figure 4.3. Despite the large-scale differences, both oxidation mechanisms predict similar wet deposition at monitoring sites in North America and Europe because of the anthropogenic influence (see Section 4.3.4). Selin and Jacob (2008) simulated similar Hg^{II} deposition to our Hg+OH/O_3 model, but with wet deposition more localized to the tropics due to suppressed cold-temperature scavenging in their model. The model contrasts imply that wet deposition measurements in the tropics and southern hemisphere could distinguish between oxidation mechanisms.

4.5 Summary of oxidant effects and conclusion

We have added Hg^0 oxidation by bromine atoms to a global 3-D atmospheric model (GEOS-Chem) to test whether this reaction is consistent with observed atmospheric mercury distribution and deposition. We compare the model performance with Br as the sole oxidant ("Hg+Br model) against a model in which OH and ozone oxidize Hg^0 ("Hg+OH/O_3 model) as found in most other models (e.g. Lin et al., 2006; Seigneur and Lohman, 2008; Selin et al., 2008).

Total emissions here are 8600 Mg a^{-1}, with 2050 Mg a^{-1} from anthropogenic sources (Streets et al., 2009), 300 Mg a^{-1} from biomass burning, 1700 Mg a^{-1} from terrestrial ecosystems, 3800 Mg a^{-1} from oceans, and 500 Mg a^{-1} geogenic. We update the light-dependence of soil emission to fit the observed TGM seasonal cycle and reduce the Hg/CO emission ratio in biomass burning based on ARCTAS data presented here. A new snowpack reservoir stores deposited mercury and reemits it under sunlight at a temperature-dependent rate. The seasonal cycle of Arctic Hg^0 implies that 60% of mercury deposited to snow is eventually reemitted (230 Mg a^{-1}) and 150 Mg a^{-1} transfers to the ocean and soils.

Hg+Br kinetics here follow Goodsite et al. (2004) and Donohoue et al. (2006), while Hg+OH/O_3 kinetics are identical to Selin et al. (2008). Global bromine distributions are specified monthly by merging Br simulations from tropospheric and stratospheric chemistry models (p-TOMCAT and GMI: Yang et al., 2005; Strahan et al., 2007). These models are constrained by biogenic and halon precursor gas measurements, and give a lower limit for Br in the free troposphere because they assume no contribution from sea-salt bromide

and no Br_y recycling on aerosols. We also specify observed BrO concentrations in the marine boundary layer and under conditions supporting polar mercury depletion events, then calculate the associated [Br] from photochemical steady state. BrO columns in our model fall in the range observed from satellites ($1-4\times10^{13}$ cm^{-2}). Hg^0 has a 6 month chemical lifetime in the Hg+Br model and a 3.7 month lifetime in the Hg+OH/O_3 model. Both mechanisms require Hg^{II} reduction to raise the TGM lifetime to 9 months and match observations, so we include UV photoreduction in cloud water. However, we find that atmospheric reduction is unnecessary if the rate coefficients for Hg+Br reactions are reduced within their published range.

We also update Hg^{II} sink processes with a new parameterization of Hg^{II} uptake and deposition through sea-salt aerosol and include Hg^{II} and Hg^{P} scavenging by snow and rime ice, as observed in field studies. Wet and dry deposition processes in the model now assume that Hg^{II} partitions evenly between gas and aerosol phases, which prolongs the Hg^{II} atmospheric lifetime compared to the previous model assuming all Hg^{II} as gas.

The Hg+Br model provides an unbiased simulation of TGM surface concentration at land sites and accounts for most spatial variance ($r^2 = 0.88$). Anthropogenic emissions drive these features, so the Hg+OH/O_3 model performs similarly. The Hg+Br model is consistent with the interhemispheric gradient of TGM, which contradicts an earlier study that argued that Hg^0 oxidation by Br only would generate an unrealistic tropical Hg^0 maximum (Seigneur and Lohman, 2008). We attribute the difference to a systematic overestimate of high-latitude tropospheric Br in their satellite-derived distribution.

TGM seasonal cycles are also consistent with the Hg+Br model. In the Arctic, high bromine concentrations in spring deplete atmospheric mercury and enrich the snowpack in both observations and the Hg+Br model. The following summer maximum is best fit if 60% of deposited mercury is eventually reemitted. Higher reemission fractions lead to unrealistic high summer concentrations. This implies 40% of deposition to snow (110 Mg a^{-1} inside the Arctic Circle) transfers to soils and the ocean.

Subsidence events over Antarctica in summer provide the clearest test for oxidation mechanisms, because the cold, dry environment prevents aqueous reduction. The $\Delta Hg^0/\Delta O_3$ and $\Delta RGM/\Delta O_3$ ratios in these events show strong oxidation aloft (Sprovieri et al., 2002; Temme et al., 2003) that are similar to the Hg+Br model, while the Hg+OH/O_3 model underpredicts oxidation by a factor of 2.

Wet deposition observations show enhanced deposition near anthropogenic Hg^{II} and Hg^{P} in Central Europe and Eastern North America that are present in the model. Deposition overestimates in the Northeast US may be due to reduction within concentrated plumes from coal-fired power plants (Edgerton et al., 2006), which future work will address. The Hg+Br model initially underestimated deposition near the Gulf of Mexico in summer by 30%, while the Hg+OH/O_3 model matches the seasonality well due to vigorous Hg^{II} production by OH in summer. If some Br from sea-salt were in the free troposphere, equivalent to 0.5 ppt BrO, then the Hg+Br model would match the lower range of observed wet deposition along the Gulf. Less BrO would be required if several ppt IO were present, although this would affect Hg^0 oxidation globally.

Aircraft vertical profiles from ARCTAS and INTEX-B show increasing Hg^0 oxidation with altitude and latitude, and the Hg+Br model is quantitatively consistent with these trends outside polar regions. Arctic profiles, however, show pervasive and complete Hg^0 oxidation in the lower stratosphere in spring that the model does not reproduce. Neither Br nor BrO can explain these features within the limits on their abundance, but Cl, Cl_2 and BrCl within the winter vortex at levels of chlorine activation reported by Thornton et al. (2003) might account for the Hg^0 oxidation. Boundary layer surveys during ARCTAS over California support the EPA emission distribution, with some evidence for additional mercury emissions near the Mexican border and from mines in Nevada. Biomass burning plumes exhibit Hg/CO enhancement ratios of 80–130 nmol mol^{-1}, similar to previous findings in the region and elsewhere.

Mercury deposition occurs mainly as Hg^{II}, with 3000 Mg a^{-1} from wet deposition, 800 Mg a^{-1} from dry deposition and 1400 Mg a^{-1} through sea-salt aerosol uptake. The deposition pattern in the Hg+Br model differs significantly from the Hg+OH/O_3 model and from Selin et al. (2008), although the differences lie outside of the mid-latitude regions with observations. The Hg+OH/O_3 model gives a strong deposition peak in the tropics due to the OH concentrations while the Hg+Br mechanism has a more even latitudinal distribution that results 2-3 times greater deposition in the mid-latitude storm tracks.

Our results show that bromine is an important global oxidant for Hg^0, producing a $\sim$6 month lifetime and TGM distribution consistent with available observations. Most reaction occurs in the free troposphere where Br concentrations here are lower limits based

on observed source gas abundance and well-known chemistry of Br_y. Given the uncertainty about whether OH and O_3 can oxidize Hg^0 under environmental conditions, and the lack of any mercury observations requiring them, Br may be the dominant global oxidant of Hg^0. If Br is dominant, then atmospheric reduction, for which there is no accepted mechanism, is unnecessary. The largest model differences between oxidation mechanisms arise in the tropics, so measurements there could clarify mercury redox chemistry.

Bibliography

Ababneh, F. A., Scott, S. L., Al-Reasi, H. A., and Lean, D. R. S. (2006). Photochemical reduction and reoxidation of aqueous mercuric chloride in the presence of ferrioxalate and air. *Sci Total Environ*, 367(2-3):831–839.

Ariya, P., Dastoor, A., Amyot, M., Schroeder, W., Barrie, L., Anlauf, K., Raofie, F., Ryzhkov, A., Davignon, D., Lalonde, J., and Steffen, A. (2004). The Arctic: a sink for mercury. *Tellus Series B*, 56(5):397–403.

Ariya, P. A., Khalizov, A., and Gidas, A. (2002). Reactions of gaseous mercury with atomic and molecular halogens: Kinetics, product studies, and atmospheric implications. *J Phys Chem A*, 106(32):7310–7320.

Ariya, P. A., Skov, H., Grage, M. M. L., and Goodsite, M. E. (2008). Gaseous elemental mercury in the ambient atmosphere: Review of the application of theoretical calculations and experimental studies for determination of reaction coefficients and mechanisms with halogens and other reactants. *Adv Quantum Chem*, 55:43–55.

Aspmo, K. and Berg, T. (2009). "Long-term" Antarctic measurements of atmospheric mercury. In *9th International Conference on Mercury as a Global Pollutant*, Guiyang, China.

Balabanov, N., Shepler, B., and Peterson, K. (2005). Accurate global potential energy surface and reaction dynamics for the ground state of HgBr2. *J Phys Chem A*, 109(39):8765–8773.

Bergan, T. and Rodhe, H. (2001). Oxidation of elemental mercury in the atmosphere; constraints imposed by global scale modelling. *J Atmos Chem*, 40(2):191–212.

Brooks, S., Arimoto, R., Lindberg, S., and Southworth, G. (2008). Antarctic polar plateau snow surface conversion of deposited oxidized mercury to gaseous elemental mercury with fractional long-term burial. *Atmos Environ*, 42(12):2877–2884.

Brooks, S., Saiz-Lopez, A., Skov, H., Lindberg, S., Plane, J., and Goodsite, M. (2006). The mass balance of mercury in the springtime Arctic environment. *Geophys Res Lett*, 33(13):L13812.

Bullock, O. R., Atkinson, D., Braverman, T., Civerolo, K., Dastoor, A., Davignon, D., Ku, J.-Y., Lohman, K., Myers, T. C., Park, R. J., Seigneur, C., Selin, N. E., Sistla, G., and Vijayaraghavan, K. (2009). An analysis of simulated wet deposition of mercury from the north american mercury model intercomparison study. *J Geophys Res*, 114:D08301.

Burrows, J., Weber, M., Buchwitz, M., Rozanov, V., Ladstatter-Weissenmayer, A., Richter, A., DeBeek, R., Hoogen, R., Bramstedt, K., Eichmann, K., and Eisinger, M. (1999). The global ozone monitoring experiment (GOME): Mission concept and first scientific results. *J Atmos Sci*, 56(2):151–175.

Butler, T. J., Cohen, M. D., Vermeylen, F. M., Likens, G. E., Schmeltz, D., and Artz, R. S. (2008). Regional precipitation mercury trends in the eastern USA, 1998-2005: Declines in the Northeast and Midwest, no trend in the Southeast. *Atmos Environ*, 42(7):1582–1592.

Caldwell, C., Swartzendruber, P., and Prestbo, E. (2006). Concentration and dry deposition of mercury species in arid south central New Mexico (2001-2002). *Environ Sci Technol*, 40(24):7535–7540.

Calvert, J. and Lindberg, S. (2004). The potential influence of iodine-containing compounds on the chemistry of the troposphere in the polar spring. II. mercury depletion. *Atmos Environ*, 38(30):5105–5116.

Calvert, J. and Lindberg, S. (2005). Mechanisms of mercury removal by O-3 and OH in the atmosphere. *Atmos Environ*, 39(18):3355–3367.

Chance, K. (1998). Analysis of BrO measurements from the Global Ozone Monitoring Experiment. *Geophysical Research Letters*, 25(17):3335–3338.

Choi, H.-D., Holsen, T. M., and Hopke, P. K. (2008). Atmospheric mercury (Hg) in the Adirondacks: Concentrations and sources. *Environ Sci Technol*, 42(15):5644–5653.

Cobbett, F. D., Steffen, A., Lawson, G., and Heyst, B. J. V. (2007). GEM fluxes and atmospheric mercury concentrations (GEM, RGM and Hg-P) in the Canadian Arctic at Alert, Nunavut, Canada (February-June 2005). *Atmos Environ*, 41(31):6527–6543.

Cohen, M., Artz, R., Draxler, R., Miller, P., Poissant, L., Niemi, D., Ratte, D., Deslauriers, M., Duval, R., Laurin, R., Slotnick, J., Nettesheim, T., and McDonald, J. (2004). Modeling the atmospheric transport and deposition of mercury to the Great Lakes. *Environmental Research*, 95(3):247–265.

Dastoor, A. P., Davignon, D., Theys, N., Roozendael, M. V., Steffen, A., and Ariya, P. A. (2008). Modeling dynamic exchange of gaseous elemental mercury at polar sunrise. *Environ Sci Technol*, 42(14):5183–5188.

Dommergue, A., Ferrari, C., Gauchard, P., Boutron, C., Poissant, L., Pilote, M., Jitaru, P., and Adams, F. (2003). The fate of mercury species in a sub-Arctic snowpack during snowmelt. *Geophysical Research Letters*, 30(12):1621.

Donohoue, D., Bauer, D., Cossairt, B., and Hynes, A. (2006). Temperature and pressure dependent rate coefficients for the reaction of Hg with Br and the reaction of Br with Br: A pulsed laser photolysis-pulsed laser induced fluorescence study. *J Phys Chem A*, 110(21):6623–6632.

Donohoue, D., Bauer, D., and Hynes, A. (2005). Temperature and pressure dependent rate coefficients for the reaction of Hg with Cl and the reaction of Cl with Cl: A pulsed laser photolysis-pulsed laser induced fluorescence study. *J Phys Chem A*, 109(34):7732–7741.

Douglas, T. A., Sturm, M., Simpson, W. R., Blum, J. D., Alvarez-Aviles, L., Keeler, G. J., Perovich, D. K., Biswas, A., and Johnson, K. (2008). Influence of snow and ice crystal formation and accumulation on mercury deposition to the Arctic. *Environ Sci Technol*, 42(5):1542–1551.

Douglass, A., Stolarski, R., Strahan, S., and Connell, P. (2004). Radicals and reservoirs in the GMI chemistry and transport model: Comparison to measurements. *J Geophys Res*, 109(D16):D16302.

Ebinghaus, R., Slemr, F., Brenninkmeijer, C. A. M., van Velthoven, P., Zahn, A., Hermann, M., O'Sullivan, D. A., and Oram, D. E. (2007). Emissions of gaseous mercury from biomass burning in South America in 2005 observed during CARIBIC flights. *Geophysical Research Letters*, 34(8):L08813.

Edgerton, E. S., Hartsell, B. E., and Jansen, J. J. (2006). Mercury speciation in coal-fired power plant plumes observed at three surface sites in the southeastern us. *Environ Sci Technol*, 40(15):4563–4570.

EMEP: European Monitoring and Evaluation Programme (2009). Co-operative programme for monitoring and evaluation of the long-range transmissions of air pollutants in Europe. http://tarantula.nilu.no/projects/ccc/emepdata.html.

EPA: US Environmental Protection Agency, Office of Wetlands, Oceans and Watersheds, Watershed Branch, (2008). Model-based analysis and tracking of airborne mercury emissions to assist in watershed planning. http://www.epa.gov/owow/tmdl/pdf/final300report_10072008.pdf.

Fain, X., Ferrari, C. P., Dommergue, A., Albert, M., Battle, M., Arnaud, L., Barnola, J. M., Cairns, W., Barbante, C., and Boutron, C. (2008). Mercury in the snow and firn at Summit Station, Central Greenland, and implications for the study of past atmospheric mercury levels. *Atmos Chem Phys*, 8(13):3441–3457.

Fain, X., Grangeon, S., Bahlmann, E., Fritsche, J., Obrist, D., Dommergue, A., Ferrari, C. P., Cairns, W., Ebinghaus, R., Barbante, C., Cescon, P., and Boutron, C. (2007). Diurnal production of gaseous mercury in the alpine snowpack before snowmelt. *J Geophys Res*, 112(D21):D21311.

Feng, J. (2009). A size-resolved model for below-cloud scavenging of aerosols by snowfall. *J Geophys Res*, 114:D08203.

Feng, X., Wang, S., Qiu, G., He, T., Li, G., Li, Z., and Shang, L. (2008). Total gaseous mercury exchange between water and air during cloudy weather conditions over Hongfeng Reservoir, Guizhou, China. *Journal of Geophysical Research-Atmospheres*, 113(D15):D15309.

Finley, B. D., Swartzendruber, P. C., and Jaffe, D. A. (2009). Particulate mercury emissions in regional wildfire plumes observed at the mount bachelor observatory. *Atmos Environ*, 43(38):6074–6083.

Gårdfeldt, K. and Jonsson, M. (2003). Is bimolecular reduction of Hg(II) complexes possible in aqueous systems of environmental importance. *J Phys Chem A*, 107(22):4478–4482.

Goodsite, M., Plane, J., and Skov, H. (2004). A theoretical study of the oxidation of Hg-0 to HgBr2 in the troposphere. *Environ Sci Technol*, 38(6):1772–1776.

Guentzel, J., Landing, W., Gill, G., and Pollman, C. (2001). Processes influencing rainfall deposition of mercury in florida. *Environ Sci Technol*, 35(5):863–873.

Gusev, A., Illiyn, I., Rozovskaya, O., Shatalov, V., Sokovych, V., and Travnikov, O. (2009). Modelling of heavy metals and persistent organic pollutants: New developments. Technical report, EMEP/MSC-E.

Gustin, M., Ericksen, J., Schorran, D., Johnson, D., Lindberg, S., and Coleman, J. (2004). Application of controlled mesocosms for understanding mercury air-soil-plant exchange. *Environ Sci Technol*, 38(22):6044–6050.

Hall, B. (1995). The gas phase oxidation of elemental mercury by ozone. *Water, Air, and Soil Pollution*, 80:301–315.

Hedgecock, I. and Pirrone, N. (2001). Mercury and photochemistry in the marine boundary layer-modelling studies suggest the in situ production of reactive gas phase mercury. *Atmos Environ*, 35(17):3055–3062.

Hedgecock, I., Trunfio, G., Pirrone, N., and Sprovieri, F. (2005). Mercury chemistry in the MBL: Mediterranean case and sensitivity studies using the AMCOTS (Atmospheric Mercury Chemistry over the Sea) model. *Atmos Environ*, 39(38):7217–7230.

Holmes, C., Jacob, D., and Yang, X. (2006). Global lifetime of elemental mercury against oxidation by atomic bromine in the free troposphere. *Geophysical Research Letters*, 33(20):L20808.

Holmes, C. D., Jacob, D. J., Mason, R. P., and Jaffe, D. A. (2009). Sources and deposition of reactive gaseous mercury in the marine atmosphere. *Atmos Environ*, 43(14):2278–2285.

Hynes, A., Donohoue, D., Goodsite, M., Hedgecock, I., Pirrone, N., and Mason, R. (2008). Our current understanding of major chemical and physical processes affecting mercury dynamics in the atmosphere and at air-water/terrestrial interfaces. In *Mercury Fate and Transport in the Global Atmosphere*. United Nations Environment Programme.

Jacob, D. J., Crawford, J. H., Maring, H., Clarke, A. D., Dibb, J. E., Ferrare, R. A., Hostetler, C. A., Russell, P. B., Singh, H. B., Thompson, A. M., Shaw, G. E., McCauley, E., Pederson, J. R., and Fisher, J. A. (2010). The ARCTAS aircraft mission: design and execution. *Atmos Phys Chem Discuss*.

Jaffe, D., Prestbo, E., Swartzendruber, P., Weiss-Penzias, P., Kato, S., Takami, A., Hatakeyama, S., and Kajii, Y. (2005). Export of atmospheric mercury from Asia. *Atmos Environ*, 39(17):3029–3038.

Johnson, K. P., Blum, J. D., Keeler, G. J., and Douglas, T. A. (2008). Investigation of the deposition and emission of mercury in arctic snow during an atmospheric mercury depletion event. *J Geophys Res*, 113(D17):D17304.

Kim, S., Talbot, R. W., and Mao, H. (2009). 2009. *Eos Transactions, Fall Meeting Suppl*, 90(52):A43A–0190.

Kirk, J. L., Louis, V. L. S., and Sharp, M. J. (2006). Rapid reduction and reemission of mercury deposited into snowpacks during atmospheric mercury depletion events at Churchill, Manitoba, Canada. *Environ Sci Technol*, 40(24):7590–7596.

Lamborg, C., Fitzgerald, W., O'Donnell, J., and Torgersen, T. (2002). A non-steady-state compartmental model of global-scale mercury biogeochemistry with interhemispheric atmospheric gradients. *Geochimica et Cosmochimica Acta*, 66(7):1105–1118.

Lamborg, C., Rolfhus, K., Fitzgerald, W., and Kim, G. (1999). The atmospheric cycling and air-sea exchange of mercury species in the South and equatorial Atlantic Ocean. *Deep-sea Research II*, 46:957–977.

Laurier, F. and Mason, R. (2007). Mercury concentration and speciation in the coastal and open ocean boundary layer. *J Geophys Res*, 112(D6):D06302.

Laurier, F., Mason, R., Whalin, L., and Kato, S. (2003). Reactive gaseous mercury formation in the North Pacific Ocean's marine boundary layer: A potential role of halogen chemistry. *J Geophys Res*, 108(D17):4529.

Leser, H., Honninger, G., and Platt, U. (2003). MAX-DOAS measurements of BrO and NO2 in the marine boundary layer. *Geophysical Research Letters*, 30(10):1537.

Liang, Q., Stolarski, R. S., Kawa, S. R., Nielsen, J. E., Douglass, A. R., Rodriguez, J. M., Blake, D. R., Atlas, E. L., and Ott, L. E. (2010). Finding the missing stratospheric Br-y: a global modeling study of CHBr3 and CH2Br2. *Atmos Chem Phys*, 10(5):2269–2286.

Lin, C., Pongprueksa, P., Lindberg, S., Pehkonen, S., Byun, D., and Jang, C. (2006). Scientific uncertainties in atmospheric mercury models I: Model science evaluation. *Atmos Environ*, 40(16):2911–2928.

Lin, J.-T. and McElroy, M. (2010). Impacts of boundary layer mixing on pollutant vertical profiles in the lower troposphere: Implications to satellite remote sensing. accepted.

Lindberg, S., Bullock, R., Ebinghaus, R., Engstrom, D., Feng, X., Fitzgerald, W., Pirrone, N., Prestbo, E., and Seigneur, C. (2007). A synthesis of progress and uncertainties in attributing the sources of mercury in deposition. *Ambio*, 36(1):19–32.

Lindqvist, O. and Rodhe, H. (1985). Atmospheric mercury - a review. *Tellus Series B*, 37(3):136–159.

Liu, B., Keeler, G. J., Dvonch, J. T., Barres, J. A., Lynam, M. M., Marsik, F. J., and Morgan, J. T. (2007). Temporal variability of mercury speciation in urban air. *Atmos Environ*, 41(9):1911–1923.

Liu, H., Jacob, D., Bey, I., and Yantosca, R. (2001). Constraints from Pb-210 and Be-7 on wet deposition and transport in a global three-dimensional chemical tracer model driven by assimilated meteorological fields. *J Geophys Res*, 106(D11):12109–12128.

Lohman, K., Seigneur, C., Edgerton, E., and Jansen, J. (2006). Modeling mercury in power plant plumes. *Environ Sci Technol*, 40(12):3848–3854.

Lyman, S. N. and Gustin, M. S. (2008). Speciation of atmospheric mercury at two sites in northern Nevada, USA. *Atmos Environ*, 42(5):927–939.

MacKenzie, D. (2009). Seasonal variations in the mixing layer in the UTLS. In *GEOS-Chem User's Meeting*, Cambridge, MA USA.

Mao, H., Talbot, R. W., Sigler, J. M., Sive, B. C., and Hegarty, J. D. (2008). Seasonal and diurnal variations of Hg0 over New England. *Atmos Chem Phys*, 8(5):1403–1421.

Mao, H., Talbot, R. W., Sive, B. C., Kim, S.-Y., Blake, D. R., and Weinheimer, A. J. (2010a). Arctic mercury depletion and its quantitative link with halogens. *Atmos Phys Chem Discuss*.

Mao, J., Jacob, D. J., Evans, M. J., Olson, J. R., Ren, X., Brune, W. H., St. Clair, J. M., Crounse, J. D., Spencer, K. M., Beaver, M. R., Wennberg, P. O., Cubison, M. J., Jimenez, J. L., Fried, A., Weibring, P., Walega, J. G., Hall, S. R., Weinheimer, A. J., Cohen, R. C., Chen, G., Crawford, J. H., Jaeglé, L., Fisher, J. A., Yantosca, R. M., Le Sager, P., and Carouge, C. (2010b). Chemistry of hydrogen oxide radicals (HOx) in the Arctic troposphere in spring. in review.

Martin, M., Poehler, D., Seitz, K., Sinreich, R., and Platt, U. (2009). BrO measurements over the Eastern North-Atlantic. *Atmos Chem Phys*, 9(24):9545–9554.

Mason, R. and Sheu, G. (2002). Role of the ocean in the global mercury cycle. *Global Biogeochem. Cycles*, 16(4):1093.

Mason, R. P. (2008). Mercury emissions from natural processes and their importance in the global mercury cycle. In Pirrone, N. and Mason, R. P., editors, *Mercury Fate and Transport in the Global Atmosphere*, chapter 7. United Nations Environment Programme.

Murakami, M., Kimura, T., Magono, C., and Kikuchi, K. (1983). Observations of precipitation scavenging for water-soluble particles. *J Meteorol Soc Jpn*, 61(3):346–358.

National Atmospheric Deposition Program (2009). Mercury Deposition Network (MDN): A NADP Network. http://nadp.sws.uiuc.edu/MDN/.

Nguyen, H. T., Kim, K.-H., Kim, M.-Y., Hong, S., Youn, Y.-H., Shon, Z.-H., and Lee, J. S. (2007). Monitoring of atmospheric mercury at a global atmospheric watch (GAW) site on An-Myun Island, Korea. *Water Air Soil Poll*, 185(1-4):149–164.

O'Brien, L., Harris, N., Robinson, A., Gostlow, B., Warwick, N., Yang, X., and Pyle, J. (2009). Bromocarbons in the tropical marine boundary layer at the Cape Verde Observatory – measurements and modelling. *Atmos Phys Chem Discuss*, 9:4335–4379.

Pacyna, E. G., Pacyna, J. M., Steenhuisen, F., and Wilson, S. (2006). Global anthropogenic mercury emission inventory for 2000. *Atmos Environ*, 40(22):4048–4063.

Pacyna, J. M., Pacyna, E. G., and Aas, W. (2009). Changes of emissions and atmospheric deposition of mercury, lead, and cadmium. *Atmos Environ*, 43(1):117–127.

Park, R., Jacob, D., Field, B., Yantosca, R., and Chin, M. (2004). Natural and transboundary pollution influences on sulfate-nitrate-ammonium aerosols in the United States: implications for policy. *J Geophys Res*, 109:D15204.

Parrella, J. P. (2010). The impact of bromine on background tropospheric ozone concentrations. in preparation.

Pehkonen, S. and Lin, C. (1998). Aqueous photochemistry of mercury with organic acids. *Journal of the Air & Waste Management Association*, 48(2):144–150.

Petersen, G., Bloxam, R., Wong, S., Munthe, J., Kruger, O., Schmolke, S., and Kumar, A. (2001). A comprehensive eulerian modelling framework for airborne mercury species: model development and applications in Europe. *Atmos Environ*, 35(17):3063–3074.

Peterson, C., Gustin, M., and Lyman, S. (2009). Atmospheric mercury concentrations and speciation measured from 2004 to 2007 in Reno, Nevada, USA. *Atmos Environ*, 43(30):4646–4654.

Pirrone, N., Cinnirella, S., Feng, X., Finkelman, R. B., Friedli, H. R., Leaner, J., Mason, R., Mukherjee, A. B., Stracher, G. B., Streets, D. G., and Telmer, K. (2010). Global mercury emissions to the atmosphere from anthropogenic and natural sources. *Atmos Phys Chem Discuss*, 10:4719–4752.

Platt, U. and Janssen, C. (1995). Observation and role of the free radicals NO_3, ClO, BrO and IO in the troposphere. *Faraday Discussions*, 100:175–198.

Pongprueksa, P., Lin, C.-J., Lindberg, S. E., Jang, C., Braverman, T., Bullock, O. R., Ho, T. C., and wei Chu, H. (2008). Scientific uncertainties in atmospheric mercury models III: boundary and initial conditions, model grid resolution, and Hg(II) reduction mechanism. *Atmos Environ*, 42(8):1828–1845.

Prestbo, E. M. and Gay, D. A. (2009). Wet deposition of mercury in the US and Canada, 1996-2005: Results and analysis of the NADP mercury deposition network (MDN). *Atmos Environ*, 43(27):4223–4233.

Pszenny, A., Moldanov, J., Keene, W., Sander, R., Maben, J., Martinez, M., Crutzen, P., Perner, D., and Prinn, R. (2004). Halogen cycling and aerosol pH in the Hawaiian marine boundary layer. *Atmos Chem Phys*, 4:147–168.

Pundt, I., Pommereau, J., Chipperfield, M., Roozendael, M. V., and Goutail, F. (2002). Climatology of the stratospheric BrO vertical distribution by balloon-borne UV-visible spectrometry. *J Geophys Res*, 107(D24):4806.

Raofie, F. and Ariya, P. (2004). Product study of the gas-phase BrO-initiated oxidation of Hg-0: evidence for stable Hg1+ compounds. *Environ Sci Technol*, 38(16):4319–4326.

Richter, A., Wittrock, F., Ladstatter-Weissenmayer, A., and Burrows, J. (2002). GOME measurements of stratospheric and tropospheric BrO. *Advances in Space Research*, 29(11):1667–1672.

Rutter, A. P. and Schauer, J. J. (2007a). The effect of temperature on the gas-particle partitioning of reactive mercury in atmospheric aerosols. *Atmos Environ*, 41(38):8647–8657.

Rutter, A. P. and Schauer, J. J. (2007b). The impact of aerosol composition on the particle to gas partitioning of reactive mercury. *Environ Sci Technol*, 41(11):3934–3939.

Saiz-Lopez, A., Plane, J., and Shillito, J. (2004). Bromine oxide in the mid-latitude marine boundary layer. *Geophysical Research Letters*, 31(3):L03111.

Sakata, M. and Asakura, K. (2007). Estimating contribution of precipitation scavenging of atmospheric particulate mercury to mercury wet deposition in Japan. *Atmos Environ*, 41(8):1669–1680.

Salawitch, R., Weisenstein, D., Kovalenko, L., Sioris, C., Wennberg, P., Chance, K., Ko, M., and McLinden, C. (2005). Sensitivity of ozone to bromine in the lower stratosphere. *Geophysical Research Letters*, 32(5):L05811.

Salawitch, R. J., Canty, T. P., Kurosu, T. P., Chance, K., Liang, Q., Pawson, S., Liu, X., Huey, G., Liao, J., Stickel, R. E., Tanner, D., Dibb, J. E., Weinheimer, A. J., Flock, F. M., Knapp, D. J., Dmontzka, D. D., Neuman, J., Simpson, W. R., Donohoue, D., Carlson, D., Blake, D. R., Kinnison, D. E., Tilmes, S., Pan, L., , Pierce, R., Hendrick, F., Kreher, K., Wang, Y., Choi, S., and Atlas, E. L. (2009). Airborne, ground-based, and satellite measurements of BrO during ARCTAS and ARCPAC. *Eos Transactions, Fall Meeting Suppl*, 90(52):A32B–07.

Sander, R., Keene, W., Pszenny, A., Arimoto, R., Ayers, G., Baboukas, E., Cainey, J., Crutzen, P., Duce, R., Honninger, G., Huebert, B., Maenhaut, W., Mihalopoulos, N., Turekian, V., and Dingenen, R. V. (2003). Inorganic bromine in the marine boundary layer: a critical review. *Atmos Chem Phys*, 3(D17):1301–1336.

Sander, S. P., Ravishankara, A. R., Golden, D. M., Kolb, C. E., Kurylo, M. J., Molina, M. J., Moortgat, G. K., Finlayson-Pitts, B. J., Wine, P. H., and Huie, R. E. (2006). Chemical kinetics and photochemical data for use in atmospheric studies: Evaluation number 15. Technical report, NASA Panel for Data Evaluation.

Seigneur, C. and Lohman, K. (2008). Effect of bromine chemistry on the atmospheric mercury cycle. *J Geophys Res*, 113:D23309.

Seigneur, C., Vijayaraghavan, K., and Lohman, K. (2006). Atmospheric mercury chemistry: Sensitivity of global model simulations to chemical reactions. *J Geophys Res*, 111(D22).

Selin, N. E. and Jacob, D. J. (2008). Seasonal and spatial patterns of mercury wet deposition in the united states: Constraints on the contribution from north american anthropogenic sources. *Atmos Environ*, 42(21):5193–5204.

Selin, N. E., Jacob, D. J., Park, R. J., Yantosca, R. M., Strode, S., Jaeglé, L., and Jaffe, D. (2007). Chemical cycling and deposition of atmospheric mercury: Global constraints from observations. *J Geophys Res*, 112(D2):1–14.

Selin, N. E., Jacob, D. J., Yantosca, R. M., Strode, S., Jaeglé, L., and Sunderland, E. M. (2008). Global 3-D land-ocean-atmosphere model for mercury: Present-day versus preindustrial cycles and anthropogenic enrichment factors for deposition. *Global Biogeochem. Cycles*, 22(2):1–13.

Shia, R., Seigneur, C., Pai, P., Ko, M., and Sze, N. (1999). Global simulation of atmospheric mercury concentrations and deposition fluxes. *J Geophys Res*, 104(D19):23747–23760.

Si, L. and Ariya, P. A. (2008). Reduction of oxidized mercury species by dicarboxylic acids (C-2-C-4): Kinetic and product studies. *Environ Sci Technol*, 42(14):5150–5155.

Sigler, J. M., Mao, H., and Talbot, R. (2009). Gaseous elemental and reactive mercury in Southern New Hampshire. *Atmos Chem Phys*, 9(6):1929–1942.

Simpson, W., von Glasow, R., Riedel, K., Anderson, P., Ariya, P., Bottenheim, J., Burrows, J., Carpenter, L., Friess, U., Goodsite, M., Heard, D., Hutterli, M., Jacobi, H., Kaleschke, L., Neff, B., Plane, J., Platt, U., Richter, A., Roscoe, H., Sander, R., Shepson, P., Sodeau, J., Steffen, A., Wagner, T., and Wolff, E. (2007). Halogens and their role in polar boundary-layer ozone depletion. *Atmos Chem Phys*, 7:4375–4418.

Singh, H. B., Brune, W. H., Crawford, J. H., Flocke, F., and Jacob, D. J. (2009). Chemistry and transport of pollution over the Gulf of Mexico and the Pacific: spring 2006 INTEX-B campaign overview and first results. *Atmos Chem Phys*, 9(7):2301–2318.

Sinnhuber, B., Rozanov, A., Sheode, N., Afe, O., Richter, A., Sinnhuber, M., Wittrock, F., Burrows, J., Stiller, G., von Clarmann, T., and Linden, A. (2005). Global observations of stratospheric bromine monoxide from SCIAMACHY. *Geophysical Research Letters*, 32(20):L20810.

Sioris, C. E., Kovalenko, L. J., McLinden, C. A., Salawitch, R. J., Roozendael, M. V., Goutail, F., Dorf, M., Pfeilsticker, K., Chance, K., von Savigny, C., Liu, X., Kurosu, T. P., Pommereau, J. P., Boesch, H., and Frerick, J. (2006). Latitudinal and vertical distribution of bromine monoxide in the lower stratosphere from scanning imaging absorption spectrometer for atmospheric chartography limb scattering measurements. *J Geophys Res*, 111(D14):D14301.

Soerensen, A. L., Skov, H., Jacob, D. J., Soerensen, B. T., and Johnson, M. S. (2010a). Global concentrations of gaseous elemental mercury and reactive gaseous mercury in the marine boundary layer. in review.

Soerensen, A. L., Sunderland, E. M., Holmes, C. D., Skov, H., Christensen, J. J., Jacob, D. J., Yantosca, R., Strode, S. A., and Mason, R. B. (2010b). A new global simulation of mercury air-sea exchange for evaluating impacts on marine boundary layer concentrations. in preparation.

Sommar, J., Gardfeldt, K., Stromberg, D., and Feng, X. (2001). A kinetic study of the gas-phase reaction between the hydroxyl radical and atomic mercury. *Atmos Environ*, 35(17):3049–3054.

Sprovieri, F., Pirrone, N., Hedgecock, I., Landis, M., and Stevens, R. (2002). Intensive atmospheric mercury measurements at Terra Nova Bay in Antarctica during November and December 2000. *J Geophys Res*, 107(D23):4722.

Stamenkovic, J., Lyman, S., and Gustin, M. S. (2007). Seasonal and diel variation of atmospheric mercury concentrations in the Reno (Nevada, USA) airshed. *Atmos Environ*, 41(31):6662–6672.

Steffen, A., Douglas, T., Amyot, M., Ariya, P., Aspmo, K., Berg, T., Bottenheim, J., Brooks, S., Cobbett, F., Dastoor, A., Dommergue, A., Ebinghaus, R., Ferrari, C., Gardfeldt, K., Goodsite, M., Lean, D., Poulain, A., Scherz, C., Skov, H., Sommar, J., and Temme, C. (2008). A synthesis of atmospheric mercury depletion event chemistry in the atmosphere and snow. *Atmos Chem Phys*, 8(6):1445–1482.

Steffen, A., Schroeder, W., Macdonald, R., Poissant, L., and Konoplev, A. (2005). Mercury in the arctic atmosphere: An analysis of eight years of measurements of GEM at Alert (Canada) and a comparison with observations at Amderma (Russia) and Kuujjuarapik (Canada). *Sci Total Environ*, 342(1-3):185–198.

Strahan, S. E., Duncan, B. N., and Hoor, P. (2007). Observationally derived transport diagnostics for the lowermost stratosphere and their application to the gmi chemistry and transport model. *Atmos Chem Phys*, 7(9):2435–2445.

Streets, D., Zhang, Q., and Wu, Y. (2009). Projections of global mercury emissions in 2050. *Environ Sci Technol*, 43(8):2983–2988.

Strode, S. A., Jaegle, L., Selin, N. E., Jacob, D. J., Park, R. J., Yantosca, R. M., Mason, R. P., and Slemr, F. (2007). Air-sea exchange in the global mercury cycle. *Global Biogeochem. Cycles*, 21(1):GB1017.

Sunderland, E. M. and Mason, R. P. (2007). Human impacts on open ocean mercury concentrations. *Global Biogeochem. Cycles*, 21(4):GB4022.

Swartzendruber, P. C., Chand, D., Jaffe, D. A., Smith, J., Reidmiller, D., Gratz, L., Keeler, J., Strode, S., Jaegle, L., and Talbot, R. (2008). Vertical distribution of mercury, CO, ozone, and aerosol scattering coefficient in the Pacific Northwest during the spring 2006 INTEX-B campaign. *J Geophys Res*, 113(D10):D10305.

Talbot, R., Mao, H., Scheuer, E., Dibb, J., and Avery, M. (2007). Total depletion of Hg0 in the upper troposphere-lower stratosphere. *Geophysical Research Letters*, 34(23):L23804.

Talbot, R., Mao, H., Scheuer, E., Dibb, J., Avery, M., Browell, E., Sachse, G., Vay, S., Blake, D., Huey, G., and Fuelberg, H. (2008). Factors influencing the large-scale distribution of hg degrees in the Mexico City area and over the North Pacific. *Atmos Chem Phys*, 8(7):2103–2114.

Talbot, R. W. and Mao, H. (2009). Boreal forest fires and pyrocumulonimbus convection as a source of Hg(0) to the troposphere. *Eos Transactions, Fall Meeting Suppl*, 90(52):A43A–0228.

Temme, C., Blanchard, P., Steffen, A., Banic, C., Beauchamp, S., Poissant, L., Tordon, R., and Wiens, B. (2007). Trend, seasonal and multivariate analysis study of total gaseous mercury data from the Canadian atmospheric mercury measurement network (CAMNet). *Atmos Environ*, 41(26):5423–5441.

Temme, C., Einax, J., Ebinghaus, R., and Schroeder, W. (2003). Measurements of atmospheric mercury species at a coastal site in the Antarctic and over the South Atlantic Ocean during polar summer. *Environ Sci Technol*, 37(1):22–31.

Thornton, B., Toohey, D., Avallone, L., Harder, H., Martinez, M., Simpas, J., Brune, W., and Avery, M. (2003). In situ observations of ClO near the winter polar tropopause. *J Geophys Res*, 108(D8):8333.

Valente, R., Shea, C., Humes, K., and Tanner, R. (2007). Atmospheric mercury in the Great Smoky Mountains compared to regional and global levels. *Atmos Environ*, 41(9):1861–1873.

Van Loon, L., Mader, E., and Scott, S. (2000). Reduction of the aqueous mercuric ion by sulfite: UV spectrum of HgSO3 and its intramolecular redox reaction. *J Phys Chem A*, 104(8):1621–1626.

Van Roozendael, M., Wagner, T., Richter, A., Pundt, I., Arlander, D., Burrows, J., Chipperfield, M., Fayt, C., Johnston, P., Lambert, J., Kreher, K., Pfeilsticker, K., Platt, U., Pommereau, J., Sinnhuber, B., Tornkvist, K., and Wittrock, F. (2002). Intercomparison of BrO measurements from ERS-2 GOME, ground-based and balloon platforms. *Advances in Space Research*, 29:1661–1666.

Vijayaraghavan, K., Karamchandani, P., Seigneur, C., Balmori, R., and Chen, S.-Y. (2008). Plume-in-grid modeling of atmospheric mercury. *J Geophys Res*, 113:D24305.

von Glasow, R., Sander, R., Bott, A., and Crutzen, P. (2002). Modeling halogen chemistry in the marine boundary layer - 1. cloud-free MBL. *J Geophys Res*, 107(D17):4341.

von Glasow, R., von Kuhlmann, R., Lawrence, M., Platt, U., and Crutzen, P. (2004). Impact of reactive bromine chemistry in the troposphere. *Atmos Chem Phys*, 4:2481–2497.

Wan, Q., Feng, X., Lu, J., Zheng, W., Song, X., Han, S., and Xu, H. (2009). Atmospheric mercury in Changbai Mountain area, northeastern China I. The seasonal distribution pattern of total gaseous mercury and its potential sources. *Environmental Research*, 109(3):201–206.

Wangberg, I., Munthe, J., Berg, T., Ebinghaus, R., Kock, H. H., Temme, C., Bieber, E., Spain, T. G., and Stolk, A. (2007). Trends in air concentration and deposition of mercury in the coastal environment of the North Sea area. *Atmos Environ*, 41(12):2612–2619.

Warwick, N., Pyle, J., Carver, G., Yang, X., Savage, N., O'Connor, F., and Cox, R. (2007). Global modeling of biogenic bromocarbons. *J Geophys Res*, 111(D24):D24305.

Weiss-Penzias, P., Gustin, M. S., and Lyman, S. N. (2009). Observations of speciated atmospheric mercury at three sites in Nevada: Evidence for a free tropospheric source of reactive gaseous mercury. *J Geophys Res*, 114:D14302.

Weiss-Penzias, P., Jaffe, D., Swartzendruber, P., Hafner, W., Chand, D., and Prestbo, E. (2007). Quantifying asian and biomass burning sources of mercury using the Hg/CO ratio in pollution plumes observed at the Mount Bachelor Observatory. *Atmos Environ*, 41(21):4366–4379.

Wesely, M. (1989). Parameterization of surface resistances to gaseous dry deposition in regional-scale numerical models. *Atmos Environ*, 23(6):1293–1304.

WMO (2007). Scientific assessment of ozone depletion: 2006. Technical Report 50, Global Ozone Research and Monitoring Project, Geneva, Switzerland.

Yang, X., Cox, R., Warwick, N., Pyle, J., Carver, G., O'Connor, F., and Savage, N. (2005). Tropospheric bromine chemistry and its impacts on ozone: A model study. *J Geophys Res*, 110(D23):D23311.

Yatavelli, R. L. N., Fahrni, J. K., Kim, M., Crist, K. C., Vickers, C. D., Winter, S. E., and Connell, D. P. (2006). Mercury, PM2.5 and gaseous co-pollutants in the Ohio River Valley region: Preliminary results from the Athens supersite. *Atmos Environ*, 40(34):6650–6665.

Zhang, H., Lindberg, S., Marsik, F., and Keeler, G. (2001). Mercury air/surface exchange kinetics of background soils of the tahquamenon river watershed in the michigan upper peninsula. *Water, Air, and Soil Pollution*, 126(1-2):151–169.